Theses and Dissertations 1. Thesis and Dissertation Collection, all items

2012-06

Formation and Development of Diabatic Rossby Vortices in a 10-Year Climatology

Shih, Nengwei Tom

Monterey, California. Naval Postgraduate School

http://hdl.handle.net/10945/7415

NAVAL POSTGRADUATE SCHOOL

MONTEREY, CALIFORNIA

THESIS

FORMATION AND DEVELOPMENT OF DIABATIC ROSSBY VORTICES IN A 10-YEAR CLIMATOLOGY

by

Nengwei "Tom" Shih
June 2012

Thesis Advisor: Richard W. Moore
Second Reader: Michael T. Montgomery

Approved for public release; distribution is unlimited

THIS PAGE INTENTIONALLY LEFT BLANK

REPORT DOCUMENTATION PAGE		*Form Approved OMB No. 0704-0188*

Public reporting burden for this collection of information is estimated to average 1 hour per response, including the time for reviewing instruction, searching existing data sources, gathering and maintaining the data needed, and completing and reviewing the collection of information. Send comments regarding this burden estimate or any other aspect of this collection of information, including suggestions for reducing this burden, to Washington headquarters Services, Directorate for Information Operations and Reports, 1215 Jefferson Davis Highway, Suite 1204, Arlington, VA 22202-4302, and to the Office of Management and Budget, Paperwork Reduction Project (0704-0188) Washington DC 20503.

1. AGENCY USE ONLY *(Leave blank)*	2. REPORT DATE June 2012	3. REPORT TYPE AND DATES COVERED Master's Thesis	
4. TITLE AND SUBTITLE Formation and Development of Diabatic Rossby Vortices in a 10-Year Climatology		5. FUNDING NUMBERS	
6. AUTHOR(S) Nengwei "Tom" Shih			
7. PERFORMING ORGANIZATION NAME(S) AND ADDRESS(ES) Naval Postgraduate School Monterey, CA 93943-5000		8. PERFORMING ORGANIZATION REPORT NUMBER	
9. SPONSORING /MONITORING AGENCY NAME(S) AND ADDRESS(ES) N/A		10. SPONSORING/MONITORING AGENCY REPORT NUMBER	

11. SUPPLEMENTARY NOTES
The views expressed in this thesis are those of the author and do not reflect the official policy or position of the Department of Defense or the U.S. Government. IRB Protocol number N/A.

12a. DISTRIBUTION / AVAILABILITY STATEMENT Approved for public release; distribution is unlimited	12b. DISTRIBUTION CODE A

13. ABSTRACT (maximum 200 words)

A diabatic Rossby vortex (DRV) is a short-scale, diabatically dominated, moist baroclinic disturbance that forms and grows in the absence of discernible upper tropospheric forcing. The overarching goal of this work is to expand on the limited amount of DRV research by examining the general characteristics of real-world DRVs that have been identified in an automated 10-year DRV climatology.

The identified 314 DRVs form preferentially over warm ocean currents. All DRVs track to the east northeast. While more DRVs form during the warm season, a larger fraction of storms that explosively deepen occur during the cold season. Composite analyses bear strong resemblance to DRV structural plots in the published literature, confirming that moisture, baroclinicity and the diabatic generation of eddy available potential energy are essential to DRV formation and development.

Upon inspection of the interaction between DRVs and the dynamic tropopause (DT), nine (30%) of the 31 explosively deepened DRVs are subjectively determined (based on how the DRVs interacted with DT to bomb) to be of type A development (as defined by Petterssen and Smebye [1971], so-called "bottom-up" development). The remaining 22 (70%) are subjectively identified as type C development (mutual interaction of pre-existing upper and lower tropospheric disturbances, as defined by Deveson et al. [2002]).

14. SUBJECT TERMS Diabatic Rossby Vortex, Moist Baroclinic Instability, Explosive Deepening, Composite Analysis Eddy Available Potential Energy, Dynamic Tropopause			15. NUMBER OF PAGES 145
			16. PRICE CODE
17. SECURITY CLASSIFICATION OF REPORT Unclassified	18. SECURITY CLASSIFICATION OF THIS PAGE Unclassified	19. SECURITY CLASSIFICATION OF ABSTRACT Unclassified	20. LIMITATION OF ABSTRACT UU

THIS PAGE INTENTIONALLY LEFT BLANK

FORMATION AND DEVELOPMENT OF DIABATIC ROSSBY VORTICES IN A 10-YEAR CLIMATOLOGY

Nengwei "Tom" Shih
Major, United States Air Force
B.S., University of Wisconsin - Madison, 2000

Submitted in partial fulfillment of the
requirements for the degree of

MASTER OF SCIENCE IN METEOROLOGY

from the

**NAVAL POSTGRADUATE SCHOOL
June 2012**

Author: Nengwei "Tom" Shih

Approved by: Richard W. Moore
Thesis Advisor

Michael T. Montgomery
Second Reader

Wendell A. Nuss
Chair, Department of Meteorology

THIS PAGE INTENTIONALLY LEFT BLANK

ABSTRACT

A diabatic Rossby vortex (DRV) is a short-scale, diabatically dominated, moist baroclinic disturbance that forms and grows in the absence of discernible upper tropospheric forcing. The overarching goal of this work is to expand on the limited amount of DRV research by examining the general characteristics of real-world DRVs that have been identified in an automated 10-year DRV climatology.

The identified 314 DRVs form preferentially over warm ocean currents. All DRVs track to the east northeast. While more DRVs form during the warm season, a larger fraction of storms that explosively deepen occur during the cold season. Composite analyses bear strong resemblance to DRV structural plots in the published literature, confirming that moisture, baroclinicity and the diabatic generation of eddy available potential energy are essential to DRV formation and development.

Upon inspection of the interaction between DRVs and the dynamic tropopause (DT), nine (30%) of the 31 explosively deepened DRVs are subjectively determined (based on how the DRVs interacted with DT to bomb) to be of type A development (as defined by Petterssen and Smebye [1971], so-called "bottom-up" development). The remaining 22 (70%) are subjectively identified as type C development (mutual interaction of pre-existing upper and lower tropospheric disturbances, as defined by Deveson et al. [2002]).

THIS PAGE INTENTIONALLY LEFT BLANK

TABLE OF CONTENTS

LIST OF FIGURES

THIS PAGE INTENTIONALLY LEFT BLANK

LIST OF TABLES

THIS PAGE INTENTIONALLY LEFT BLANK

LIST OF ACRONYMS AND ABBREVIATIONS

2D	Two-Dimensional
3D	Three-Dimensional
APE	Available Potential Energy
CH	Diabatic Heating
DRV	Diabatic Rossby Vortex
ECMWF	European Centre for Medium-Range Weather Forecasts
HR	Hour
IWC	Ice Water Content
K	Kelvin
KM	Kilometer
LWC	Liquid Water Content
MCS	Mesoscale Convective System
MCV	Mesoscale Convective Vortex
MM5	Mesoscale Model Version 5
MSLP	Minimum Sea Level Pressure
NCAR	National Center for Atmospheric Research
PV	Potential Vorticity
PVU	Potential Vorticity Unit
Q	Specific Humidity
RH	Relative Humidity
SST	Sea Surface Temperature
TH	Potential Temperature
UVM	Upward Vertical Motion

THIS PAGE INTENTIONALLY LEFT BLANK

ACKNOWLEDGMENTS

I want to thank God, who put me together.

I want to thank Beth, who made me join the USAF.

I want to thank USAF, which sent me to NPS.

I want to thank Bob, who got me the coveted corner desk.

I want to thank Zaak and Joe, who fought the battle with me.

I want to thank Rob, my lunch and cribbage Navy buddy.

I want to thank Mary, who laid the foundation of sound programming.

I want to thank Saurabh, who knew everything about computers.

I want to thank Prof. Murphree, who knew how to explain stuff.

I want to thank Prof. Harr, who gave generously to his students.

I want to thank Prof. Nuss, the coolest department chair in this century.

I want to thank Prof. Montgomery, who read every word in this thesis.

But I am most grateful to my advisor, who led me every step of the way.

THIS PAGE INTENTIONALLY LEFT BLANK

I.   INTRODUCTION

A.   DEFINITION OF DIABATIC ROSSBY VORTEX

The diabatic Rossby vortex (DRV) is best described as a short-scale, diabatically-dominated, moist baroclinic disturbance in the absence of discernible upper-tropospheric (UT) forcing. It is insightful to individually contrast each of these characteristics with a typical extratropical cyclone (EC):

- Short-Scale: A DRV is significantly shorter in both its horizontal and vertical extent.

- Diabatically-Dominated: A DRV is termed "diabatically-dominated" due to the primacy of diabatic effects, as opposed to baroclinic processes.

- Moist Baroclinic: Sufficient moisture and baroclinicity are *necessary* ingredients for disturbance growth.

- Absence of Discernible Upper Tropospheric Forcing: A DRV does not require upper tropospheric forcing. In contrast, it is a self-sustaining entity that thrives on the diabatic production of positive potential vorticity (PV).

Many of these characteristics are evident when viewing an observed DRV in satellite imagery, where the short-scale of the DRV is apparent, as shown inside the red ellipse of Figure 1. It can also be seen that cloud diabatic processes are at work, speaking to both the diabatic dominance and the importance of moisture content.
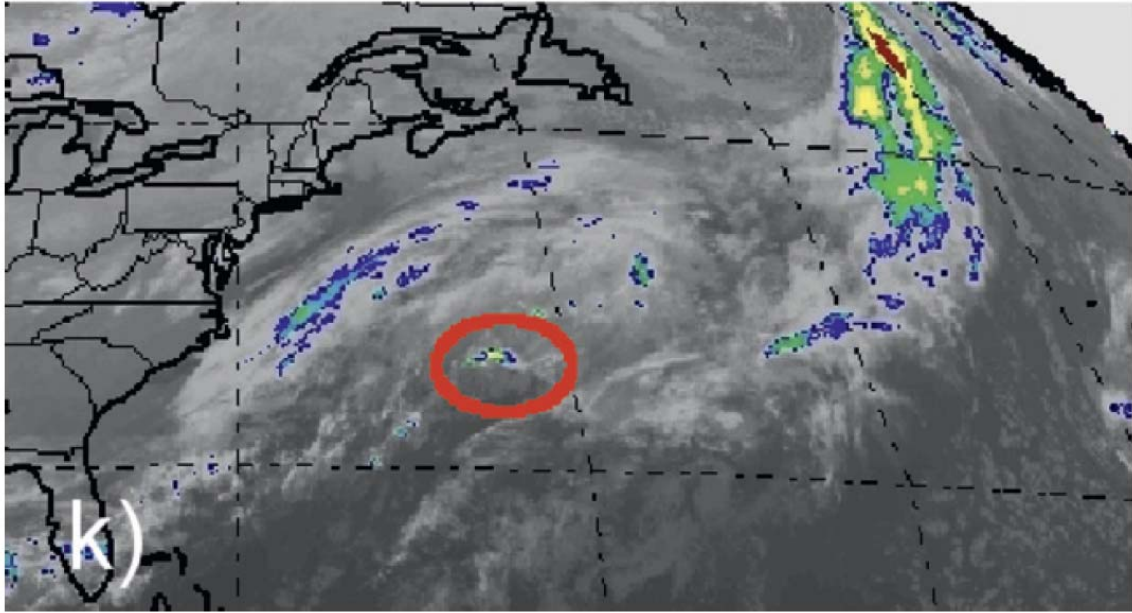
Figure 1.   IR satellite image from GOES East at 12 UTC 19 December 2005, with red ellipse marking the DRV (Figure 2k from Boettcher and Wernli 2011).

DRVs are important in terms of weather research for a number of reasons. The characteristic DRV growth mechanism has been linked to a variety of atmospheric phenomena that can generate high impact weather. In addition, there is mounting evidence that today's numerical weather prediction (NWP) models have difficulty in properly simulating these disturbances.

The case of extreme winter storm "Lothar" provides a motivating example. It has been shown that a DRV played an integral role in the dynamical evolution of Lothar, serving as a precursor disturbance to the subsequent explosive cyclogenesis (Wernli et al. 2002). The storm system left a path of destruction over central Europe from Great Britain to Switzerland, as shown in Figure 2. It resulted in significant societal impacts: roughly 50 lives were lost and over 3.5 billion Euros in damages were reported.   Exacerbating the problem, it was very poorly forecast.

Figure 2.   Photos of damage from Winter Storm "Lothar" (AIR WORLDWIDE, cited 1999).

## B.	DRV FUNDAMENTALS

### 1.	Growth Rate vs. Wavelength of Dry vs. Moist Cyclogenesis

To investigate how moisture fundamentally alters storm dynamics, Moore and Montgomery (2004), hereafter MM04, conducted a stability analysis of the moist baroclinic atmosphere. They utilized a two-dimensional (2D), semigeostrophic (SG) model (with a parameterization of latent heat release) to diagnose the structure, energetics, and propagation characteristics of short-scale, diabatic normal modes in a moist, baroclinic atmosphere with the Eady basic state. A main conclusion of their work is that the presence of moisture can not only modify the dry dynamics of extratropical cyclones, but also gave rise to disturbances that have no dry counterpart.

The stability analysis of MM04 can be summarized via an examination of disturbance growth rate as a function wave scale. With the inclusion of the results for the dry system for direct comparison, these data are presented in Figure 3. The inclusion of moisture serves to increase the maximum growth rate by 1.14 times the dry value, and has shifted the wavelength of the most unstable mode from 3900 km in the dry system to approximately 3490 km. The data also illustrate that, when a thermodynamically consistent vertical profile of latent heat release is used, the short-wave cutoff apparent in the dry system vanishes, and the disturbance growth rate becomes independent of zonal wavelength for zonal wavelengths shorter than 1900 km.

For the moist system, MM04 noted two distinct growth regimes. Following the terminology of Eady (1949), MM04 referred to disturbances longer than 1900 km (where disturbance growth rate varies with wave scale) as "long waves" and disturbances shorter than 1900 km (where the disturbance growth rate is constant with wave scale in the absence of friction) as "cyclone waves." As will be seen in the next subsection, at longer wave scales, the disturbance qualitatively resembles a dry baroclinic wave, intimating that dry dynamics are of primary importance. In contrast, at shorter wave scales, it is diabatic processes that dominate the disturbance evolution. These "cyclone waves" have been termed a diabatic Rossby wave (Parker and Thorpe 1995), and subsequently due to their hybrid wave-vortical structure in three dimensions, a diabatic Rossby vortex (MM04).
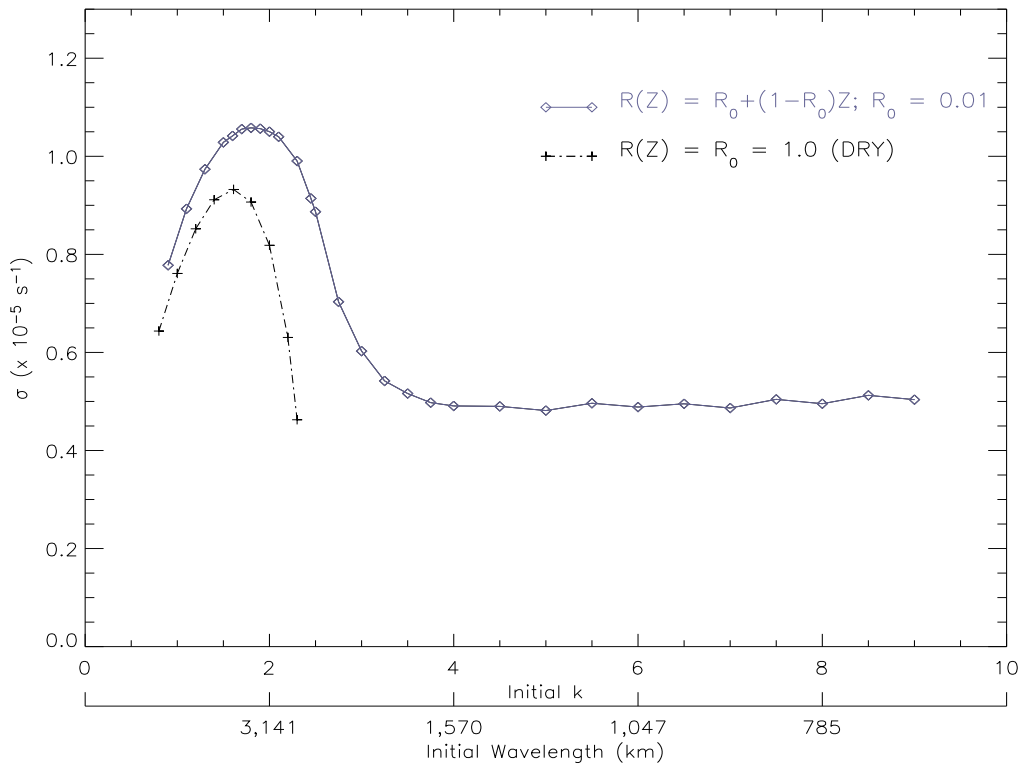
Figure 3.   Growth rate (vertical axis) as a function of initial nondimensional wavenumber and dimensional wavelength in km (horizontal axis) for dry (short/black curve) versus moist (long/blue curve) cyclogenesis (Figure 1 after MM04).

5

2.   Disturbance Structure

To further investigate the dynamical processes at work, disturbance structure in both the long wave and cyclone wave regimes are reviewed using the results of MM04. Vertical cross sections (longitude versus height) of the meridional wind and potential temperature for the most unstable moist mode (dimensional wavelength of 3490 km, top panels), and for a disturbance shorter than the shortwave cutoff of the dry system (dimensional wavelength of 1047 km), are presented in the top and bottom panels of Figure 4.

There is a strong qualitative resemblance between the most unstable moist mode and that of a dry baroclinic wave. One can see the characteristic westward tilt with height of meridional wind and eastward tilt with height of potential temperature perturbation in top panel of Figure 4. This disturbance structure maximizes the poleward heat transport and is representative of the conversion of available potential energy to kinetic energy via baroclinic processes (e.g., Holton 1992, Chapter 8). For the cyclone wave, a decidedly different disturbance structure is evident as shown in bottom panel of Figure 4. It in no way resembles the structure of a dry baroclinic wave. There is no evidence of an upper-level disturbance.   This incongruity implies that a growth mechanism other than dry baroclinic instability must be at work.
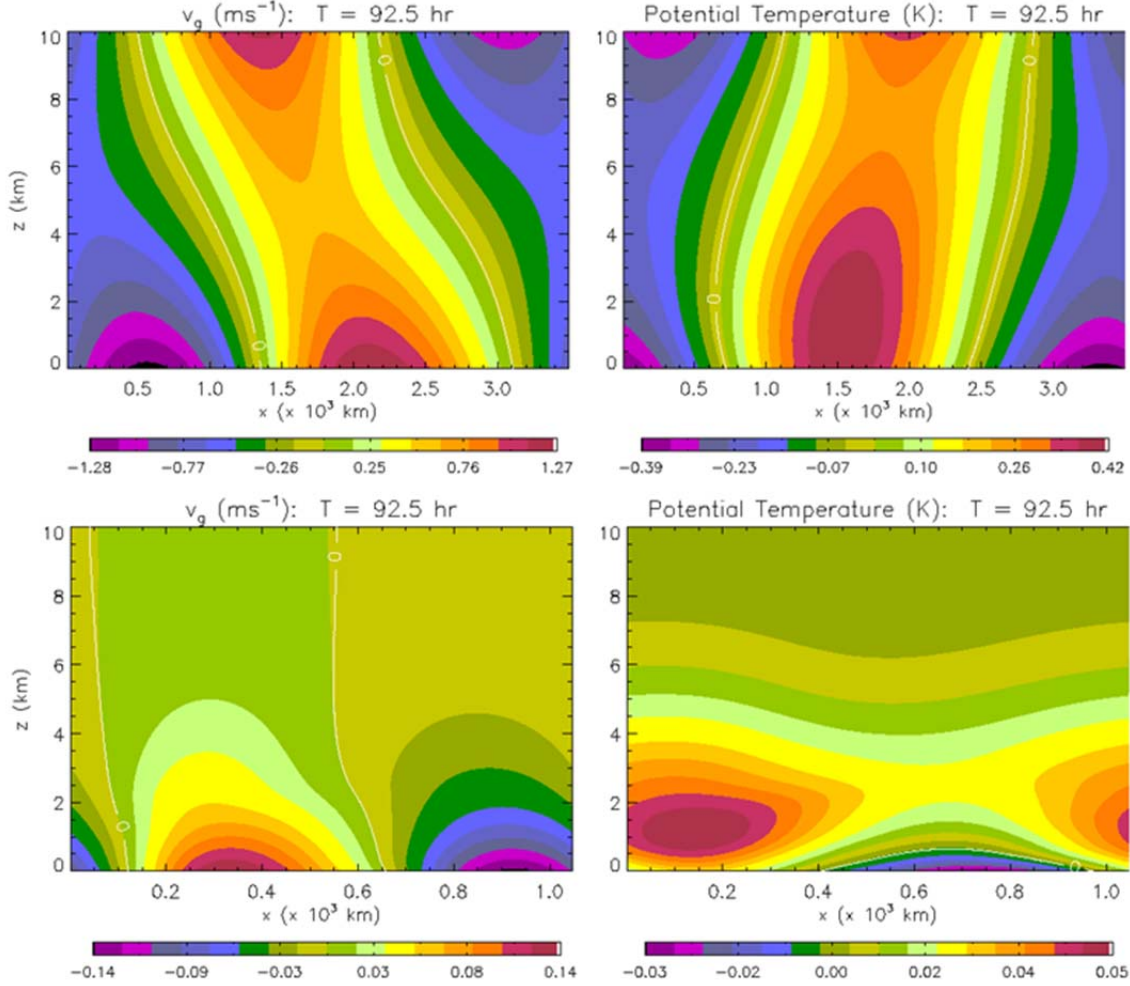
Figure 4.   Top panel: Vertical cross section of disturbance structure of most unstable, moist mode (initial nondimensional wavenumber $k = 1.8$; dimensional wavelength = 3490 km). Bottom panel: Vertical cross section of disturbance structure of a previously neutral wave (initial nondimensional wavenumber $k = 6.0$; dimensional wavelength = 1047 km). Meridional wind or v_g (shading; m/s) is shown on the left, and potential temperature perturbation (shading; K) is shown on the right, at time $T = 92.5$ hr (Figure 3a and 4a from MM04).

In similar fashion, vertical cross sections of the vertical velocity and anomalous PV are presented for both wave scales in Figure 5. The most obvious feature evident in these plots is the drastically reduced horizontal and vertical scale of the cyclone wave (bottom panel), in comparison to the long wave (top panel).
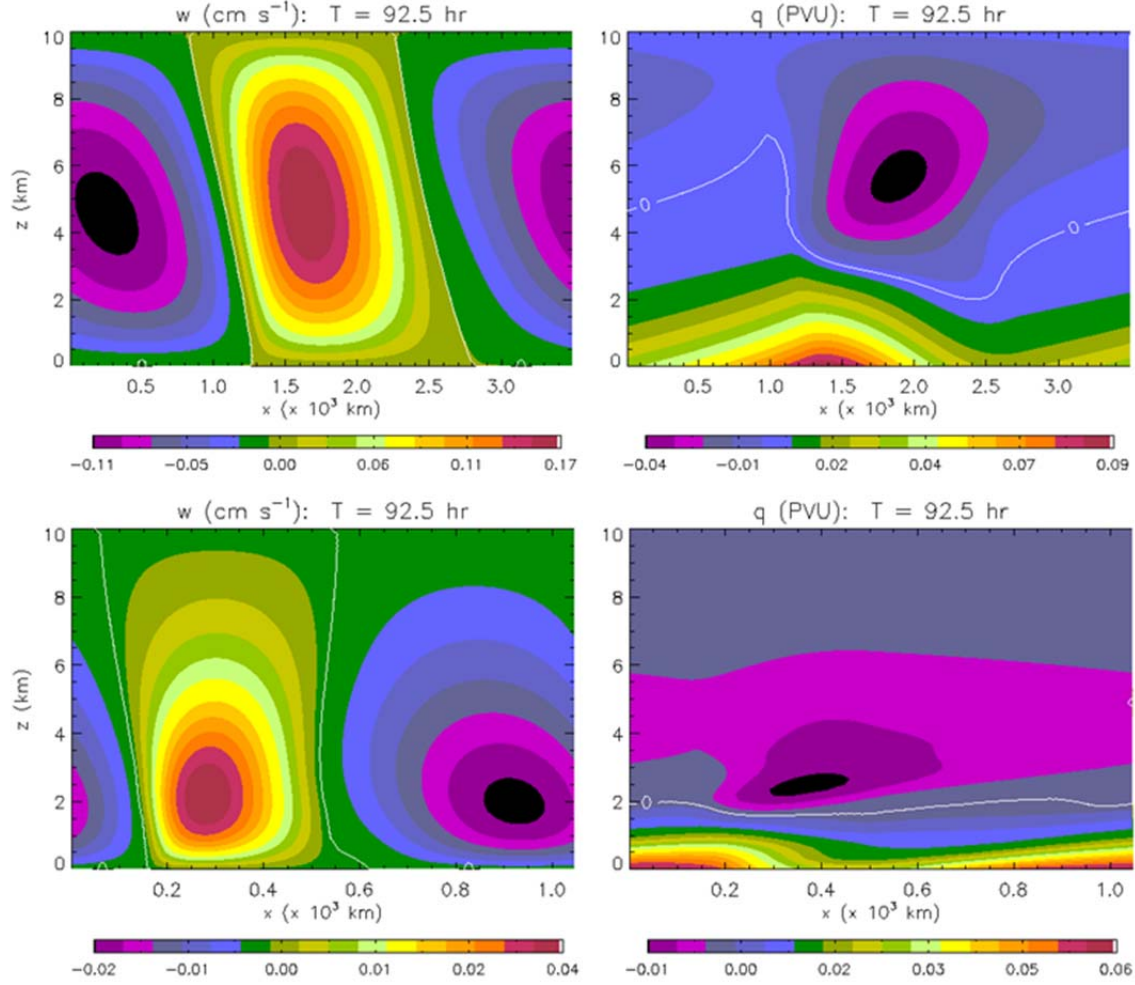
Figure 5.   Top panel: Vertical cross section of disturbance structure of most unstable, moist mode (initial nondimensional wavenumber $k = 1.8$; dimensional wavelength = 3490 km). Bottom Panel: Vertical cross section of disturbance structure of a previously neutral wave (initial nondimensional wavenumber $k = 6.0$; dimensional wavelength = 1047 km). Vertical velocity or w (shading; cm/s) is shown on the left, and anomalous dry PV or q(shading; PVU) is shown on the right (white line is the 0 PVU isoline), at time T = 92.5 hr (Figure 3b and 4b from MM04).

3.   DRV Growth Mechanism

Raymond and Jiang (1990; hereafter RJ90) proposed that certain mesoscale convective systems (MCS), such as supercell thunderstorms and squall lines, maintain themselves through an interaction between vertical motions and the diabatic effects of moist convection. RJ90 asserted that within a convective column, the latent heat release

8

through water vapor condensation, and to a lesser degree evaporation/melting of precipitation and thermal radiation, contributes to the creation of a positive PV anomaly in the lower troposphere and a negative PV anomaly near the tropopause, as shown in Figure 6.
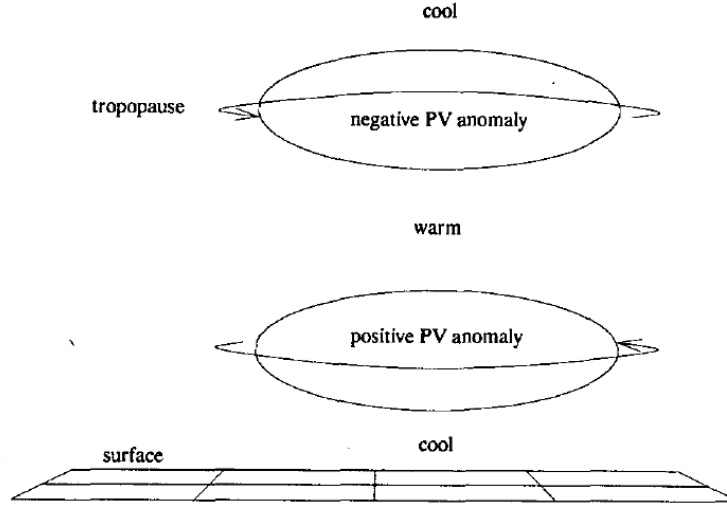
Figure 6. Structure of PV anomalies produced by a region of convection and the associated changes in temperature and wind structure. The circulation is cyclonic around the lower, positive PV anomaly, and anticyclonic around the upper, negative PV anomaly, as shown by the arrows (Figure 1 from RJ90).

The result is a cyclonic circulation around the positive PV at lower tropospheric (LT) levels and an anticyclonic circulation around the negative PV at upper tropospheric (UT) levels. In addition, the air temperatures above the negative PV anomaly and below the positive PV anomaly would be cooler than the surrounding air, and the air temperature between the positive and negative PV anomalies would be warmer than the surrounding air. In the lower troposphere, the increase in lapse rate would increase the static stability, which results in PV enhancement, according to Ertel's definition of PV (Equation 1). In the upper troposphere, the decrease in lapse rate would decrease the static stability, which results in PV dilution.

$$PV = (\zeta_\theta + f)(-g\frac{\delta\theta}{\delta p})$$ (1)

9

RJ90 estimated the vertical to horizontal ratio of radius of influence/deformation of the convectively induced PV anomalies to be about 0.01 (corresponding to f/N, the so-called Prandtl's ratio). Given that a typical MCS is several hundred kilometers in horizontal extent, this would yield a vertical radius of influence of several kilometers. Given this estimation, the negative PV anomaly aloft would have no influence near the surface. On the other hand, the positive PV anomaly could influence further convection by affecting circulation and isentropic lifting in the presence of baroclinicity, as shown in Figure 7. This figure depicts a positive PV anomaly within a westerly flow (coming out of the page), with potential temperature surfaces sloping upward to the north (page right). The cyclonic circulation within the positive PV anomaly would cause air parcels to rise toward the east, triggering convection in a conditionally unstable atmosphere, and sink toward the west, diminishing convection there. This mechanism also contributes to the eastward propagation of the PV anomaly and vertical expansion over time. This same mechanism also sustains and propagates a DRV.
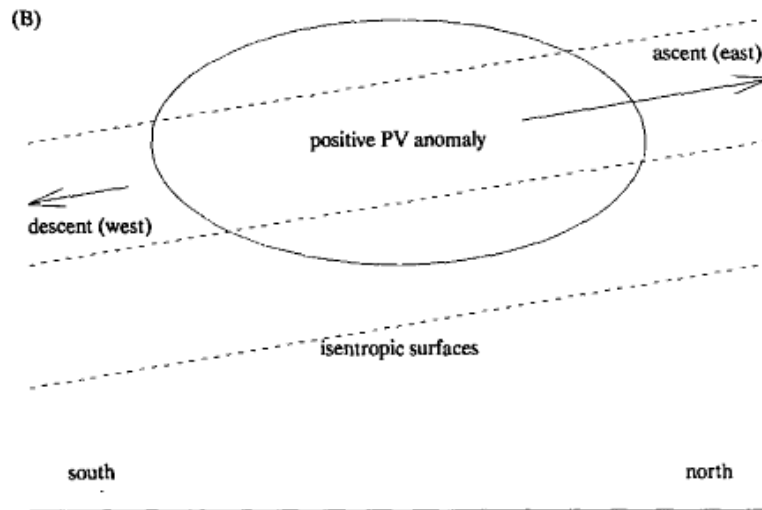
Figure 7.   View of the positive PV anomaly (think DRV) from the east. The tilted isentropic surfaces (dashed lines) are associated with uniform ambient westerly shear through the depth of the illustration. The cyclonic circulation around the anomaly causes ascent in the northward-moving air on the east side, and descent in the southward-moving air on the west side of the DRV (Figure 2B from RJ90).

10

The concept of PV redistribution through diabatic heating was revisited by Mak (1994). Mak demonstrated that perturbation PV would increase where latent heating increases with height and decrease where latent heating decreases with height. In other words, diabatic heating would give rise to significant local positive or negative PV anomalies wherever there is a sharp vertical gradient in the heating rate, even though there is no net change of PV within the convective column.

Therefore, given strong diabatic heating associated with intense convection, one would expect to see a PV dipole—a positive PV anomaly above, and a negative PV anomaly below the level of convection. This PV dipole was observed by Moore and Montgomery (2005) in the longitude-pressure cross section of DRV model (MM5) simulation at Day 4, exhibiting an approximate phase locking and mutual amplification of two diabatically-generated PV anomalies, as shown in Figure 8.
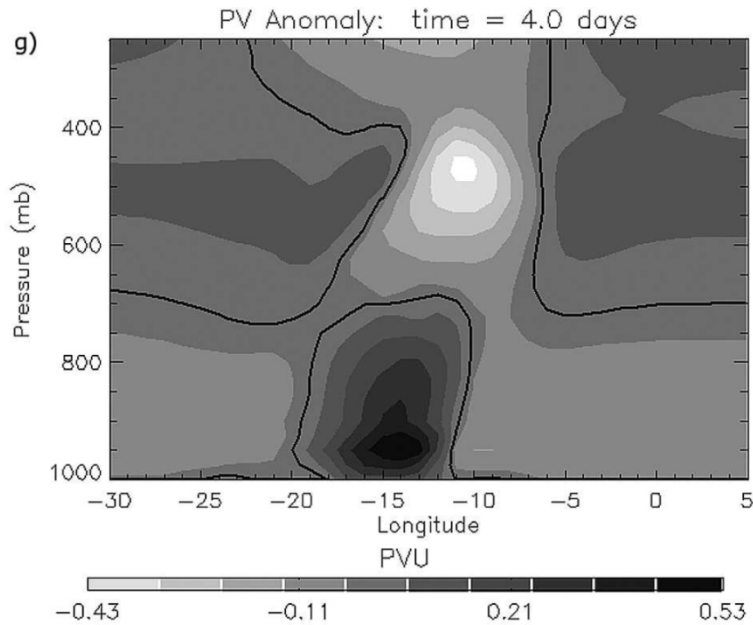
Figure 8.   Longitude-pressure cross section of PV anomaly (shading; PVU) simulated by MM5 at Day 4 of DRV evolution, showing the interaction of two diabatically generated PV anomalies (Figure 5g from MM05).

Parker and Thorpe (1995; hereafter PT95) introduced the term "diabatic Rossby wave," a distinctly different phenomenon from the "ordinary dry baroclinic Rossby wave." In modeling convective frontogenesis using 2D SG model with the Eady basic

state, PT95 found that once diabatic heating reached a certain threshold, the energetics of the frontogenesis shifted predominantly to cross-front diabatic conversion, which was an order of magnitude greater than the along-front temperature gradient contribution. PT95 named such convective fronts "diabatic Rossby waves," and illustrated their propagation and development schematically as shown in Figure 9.
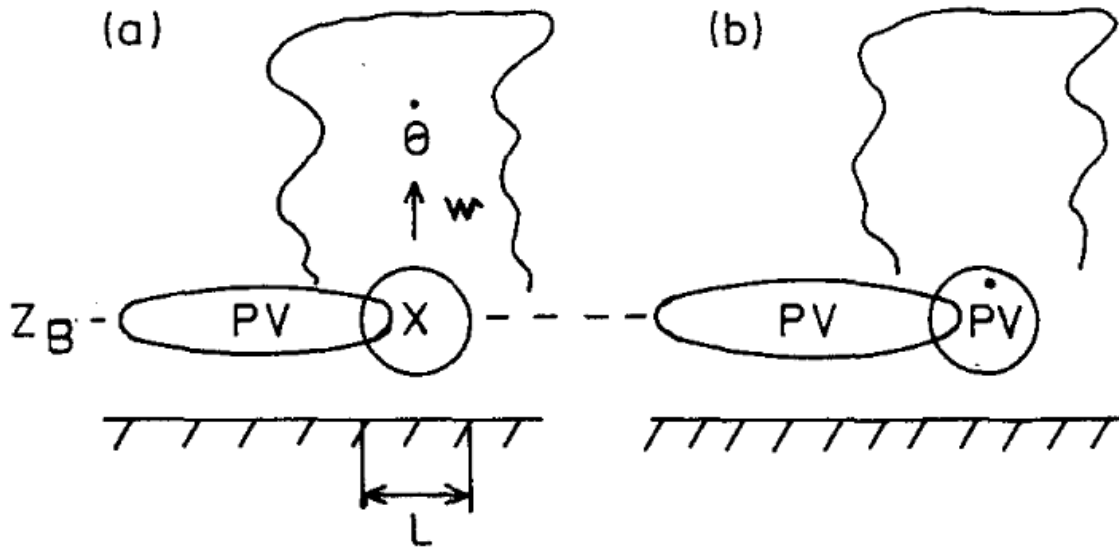
Figure 9.   Schematic representation of the dynamics of the diabatic Rossby wave. Here L is the horizontal scale of the jet on the eastern side of the PV anomaly. The poleward jet (marked by "X") associated with the lower tropospheric PV anomaly gives positive thermal advection, leading to upward motion and diabatic heating (Figure 6a and 6b from PT95).

Figure 9(a) depicts a vertical cross section (longitude vs. height) of a pre-existing low level PV anomaly. The cyclonic rotation around the PV anomaly is implied, which enhances the low level jet (LLJ) marked by "X" with horizontal scale of "L," serves to advect warm moist air into the page (to the north). As the LLJ ascends (depicted by vertical motion w) the isentropic surfaces (which slant upward from south to north), air parcels expand and cool, achieving saturation and latent heat release of condensation (depicted by the potential temperature tendency). Differential diabatic heating in the vertical results in PV generation below the level of maximum heating and PV depletion above the level of maximum heating. The low-level PV generation indicated by the PV tendency in Figure 9(b) results in a positive PV anomaly to the east of the initial positive

PV anomaly, resulting in disturbance propagation to the east. As outlined here, this represents a self-sustaining growth mechanism.

PT95 then contrasted the growth mechanisms of a classical Rossby wave and diabatic Rossby wave in Figure 10. Both result in a PV tendency, however the dynamical pathways are drastically different. For a classical Rossby wave, the PV tendency is a result of the meridional advection of the mean meridional gradient of background PV. In contrast, it is the diabatic generation of PV (via the process outlined above) that results in a PV tendency for the diabatic Rossby wave. A repercussion of these differences is evident in the respective propagation direction: classical Rossby waves propagate to the west, whereas a diabatic Rossby wave propagates to the east.
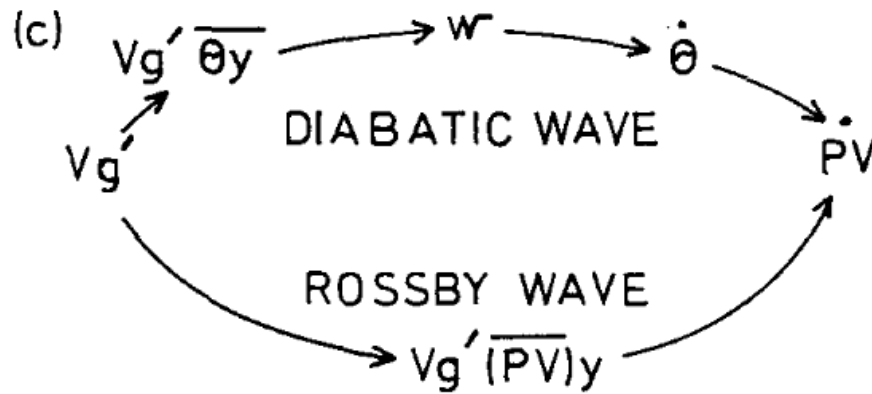
Figure 10.   A comparison between the dynamical processes for the diabatic Rossby wave versus the classical Rossby wave, linking meridional advection with the PV tendency (Figure 6c From PT95).

4.   Necessary Ingredients for DRV Growth

Moore and Montgomery (2005; hereafter MM05) utilized the fifth-generation Pennsylvania State University—National Center for Atmospheric Research (NCAR) Mesoscale Model (MM5) to study the formation, structure, and evolution of DRVs. In their previous paper, MM04 suggested using the term diabatic Rossby "vortex" (instead of "wave) because the disturbance is best viewed as a coherent vortex (as opposed to an idealized wavelike disturbance with an alternating high/low pattern). Using an idealized model setup, MM05 confirmed that an alternate growth mechanism to that of dry

baroclinic instability is viable within a moist baroclinic environment. Their MM5 simulations illustrated that, in this alternate growth scenario, a DRV's growth depended on the presence of sufficient environmental moisture *and* baroclinicity. The lack of either necessary ingredient precluded disturbance growth, as demonstrated in Figure 11. In the presence of both moisture and baroclinicity, a growing disturbance emerges. In contrast, the simulations without moisture or baroclinicity, respectively, exhibit a vortex that decays with time.
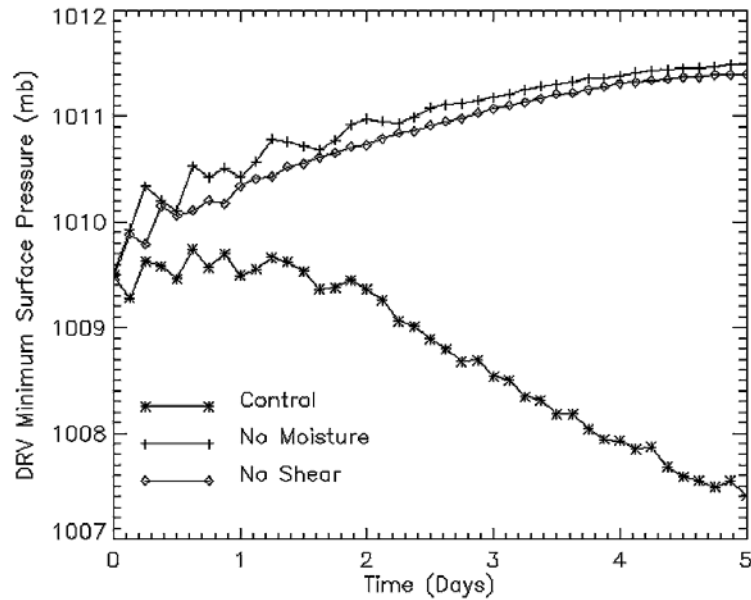
Figure 11. Temporal evolution of the minimum DRV surface pressure for the following MM5 simulations: the control run (asterisk), no moisture (plus sign), and no shear/baroclinicity (diamond) (Figure 3 from MM05).

MM05 then conducted a sensitivity study to quantify the dependence of the DRV dynamics on various parameters. They concluded that the track and intensity of a DRV are most sensitive to the environmental baroclinicity and moisture, while the vertical profile of the moisture determines the characteristic depth of a DRV.

14

5.   Energetics

Leveraging the same 2D SG model designed to study DRV and moist cyclogenesis, MM04 gained insight into cyclone growth energetics by calculating the contribution terms (positive terms on RHS) to the diagnostic eddy available potential energy (APE) equation (Lorenz 1955 and Norquist et al. 1977):

$$\frac{\delta A_E}{\delta t} = C_A - C_E + G_E \tag{2}$$

where A_E is the eddy APE, and the positive contribution term C_A is the conversion from basic state APE to A_E, while the other positive contribution term $C_A G_E$ is the conversion from diabatic heat sources to A_E . C_A and G_E are defined in Equations 3 and 4, respectively.

$$C_A = \frac{f\overline{U_z}}{2\overline{\theta_z}} \overline{(\upsilon_g'\theta')} \tag{3}$$

$$G_E = \frac{g}{2\theta_o\overline{\theta_z}} \overline{(\theta'S')} \tag{4}$$

All variables have their usual meteorological meaning S is the diabatic heating rate in K/day. The apostrophe following a parameter denotes perturbation. A parameter with overbar and subscript z is the vertically averaged value of that parameter. An overbar within parentheses represents a spatially integrated quantity. Note that the covariance term on RHS of C_A is simply the meridional temperature advection.   In addition, the covariance term on RHS of G_E is the temperature perturbation multiplied by the diabatic heating rate. If both the temperature perturbation and diabatic heating are positively correlated, then the covariance term would also be positive, leading to a positive diabatic contribution term G_E, (illustrated in the center of Figure 12).
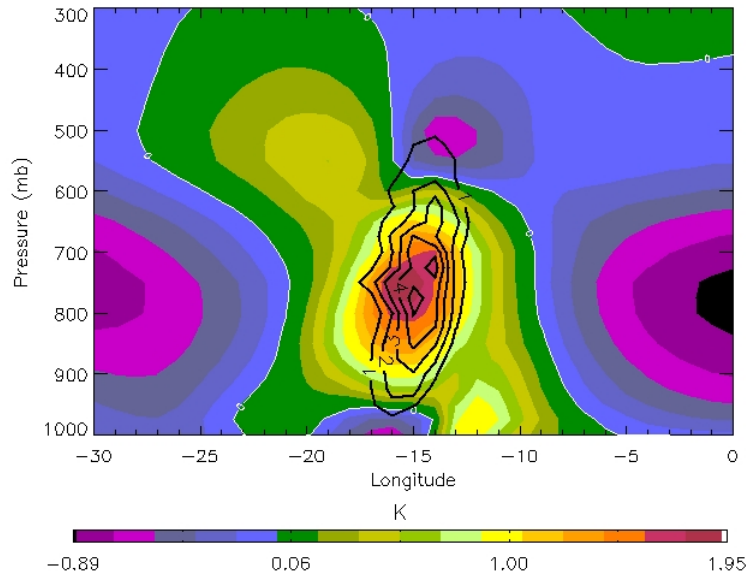
Figure 12.   Longitude-pressure cross section of temperature anomaly (shading; K) and diabatic heating or CH (black contour; K/day) for 2D SG model simulation of DRV growth at day=4.5 (From Figure 5d of Moore, Montgomery and Davies, 2012 [submitted]).

MM05 further defined the "conversion ratio" to be G_E/C_A, which proved to be a useful diagnostic for differentiating between the dynamics associated with a long (baroclinic) wave and a cyclonic/short (DRV) wave. The conversion ratio as a function of wave scale (using results from 2D SG model) is presented in Figure 13. It is apparent that, for disturbances in the long wave regime (dimensional wavelength > 1900 km, such as an extratropical cyclone), the conversion ratio is small, highlighting the dominance of the baroclinic eddy APE conversion term (C_A). In contrast, in the cyclone wave regime (dimensional wavelength < 1900 km) the conversion ratio increases (becomes much larger than one) with decreasing wave scale, highlighting the dominance of the diabatic eddy APE conversion term (G_E).

16
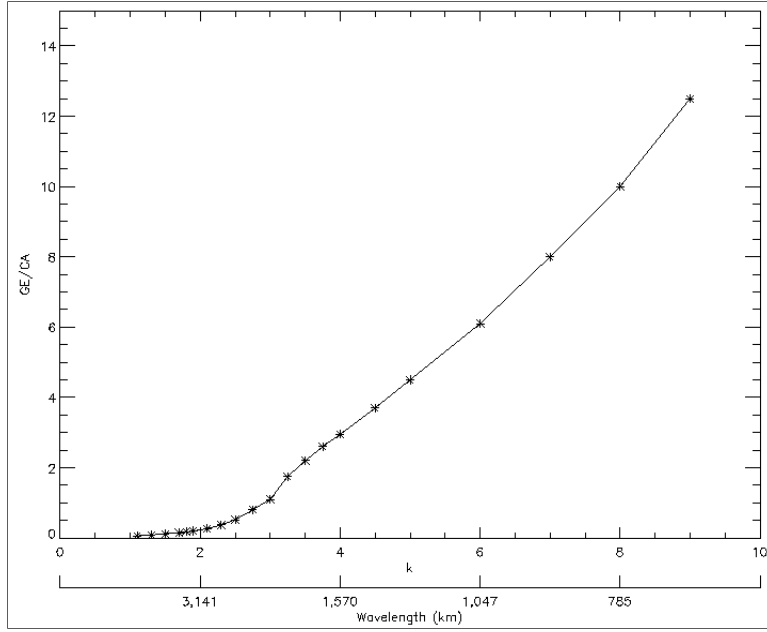
Figure 13.   Ratio of the conversion of diabatic heat sources to eddy APE (G_E) over the conversion of basic-state APE to eddy APE (C_A), plotted as a function of initial nondimensional wavenumber and dimensional wavelength (km) for simulation of moist cyclogenesis (Figure 5 from MM04).

6.   DRV as Precursor to Type A or Type C Cyclogenesis

Petterssen and Smebye (1971; hereafter PS71) surmised that there are at least two distinct mechanisms that would initiate and support the development of extratropical cyclones; they named these two mechanisms Type A and Type B cyclogenesis. In contrast to Type B cyclogenesis, which starts with a pre-existing upper trough with strong vorticity advection over area of warm advection below, the Type A cyclogenesis starts with a pre-existing surface cyclone (think frontal wave) without upper-level support, but eventually affects an upper cold trough as the surface low intensifies. Deveson et al. (2002) introduced a third mechanism (Type C) whereby both the upper and lower tropospheric level disturbances are pre-existing, but the upper tropospheric level plays a greater role in forcing the cyclogenesis. Out of the 16 cyclones Deveson et al. (2002) analyzed, three of them were determined to be Type C which formed at high latitudes and resembled the comma-cloud-type polar lows in their initial stages. The concept of DRV is not unlike the pre-existing surface cyclone in the early stage of Type A or Type C cyclogenesis.

17

7.   Definition of Bomb

Sanders and Gyakum (1980; hereafter SG80) gave credit to Tor Bergeron for characterizing a "rapidly deepening" extratropical low as one in which the central pressure at sea level falls at the rate of at least 1 hPa/hr for 24 hours. In that same vein, SG80 defined a "bomb" as an extratropical surface cyclone whose central pressure fall averages at least 1 hPa/hr for 24 hours. Since Tor Bergeron's characterization pertained to cyclones near the latitude of Bergen (60^oN), his "bomb" rate was adjusted geostrophically for cyclones at other latitudes by a factor of ($\sin \varphi$ / $\sin 60^o$). The resulting critical rate was termed "one Bergeron" as shown in equation 5.

$$1 \; Bergeron = 24 * (\sin \varphi \, / \sin 60^o) \; hPa \; pressure \; drop \; in \; 24 \; hours \qquad (5)$$

For example, a cyclone near 45^oN that dropped at least 20 hPa in 24 hours would be defined as a bomb, because at 45^oN latitude 1 Bergeron calculates to be 20 hPa. Similarly, a cyclone near 33^oN that dropped 15 hPa or more in 24 hours would be considered a bomb. In addition, SG80 found these bombs were predominantly maritime, cold-season events.

8.   DRV as Pathway to Explosive Cyclogenesis

Through systematic study of a large sample of cyclones in both North Pacific and North Atlantic basins, Gyakum et al. (1992) found that the subsequent intensification of a cyclone was proportional to the intensity of the pre-existing (surface) circulation. By examining 794 cyclones in the North Pacific basin, they found those cyclones which explosively deepened were preferentially characterized by at least 12 hours of antecedent development. Computations with model-based surface convergence further indicated that the response to the upper tropospheric forcing is conditioned by the antecedent lower tropospheric vorticity development. Gyakum et al. (1992) concluded that explosive development was typically characterized by a nonlinear interaction between upper and lower cyclonic disturbances, which might have formed synergistically (Type A mechanism), or independently (Type C mechanism). The notion of a DRV provides a mechanism via which antecedent lower tropospheric vorticity spin-up might occur. Therefore, it seems reasonable to hypothesize that DRVs can play an important role in at least some cases of explosive cyclogenesis, thereby describing a DRV pathway to explosive cyclogenesis.

C.   DRV CASE STUDIES

1.   Extreme Winter Storm Lothar (1999 Christmas)

Wernli et al. (2002; hereafter W02) addressed the importance of diabatic processes (release of latent heat of condensation) for rapid extratropical cyclone intensification. The prime example is the extreme winter storm "Lothar" (24–26 December 1999 over central Europe, see Figure 14) which demonstrated that cloud condensational processes can play a primary role in the formation of an antecedent positive low-level PV anomaly (reminiscent of a DRV) and that antecedent spin-up can lead to explosive intensification.
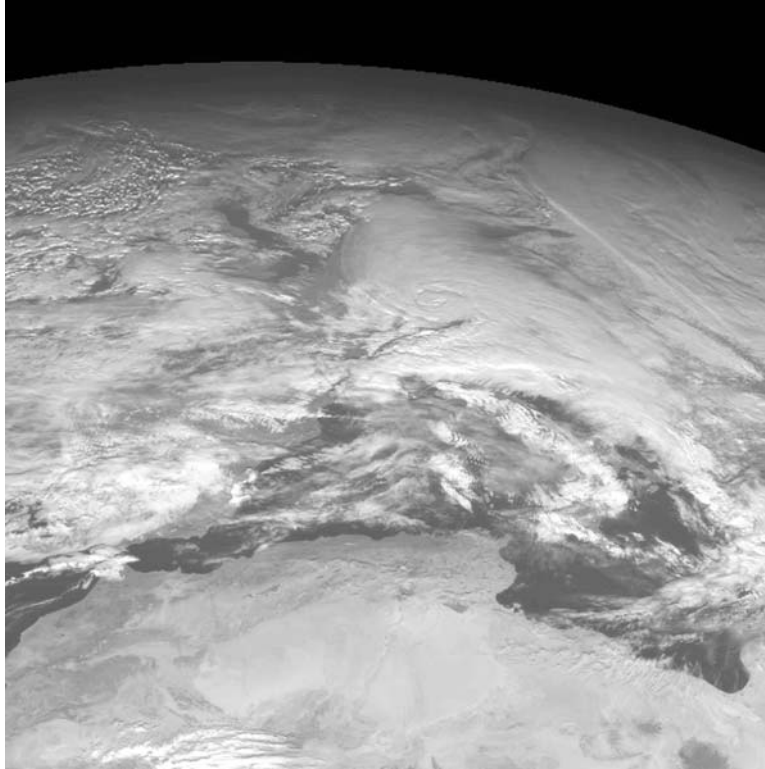
Figure 14. Satellite image of winter storm "Lothar" over Christmas of 1999 (From oiswww.eumetsat.org).

W02 found that neither the ECMWF (European Centre for Medium-Range Weather Forecasts) analysis, nor the HRM (high resolution model) mesoscale model ran in hindsight, was able to capture the full amplitude of Lothar's extreme pressure fall and surface wind speeds, as shown in Figure 15.
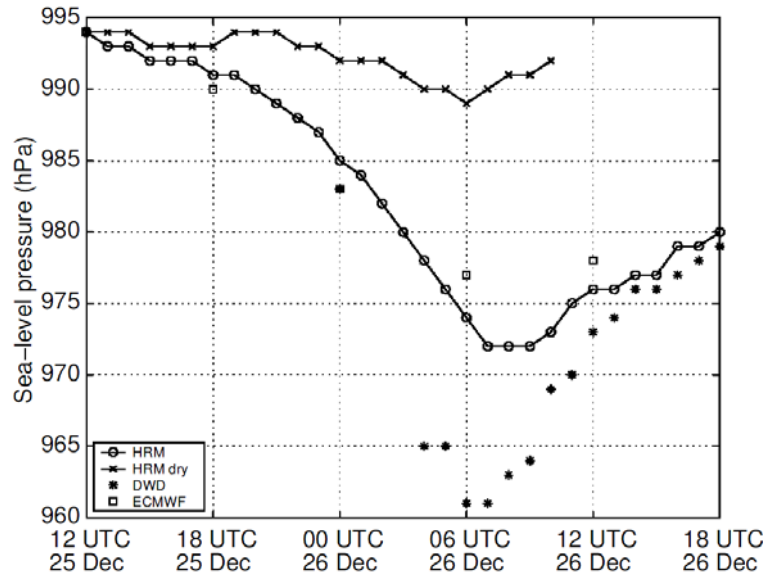
Figure 15.   Time evolution of the minimum sea-level pressure in the core of the cyclone Lothar, showing actual observations (German Weather Service DWD), ECMWF analyses, and HRM (high resolution model, moist and dry) mesoscale hindcast simulations (Figure 6 from W02).

From HRM, W02 created a three-dimensional (3D) rendition of the 2 PVU isosurface for the case of Lothar at six hour intervals from 18 UTC 25 December 1999 (end of DRV phase, beginning of explosive deepening), to 00 UTC 26 December 1999 (lowest pressure achieved—drop of 30 hPa in 12 hours), as shown in Figure 16. At 18 UTC 25 December 1999, the positive lower tropospheric PV anomaly (DRV) existed autonomously over the Atlantic ocean, roughly 1000 km west of Great Britain Aloft, there is no indication of an upper-level anomaly. At 00 UTC 26 December 1999, the DRV has moved just offshore of Great Britain, exhibiting vertical growth toward the midtroposphere. Between 18 UTC 25 December and 00 UTC 26 December 1999, the DRV has intensified enough to project its cyclonic circulation upward, resulting in a "kink" in the 2 PVU ceiling, forming a tropopause fold that began to push higher PV values down toward the DRV. By 06 UTC 26 December 1999, both the tropopause fold and DRV have extended further to form a "PV tower" (defined as a continuous column of cyclonic PV), coinciding with the time of maximum deepening. This is an example of Type A cyclogenesis (bottom-up intensification) as defined by PS71.

21
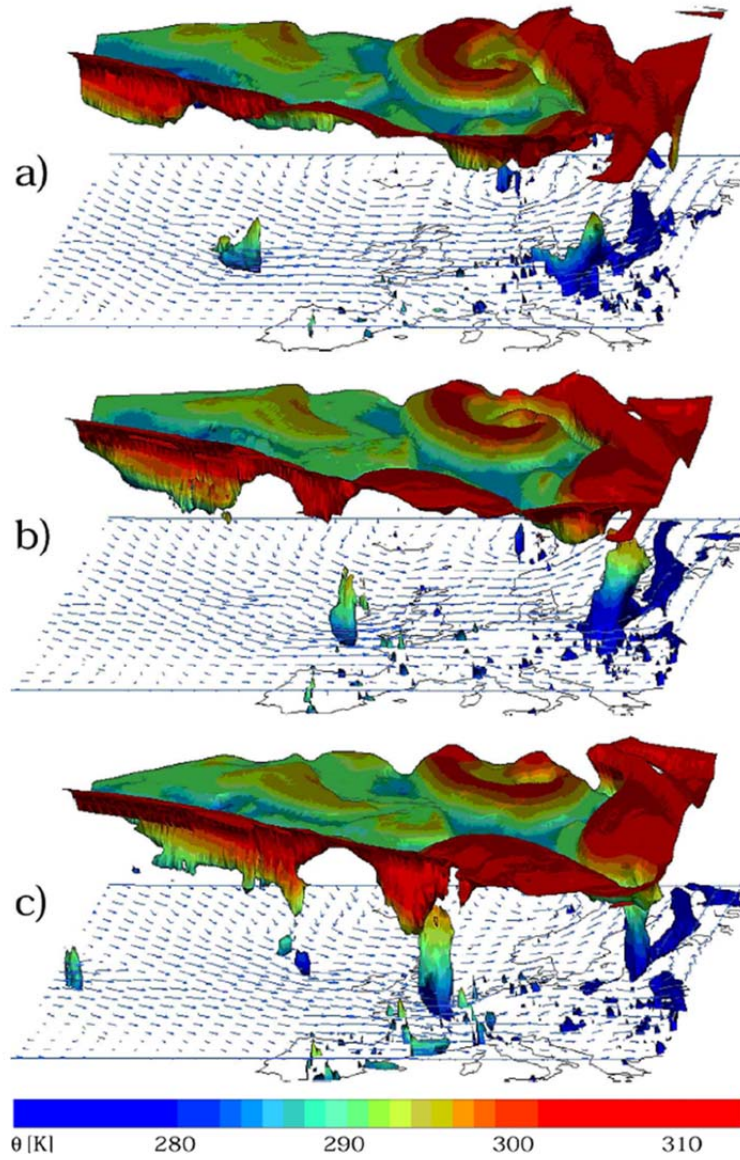
Figure 16.   The 2 PVU isosurface from the moist HRM simulation of Lothar at (a) 18 UTC 25 December (DRV stage), (b) 00 UTC 26 December and (c) 06 UTC 26 December (explosive deepened stage). The surfaces are colored with the potential temperature values. Also shown are the 850 hPa horizontal wind vectors (Figure 7 from W02).

To capture the disturbance structure during the DRV phase of extreme winter storm Lothar, W02 extracted longitude-pressure cross sections of the disturbance as shown in Figure 17. PV, potential temperature (PT) and meridional wind are shown in the left-panel; PV generation rate and vertical velocity are shown in the right-panel.

22

There is a distinct positive PV anomaly associated with this feature. To the east of this anomaly, there is strong flow from the south to the north. Additionally, there is a clear warm core structure evident in the TH field. In response to the warm moist advection to the east of the PV anomaly, there is rising motion (and latent heat release). Positive PV production is evident at the lower-troposphere (LT), with PV depletion at higher levels and on the western flank of the updraft region. Eastward propagation of the disturbance is implied due to the generation of positive PV to the east of the PV anomaly.
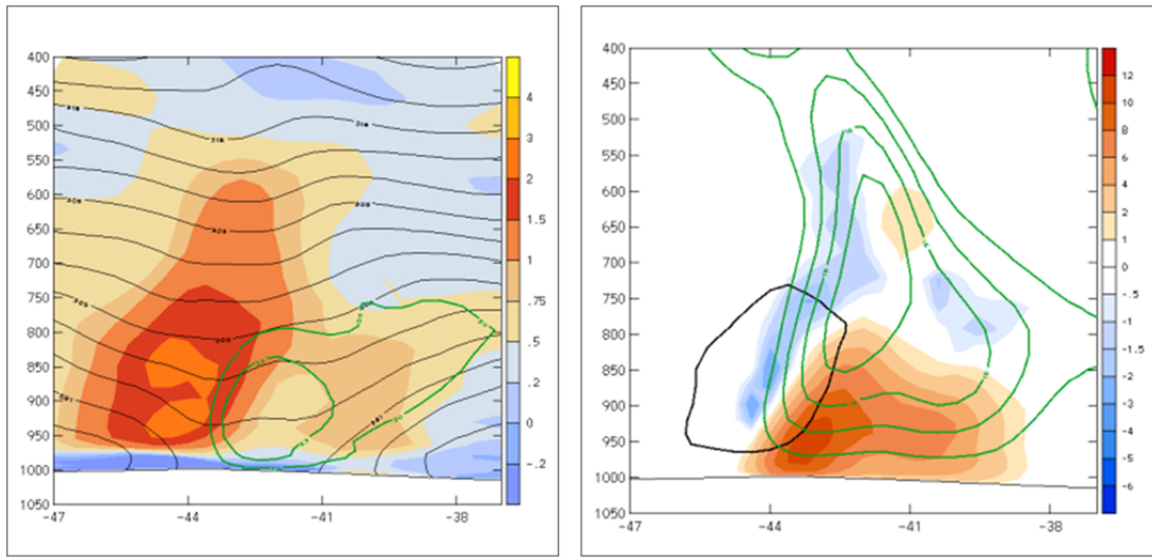
Figure 17.   Longitude-pressure cross sections at 00 UTC 25 December 1999 (from ECMWF analysis fields) for the DRV stage of the development near center of winter storm "Lothar." Left-panel: PV (shading; PVU), TH (black contours; 3K interval), and meridional wind or V (green contours; 20 and 23 m/s). Right-panel: diabatic PV generation rate or PVR (shading; PVU/hr), vertical velocity or W (green contours; ascending only; cm/s), and 1.5 PVU outline of DRV in black (Figure 13 from W02).

W02 attributed the explosive development of Lothar to the "bottom-up development" mechanism and diabatic tropopause-fold triggering, as shown in Figure 18. A mature DRV is able to project its cyclonic circulation upward to the tropopause, resulting in a wave perturbation along the tropopause. In this manner, high PV stratospheric air flows down steep isentropic surface upstream (west) of the DRV, and

low PV tropospheric air flows up the same isentropic surface downstream (east) of the DRV. This eventually leads to the formation of the PV tower, which is conducive to explosive cyclogenesis.
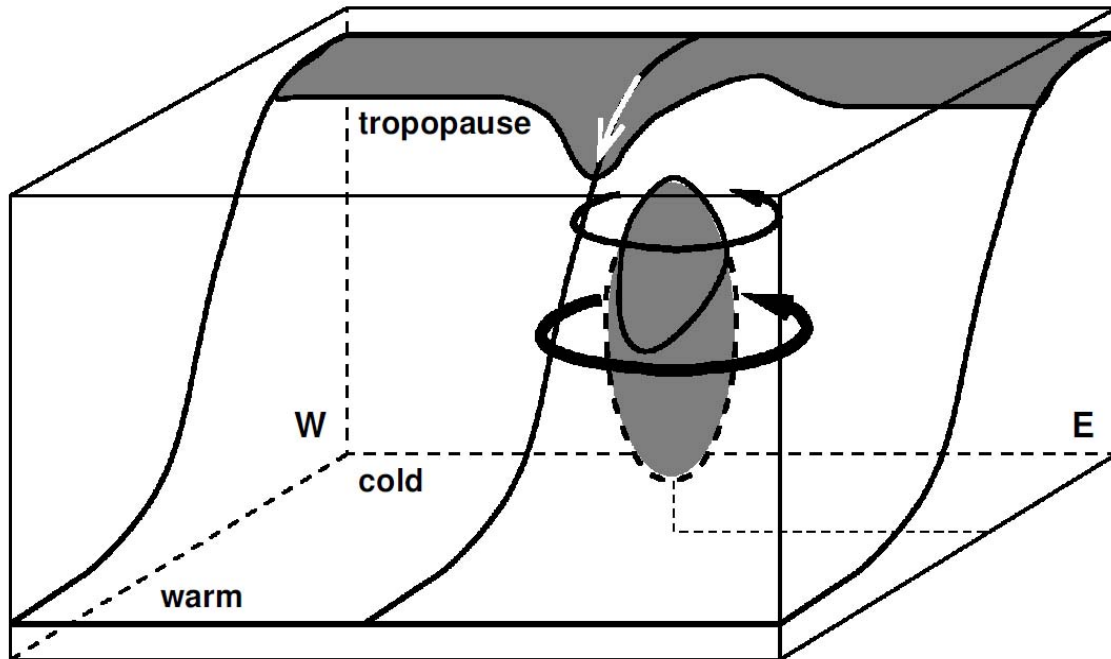
Figure 18.   Schematic illustration of the formation of PV anomalies near the tropopause level associated with the arrival of a positive PV anomaly below an intense upper tropospheric jet region. Grey shading indicates PV values larger than 2 PVU and denotes the diabatically produced PV anomaly in the lower and middle troposphere and the stratospheric part of a steeply sloping isentropic surface which intersects the low-level vortex. The circulation induced by the low-level vortex (shown by black arrows) leads to northward advection of tropospheric air to the east of the vortex, and to southward and downward advection (indicated by the white arrow) of stratospheric air on the western side (Figure 14 from W02).

W02 noted that three ingredients were present at the onset of the rapid intensification of Lothar: strong baroclinicity (implied by an intense upper tropospheric jet), proximity of DRV to the jet, and a relatively low tropopause, making high stratospheric PV air readily available.

2. 2005 East Coast Snowstorm

Another DRV case study was done on a pre-existing low-level (LL) vorticity spin-up (reminiscent of DRV) which interacted with a distinct, pre-existing upper tropospheric PV anomaly and explosively deepened (dropped 24 hPa in 24 hr from 18 UTC 24 February to 18 UTC 25 February 2005) over the northern Atlantic off the New England coast, as shown on Figure 19. Using PV inversion technique, model simulation and Lagrangian evolution perspectives, Moore, Montgomery and Davies (2008; hereafter MMD08) drew the connection between a precursor DRV, and the eventual February 2005 Snow Storm (hereafter East Coast Snow Storm), which deposited 4 to 12 inches of snow over northeastern United States 15 hours later.
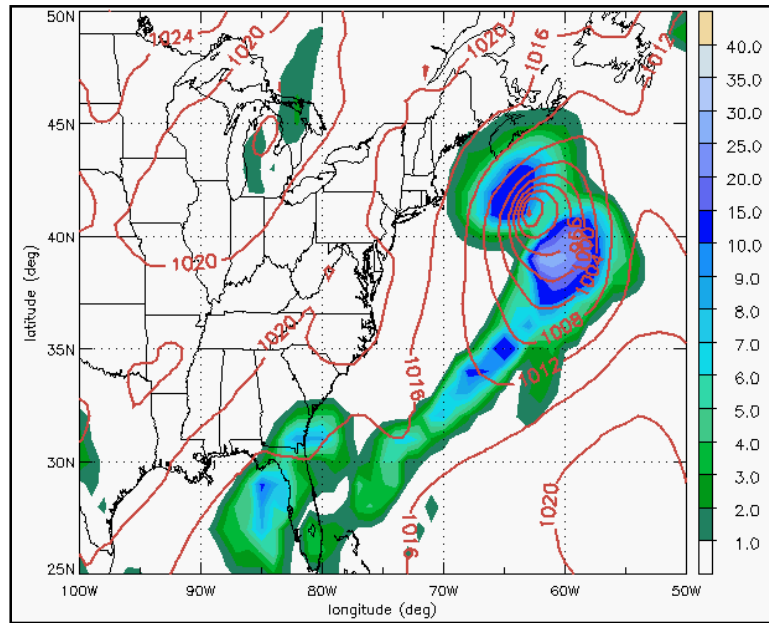
Figure 19. SLP (contours in 4 hPa intervals) and previous 6-h accumulated precipitation (shading; mm) from ECMWF analysis data at 18 UTC 25 February 2005, which was the time of maximum deepening for the East Coast Snowstorm (Figure 2f from MMD08).

MMD08 ran a full-physics MM5 simulation of the snow event (CNTRL), which yielded a reasonable approximation of the actual storm deepening (ECMWF analysis), as show in Figure 20. MMD08 then simulated the storm without latent heat release (NL; marked with diamonds), resulting in a weaker storm in comparison with CNTRL.

MMD08 simulated the storm again by removing surface fluxes (NF; marked with triangles), which resulted in an even weaker storm in comparison with CNTRL. Lastly MMD08 simulated the storm (DRY) with neither latent heat release nor surface flux, and the resultant storm was 24 hPa weaker than CNTRL. This series of MM5 simulation demonstrated the importance of diabatic effects (antecedent DRV stage) to the East Coast Snowstorm.
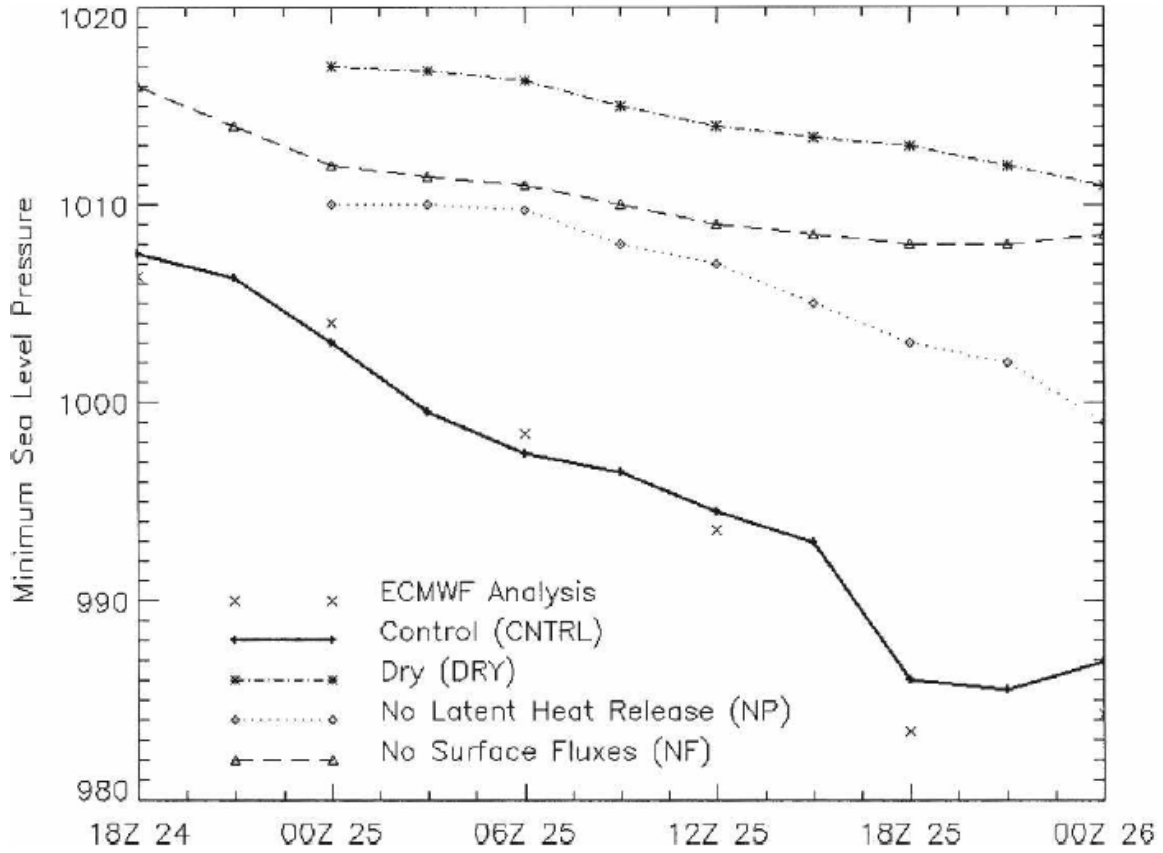
Figure 20.   MSLP evolution for ECMWF analysis data (no line; crisscrosses only) and MM5 simulations: CNTRL (solid; pluses), Dry (dotted-dashed; asterisks), NF (no surface fluxes, dashed; triangles), and NL (no latent heat release, dotted; diamonds) (Figure 10 from MMD08).

As discussed previously in MM04, the conversion ratio of G_E/C_A gave insight into the dynamics of moist baroclinic instability, specifically allowing for a separation between long waves and DRVs. The larger the G_E/C_A ratio, the more dominant a role moist processes play. Recall that on the RHS of the eddy APE equation, G_E is the

26

generation of eddy APE by diabatic processes, and C_A represents the conversion of basic state (zonal) APE to eddy APE. For the East Coast Snowstorm, MMD08 plotted the conversion ratio for two volumes, as shown in Figure 21. The dashed line (bottom curve) represents the volume encompassing both the upper tropospheric short wave trough and the lower tropospheric cyclone, and the G_E/C_A ratio was approximately one. The solid line (top curve) represents the volume encompassing only the low level cyclone (DRV), and the G_E/C_A ratio surged between 12 UTC 24 February and 00 UTC 25 February, 2005, indicating the dominant role moisture played in maintaining the DRV stage of cyclogenesis.
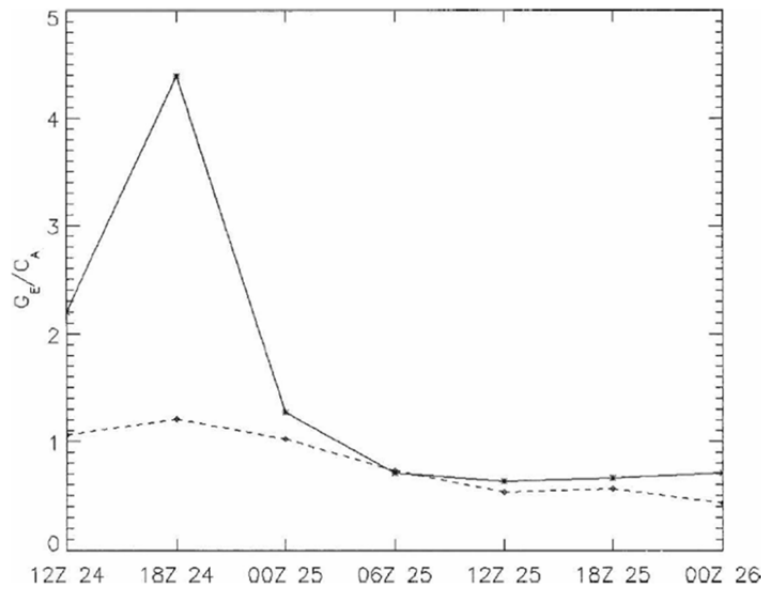
Figure 21. The ratio of the diabatic generation to the baroclinic generation of eddy APE for the volume encompassing both the lower tropospheric cyclone and upper tropospheric short-wave trough (dashed; bottom curve), versus that of the volume centered on the lower tropospheric cyclone only (solid; top curve) (Figure 8 from MMD08).

The notion of two-stage storm evolution is further demonstrated by the 24-hr backward trajectory analyses, first during the DRV phase at 00 UTC 25 February 2005, as shown in left-panel of Figure 22, next during the mature storm phase at 18 UTC 25 February 2005 (maximum deepening), as shown in right-panel of Figure 22. The first set of backward trajectories in left-panel Figure 22 (initialized at 00 UTC 25 February 2005 and composed of air parcels with PV value greater than 1.5 PVU within the 3D box

27

[35–40ºN, 70–75ºW and 900–600 hPa]) shows that during the DRV phase, the air parcels primarily originated from warm/moist regions at low levels (below 950 hPa). As these air parcels approached the DRV center they experienced isentropic lifting (rise toward 850 hPa) with accompanied latent heat release and PV generation. The second set of backward trajectories in right-panel of Figure 22 (initialized at 18 UTC 25 February 2005 and composed of air parcels with PV value greater than 1.5 PVU within the 3D box [39–42ºN, 63–66ºW and 900–600 hPa]) shows that during the mature storm phase, air parcels not only originated from the lower pressure levels, but also came from higher pressure levels (300–400 hPa) northwest of the DRV. The latter air stream represents the dry intrusion, a common feature of extratropical cyclones (but not DRVs). This is indicative of the interaction of the incipient DRV with an upper-level PV anomaly
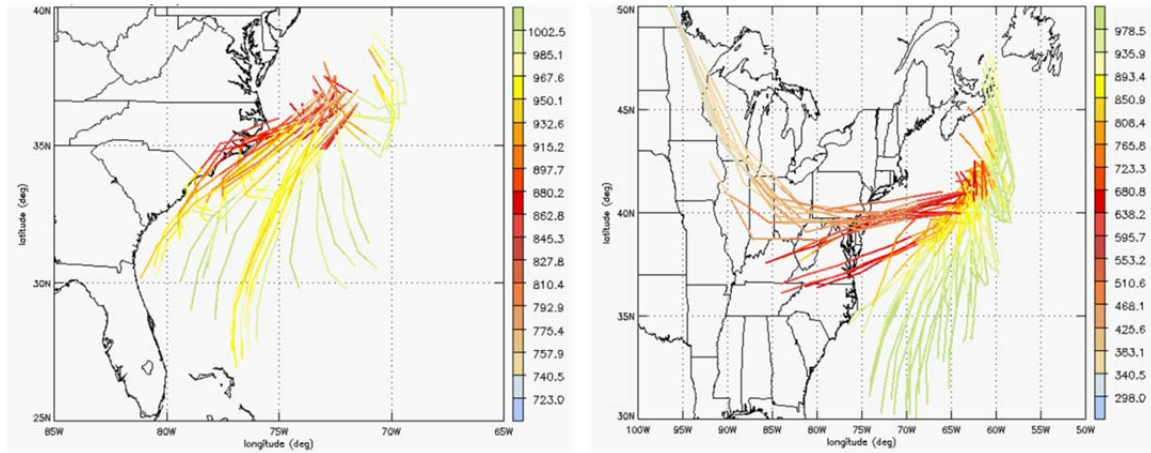
Figure 22.   Left-panel: 24-hr backward trajectory analysis using ECMWF analysis data initialized at 00 UTC 25 February 2005 and composed of air parcels with PV value greater than 1.5 PVU within the 3D box (35–40ºN, 70–75ºW and 900–600 hPa). Right-panel: 24-hr backward trajectory analysis using ECMWF analysis data initialized at 18 UTC 25 February 2005 and composed of air parcels with PV value greater than 1.5 PVU within the 3D box (39–42ºN, 63–66ºW and 900–600 hPa) (Figure 9 from MMD08).

Qualitatively similar to W02, MMD08 also extracted longitude-pressure cross sections of DRV in Figure 23, showing first the PV, TH and meridional winds in left-panel and then the PV generation rate and vertical velocity in right-panel. Left panel of Figure 23 shows a positive lower tropospheric PV anomaly (warm shading) marking the DRV, sagging TH lines exhibiting the warm-core nature of the DRV (due to diabatic

28

heating and WAA), and the LLJ (white contours; positive meridional winds only) east of the DRV. Right panel of Figure 23 illustrates the isentropic lifting associated with the warm moist advection and the characteristic PV generation pattern (positive PV tendency below and negative PV tendency above the level of maximum heating).
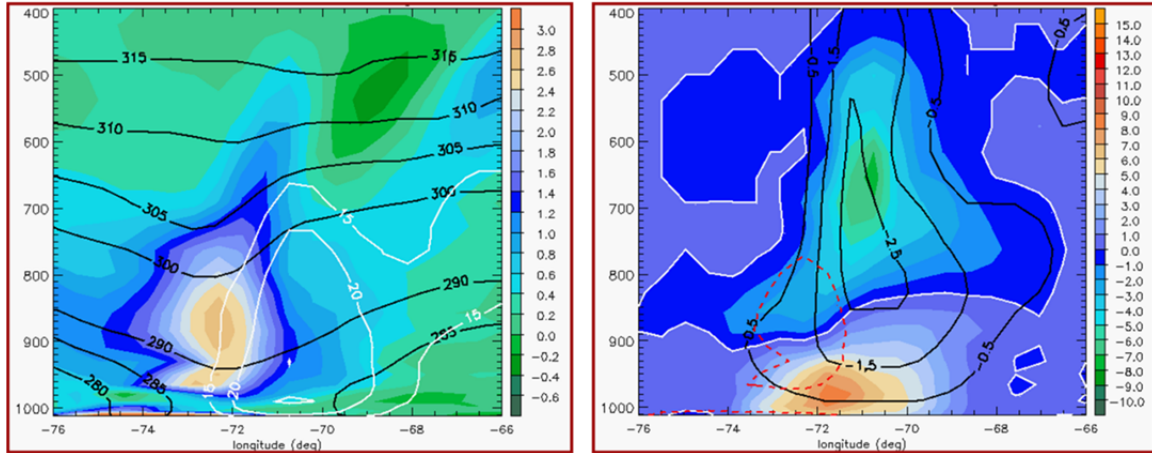
Figure 23.   Longitude-pressure cross section along 37°N from ECMWF analysis data through the surface cyclone at 00 UTC 25 February 2005 (near end of DRV stage). Left-panel: PV (shading; PVU), potential temperature or TH (black contours; K), and the 15, 20 and 25 m/s meridional wind isotachs (white contours). Right-panel: PV generating rate or PVR (shading; PVU/hr), 0 PVU/hr isoline (solid white), vertical velocity or w (black contours; hPa/s), and the 1.5 PVU isoline (red dashed contour) (Figure 7 from MMD08).

Telling a parallel yet distinct story as the 3D 2 PVU isosurface figures from Wernli et al. (2002), MMD08 generated a series of vertical cross sections in order to elucidate the two-stage development of East Coast Snowstorm, as shown in Figure 24. The orientation of the slices was chosen in such a way to capture both the DRV and the upper tropospheric trough from 18 UTC 24 February to 18 UTC 25 February, 2005, at six hour intervals. Note that at 18 UTC 24 February 2005 (Figure 24[a]) both the DRV and the upper tropospheric trough were pre-existing, approximately 1500 km apart. Over the next twelve hours there was visible vertical growth for the DRV and upper tropospheric trough, upward and downward respectively (Figure 24[b] and [c]). At 12 UTC 25 February 2005 (Figure 24[d]) there seems to be interaction (phase-locking) between the upper tropospheric trough and the DRV. By 18 UTC 25 February 2005 (Figure 24[e]) the PV tower forms as the explosive cyclogenesis is complete. The diagnosed PV

29

evolution is consistent with the energetics calculations. In addition, the case in question appears to be a representative example of Type C cyclogenesis (interaction of pre-existing upper and lower disturbances) as defined by Deveson (2011).
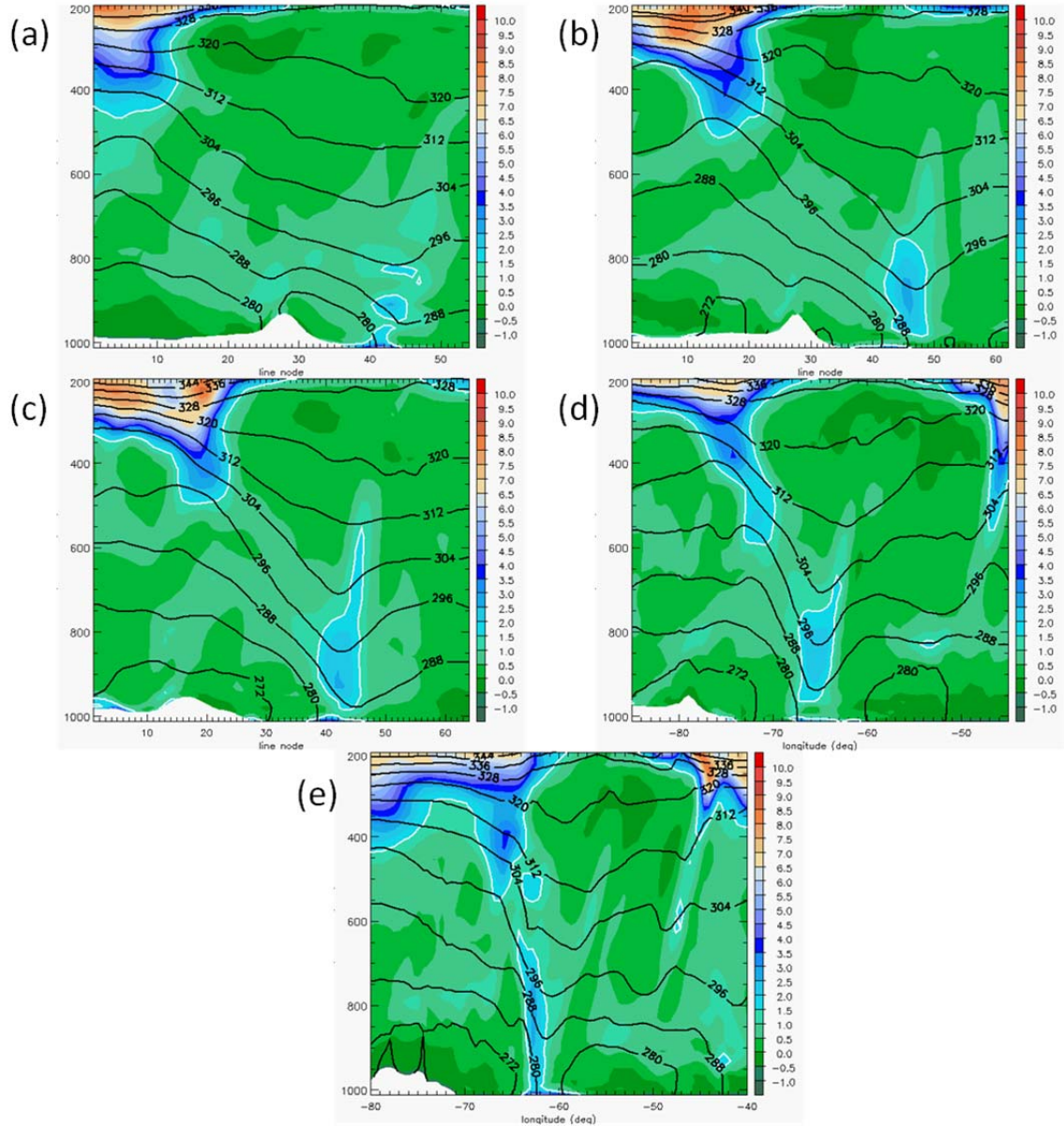
Figure 24.   Vertical cross-section analysis of PV (shading; PVU; white contour is 1.5 PVU isoline) and TH (black contours; K) from ECMWF analysis data at (a) 18 UTC 24 February, (B) 00 UTC 25 February, (c) 06 UTC 25 February, (d) 12 UTC 25 February, and (e) 18 UTC 25 February 2005. The cross sections go through both the DRV and the upper tropospheric trough (Figure 6 from MMD08).

3. 2005 North Atlantic Cyclone

Boettcher and Wernli (2011; hereafter BW11) presented the lifecycle of a December 2005 North Atlantic winter storm (hereafter N ATL Cyclone). They propose this case is another representative example of a storm evolution characterized by a predecessor DRV phase, followed by the interaction of distinct upper and lower tropospheric anomalies (Type C cyclogenesis). In their study, they diagnosed four distinct phases: DRV generation, DRV propagation, intensification and decay, as shown in Figure 25.
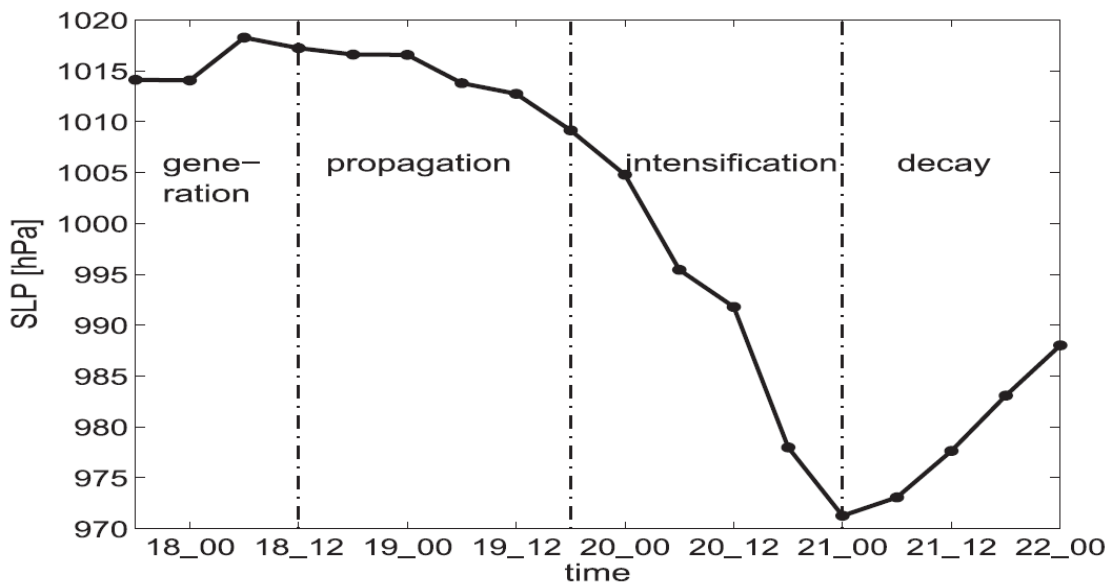
Figure 25. Minimum SLP (hPa) time development of the N ATL winter storm 17–22 December 2005 showing four development phases (Figure 1 from BW11).

The first phase was the generation of the DRV. It emerged as a remnant of a Mesoscale Convective Vortex (MCV) in the Gulf of Mexico, which was formerly supported by an upper tropospheric trough. The second phase involved the propagation of the DRV, where the upper tropospheric support waned with the flattening dynamic tropopause (DT) and distancing of a straight upper tropospheric jet. Lack of upper tropospheric support equates to no quasi-geostrophic lifting and, in this case, resulted in reduced vertical velocities and condensation when compared to the MCV. This led to less change in static stability, as well as less PV generation at the lower- and mid-levels

during the propagation phase. The culmination of factors like the absence of well-defined upper tropospheric features, the relatively fast propagation speed of the positive lower tropospheric PV anomaly (13 m/s, twice that of ambient wind speed), the proximity of the existing baroclinic zone, the abundant moisture supply and observed precipitation, indicate that during the first 30 hours this system was, in fact, a DRV.

During the propagation phase, the DRV can be considered as a shallow, diabatically driven lower tropospheric cyclonic system. A vertical cross section of the propagating DRV was captured in Figure 26. As seen in previous case studies, the lower tropospheric PV anomaly (warm shading) is the telltale to a DRV (bimodal in this case, indicating leap frog propagation), while the positive meridional winds in green contours (going into page) depicts cyclonic circulation and WAA, and positive diabatic heating in black dashed contours underlining the importance of moisture in DRV energetics.
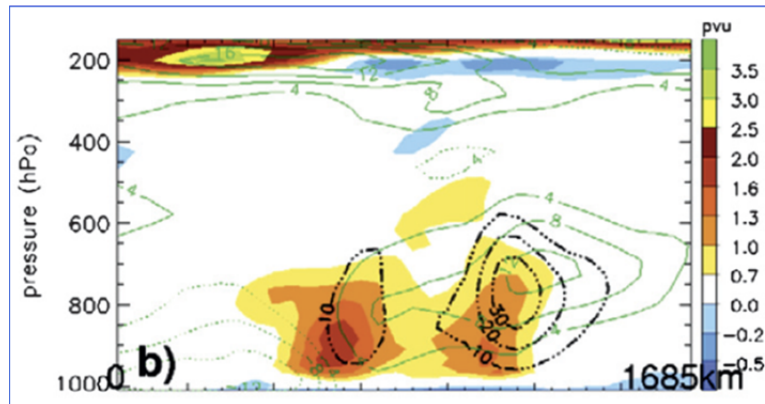
Figure 26. Vertical cross section through N ATL 2005 winter storm at 00 UTC 19 December 2005 (DRV propagation phase) showing PV in shading (PVU), meridional wind in green contours (interval 4 m/s), and latent heating in black dashed contours (interval 10 K/6 hr) (From BW11).

In the third phase, the disturbance underwent a transformation to an extratropical cyclone (with a horizontal extent of greater than or equal to 1,500 km). The disturbance began to exhibit typical frontal features and interact with an approaching upper-tropospheric wave. Twelve hours into the intensification phase, the DRV low is now on the upward vertical motion (UVM) side of entrance region of jet, which furthers explosive deepening, as shown in Figure 27. At 00 UTC 21 December 2005, a minimum

32

sea level pressure (971 hPa) is reached and the cyclone has formed a well-defined PV tower corresponding to a vertical column of air with high PV values (>1.3 PVU) throughout the troposphere. The high values of lower tropospheric PV in the mature cyclone resulted from the moist diabatic processes, whereas in the upper part of the PV tower, the high PV values trace back to the stratospheric air descending to the mid-troposphere (~500hPa).
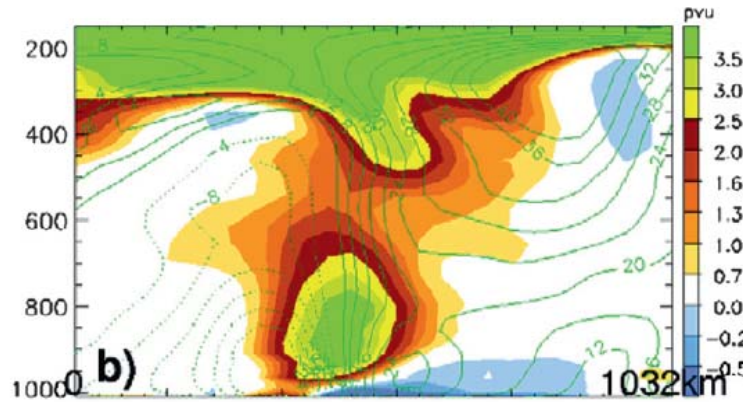
Figure 27.   Vertical cross section through N ATL 2005 winter storm at 00 UTC 21 December 2005 (maximum deepening) showing PV (colors, PVU) and meridional wind (green contours, interval 4 m/s) (From BW11).

BW11 acknowledged that for this storm, the MCV was the precursor to the DRV, but this pathway is not exclusive. Other mechanisms for DRV formation are possible, but they all share the proximity to intense baroclinic zone and moisture supply. The DRV genesis stories are similar: they all begin with a low level PV anomaly, superposed on a baroclinic zone. The circulation induced by the anomaly results in strong WAA downstream, leading to moist-diabatic processes, and subsequent low-level PV generation.

4.   The "Perfect Storms"

Cordeira and Bosart (2011; hereafter CB11) noted there were two intense extratropical cyclones (EC1 and EC2) contemporary to the well-known Perfect Storm of 1991. In particular, EC1 developed in two distinct phases, outlining the so-called DRV pathway to explosive cyclogenesis. Specifically, CB11 noted that there were three

33

ingredients that came together to fuel the Perfect Storm, as illustrated in Figure 28. The first ingredient is the warm air coming from one direction due to a low-pressure system, represented by the symbol "1" (DRV phase of EC1). The second ingredient is the flow of cool and dry air from another direction, generated by a high-pressure system, marked by the symbol "H." The third ingredient is the tropical moisture provide by Hurricane Grace, marked by the symbol "G."
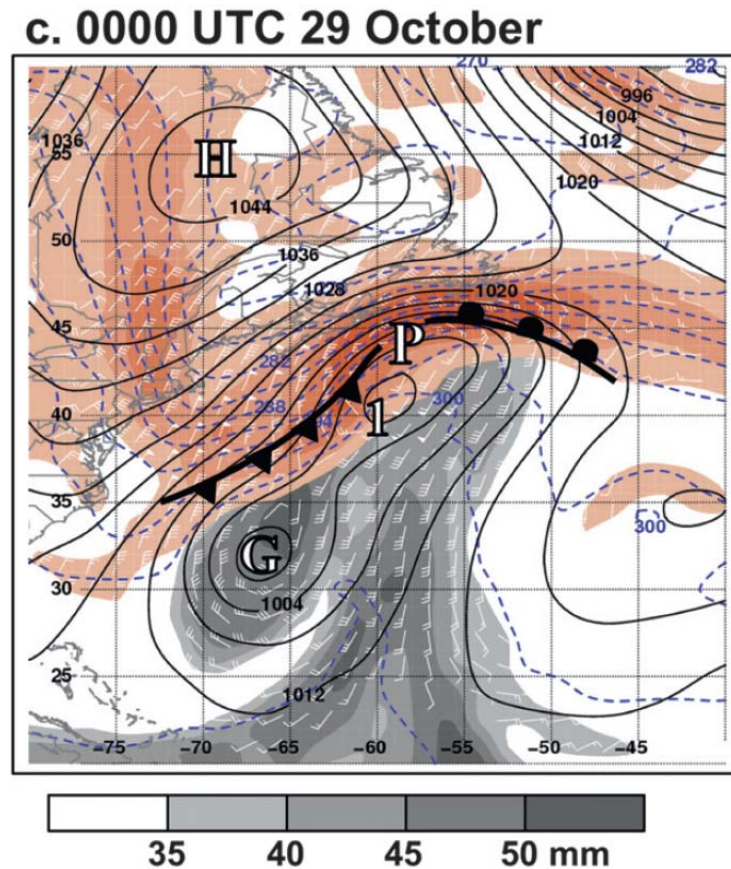
Figure 28.   "P" represents the Perfect Storm; "H" represents the anticyclone that provided dry cool air to "P"; "G" represent Hurricane Grace that provided moisture to "P"; "1" is the DRV phase of EC1 that provided warm air to "P." The 850-hPa TH (dashed blue contours every 3 dam), TH gradient (shaded red; K/100km), wind (half barb = 2.5 m/s; full barb = 5.0 m/s; pennant = 25.0 m/s; plotted for magnitudes > 5 m/s only), SLP (solid black contours every 4 hPa), and precipitable water (shaded gray; mm) on 00 UTC 29 October 1991 (From CB11).

CB11 determined that phase 1 of EC1 is indeed a DRV by plotting the relevant energy conversion terms (diabatic [G_E] and baroclinic [C_A]), as shown on Figure 29. The G_E curve is highlight with solid green line, while the C_A curve is highlight by dashed brown line. Note that during almost the entire phase 1 of EC1, the green (G_E) curve sits on top of the brown (C_A) curve, which indicates diabatic conversion played a dominant role energetically during phase 1. This is consistent with energetics of previously reported DRVs.
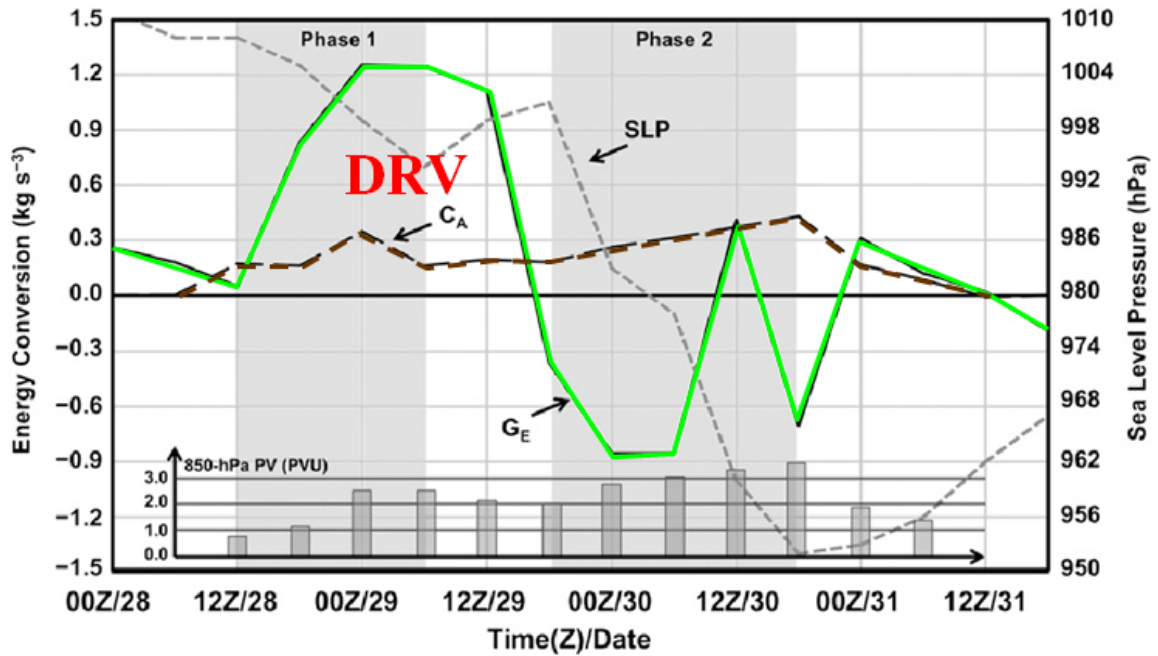
Figure 29.   Two phase development of EC1; depicting phase 1 as DRV. Lagrangian time series of the MSLP (hPa; short-dashed contour), baroclinic conversion of basic-state APE to eddy APE (C_A; kg/s^3; long-dashed contour), diabatic generation of eddy APE (G_E; kg/s^3; solid contour), and the 850-hPa maximum PV (PVU; inset bar chart) computed for a ~500km X ~500 km box centered on EC1 (From CB11).

35

D.   MOTIVATION FOR FURTHER UNDERSTANDING OF DRVS

Previous studies have linked DRV type of growth mechanism to explosive cyclones (Gyakum et al. 1992; W02; MMD08; BW11; CB11), mesoscale convective vortices (MCVs) in baroclinic environments (RJ90; Davis and Weisman 1994; Jiang and Raymond 1995; Conzemius et al. 2007; Conzemius and Montgomery 2010), squall lines (PT95), and polar lows (Montgomery and Farrell 1992; Fantini and Buzzi 1993; Mak 1994), as depicted in Figure 30.
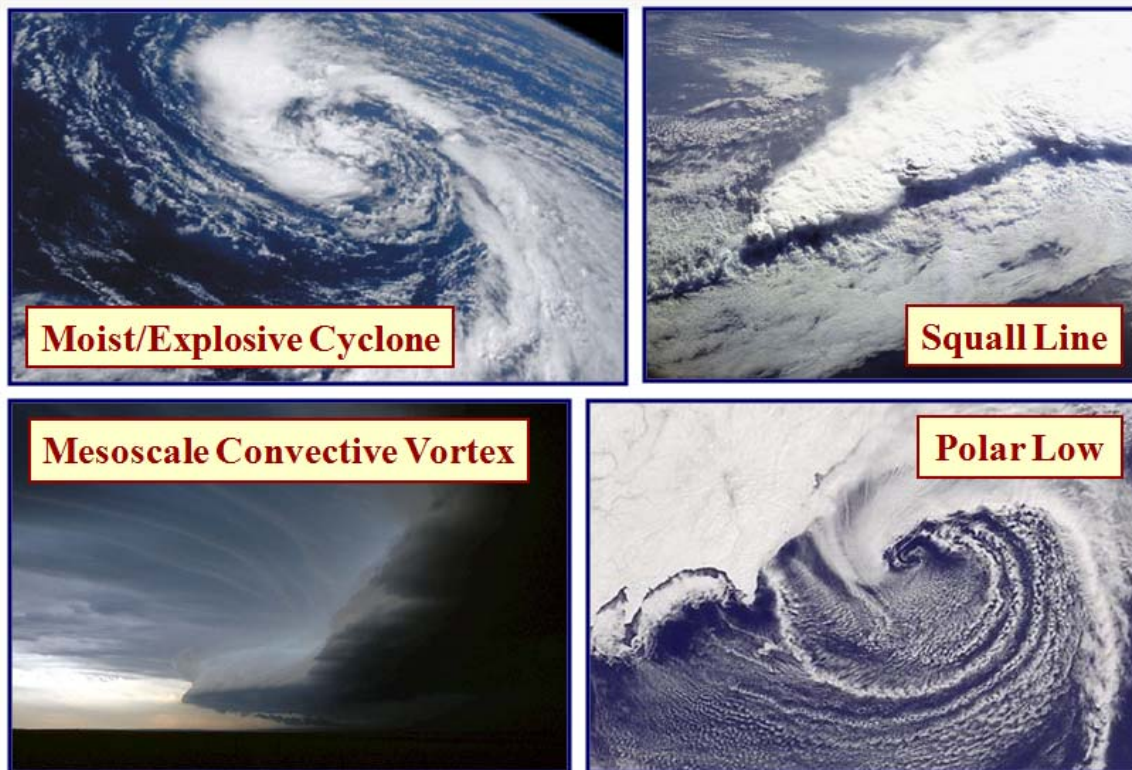
Figure 30.   High impact weather with precursor/pathway linked to DRVs (image courtesy of Richard Moore)

Recent work has emphasized the fact that DRVs are, in general, not well represented in today's numerical forecast systems (Wernli and Kenzelmann 2006; BW11). As such, there is an urgent need for better understanding of DRV dynamics and their inherent predictability. Numerical weather prediction (NWP) models often struggle to properly predict high impact events, such as the "Surprise" snowstorm of January 2000, which dropped record snow over North Carolina, or the aforementioned

devastating winter storm "Lothar," where the operational forecast model failed to capture its explosive nature. While there are many possible sources of forecast error, ranging from insufficient and/or erroneous initial condition, to deficiencies in the representation of the physical processes in the models themselves, a common denominator of many forecast "busts" is the primacy of diabatic processes in these high-impact weather events.

As outlined above, the DRV growth mechanism and characteristics have been explored in a number of idealized settings, as well in a very limited number of case studies. However, there remains a need to further explore the dynamics and predictability of "real-world" DRVs.

E. THESIS ORGANIZATION

The remainder of this thesis is outlined as follows. Data and methodology are described in Chapter II. The DRV climatology is surveyed in Chapter III. Results from the DRV composite analysis are highlighted in Chapter IV. Chapter V focuses on DRVs which explosively deepened. Chapter VI contains the discussion and conclusion.

THIS PAGE INTENTIONALLY LEFT BLANK

II.   DATA AND METHODOLOGY

A.   DATA

1.   Primary Data

The primary source of meteorological data for this thesis is the ERA-interim dataset, specifically from January 2001 through December 2010 (total 120 months). ERA-interim is an "interim" reanalysis of the European Center for Medium-Range Weather Forecasts (ECMWF) data, available from 1989 to the present, in preparation for the next-generation extended reanalysis. These data are interpolated onto a Gaussian grid with a nominal resolution of one degree in the horizontal (361 longitude degrees by 181 latitude degrees), 60 levels in the vertical, and are available in six-hourly time steps. All data files utilize the Network Common Data Form (NetCDF) format.

a.   Primary Files

As downloaded from the ERA-interim source, the primary data files (P-files) contain the variables in Table 1, for each time step (a time step could be 12 UTC 19 December 2005, for example).

Q	Specific Humidity
LWC	Liquid Water Content
IWC	Ice Water Content
T	Temperature
U	Zonal Wind Speed
V	Meridional Wind Speed
OMEGA	Pressure Tendency
PS	Pressure
SLP	Sea Level Pressure

Table 1.   Type of variables available within each P-file (primary file).

b.   *Secondary Files*

The built-in UNIX command (p2s) is able to take primary atmospheric parameters (say U and V for example) from P-files, and convert them to secondary parameters (like VEL) in S-files (secondary files), with the same horizontal and vertical resolution (361 X 181 X 60), in six-hourly time steps.   Table 2 shows the variables generated for this thesis within each S-file:

CH	Diabatic Heating
VORT	Vorticity
W	Vertical Velocity
VEL	Velocity
PV	Potential Vorticity
PVR	Potential Vorticity Generation Rate
RH	Relative Humidity
TH	Potential Temperature
THE	Equivalent Potential Temperature

Table 2.   Type of variables generated within each S-file (secondary file).

Using a different built-in UNIX command (nput2p), another type of secondary files called levels files (L-files) were created containing all the same variables as S-files (except CH) at set pressure levels of 1000, 925, 850, 700, 500 and 250 hPa. L-files have the same horizontal resolution as the P and S files (361 X 181), but only six levels (1000, 925, 850, 700, 500 and 250 hPa) in the vertical.

A third type of UNIX command (nput2pv) generated a different type of secondary files called T-files, which contain TH (potential temperature) on the 2.0 PVU PV isosurface. These T-files have the same horizontal resolution as the P and S files (361 X 181), but since they have only one vertical level, they are in essence two-dimensional files.

A fourth type of UNIX command (nput2th) also generated T-files, but this type of secondary files contains the PV values on TH levels of 310, 320, 330, 340 and 350 K. These T-files have the same horizontal resolution as the P and S files (361 X 181), but only five levels (310, 320, 330, 340 and 350 K) in the vertical.

2.   Secondary Data

To create the monthly climatological data, each atmospheric parameter (take TH for example) at every grid point (within the 3D cube of 361 X 181 X 60) is averaged over all days (28 days in February, for example) and hours (00, 06, 12 and 18 UTC) from the same month (February), through all ten years (February 2001, February 2002, February 2003, and so forth through February 2010). The computation process yielded 12 monthly climatology files (January, February, March and so forth through December) for the P-files, and another 12 monthly climatology files separately for the S-files, L-files, and T-files (TH on the 2.0 PVU PV isosurface). The monthly climatological data provided a reference point (background value) for each atmospheric variable at each grid point. Take potential temperature again for example. If the 850 hPa TH at 40N/141E was known to be 300K on 12Z of 22 February 2002, it is then possible to reference the monthly climatological file for February and obtain the monthly average TH at the same grid point (40N/141E) to be 276K. The difference of the two TH is +24K, which represents a positive TH anomaly when compared to the monthly mean.

B. DRV IDENTIFICATION METHOD

All work herein is based on the 10-year DRV climatology compiled by Boettcher and Wernli (2012; hereafter BW12). They designed an objective, automated algorithm to identify Northern Hemisphere DRVs, applying to 10 years of ECMWF analysis data during the years 2001–2010. In order to prevent the identification of non-DRVs, each storm must meet the following five criteria to qualify for inclusion:

1. SLP Minimum and Lower Tropospheric PV Maximum

The DRV identification algorithm looked for two co-existing criteria as the initial criteria for tracking a disturbance. One criterion is a local SLP minimum, which must be enclosed by a closed SLP contour of at least 0.5 hPa larger than the SLP minimum. The other criterion is high values of 850 hPa PV which, when averaged over the SLP minimum location plus its eight neighboring grid points (think 3 X 3 matrix), must be greater than 0.8 PVU. These two criteria must both be met for a minimum of 24 consecutive hours, in order to trigger identification as a potential DRV. To visualize these two criteria at work, reference Figure 31 and Figure 32 for evolution of the ATL DRV#56 from 00 to 06 UTC of 19 December 2005 (same DRV/storm investigated by BW11).
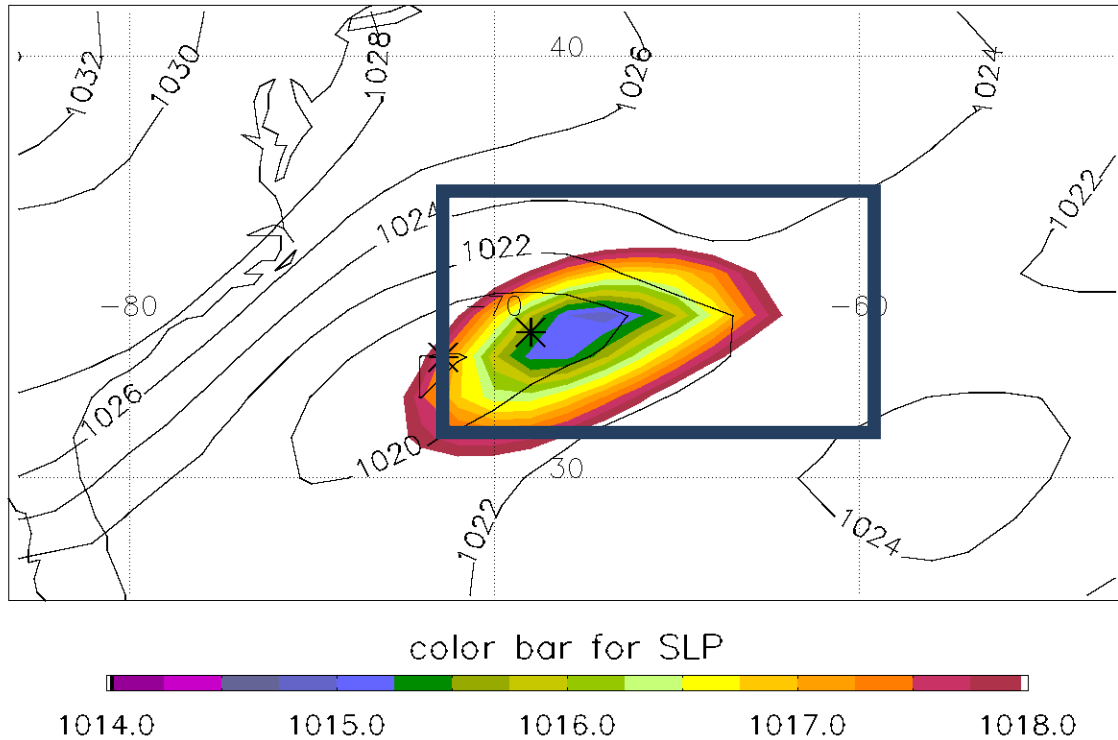
Figure 31. SLP minimum (2 hPa interval) at 00 UTC 19 December 2005 (black lines) and 06 UTC 19 December 2005 (shading; only 1014 to 1018 hPa shown), superposed by the DRV locations, left asterisk marking 00 UTC 19 December 2005, and right asterisk marking 06 UTC 19 December 2005, as determined by BW12 algorithm. Note that another SLP minimum was successfully found (which enables further tracking) within a box which extends 12° eastward, 2° southward, and 4° northward from the former DRV position at 00 UTC 19 December 2005.

The 0.8 PVU threshold was determined empirically and was found to work well for identifying the early stage of a DRV when the diabatically produced PV might not be very strong (BW12). The BW12 algorithm then continues only if, at the next time step (six hours later), another SLP minimum possessing threshold value of 850-hPa PV can be found within a box (blue box inside Figure 31 and Figure 32) which extends 12° eastward, 2° southward, and 4° northward from the current position at 00 UTC 19 December 2005 (left asterisk). If multiple DRV candidates qualify, the one with the highest PV value is selected. To exclude ECs and TCs, which would also meet the criteria thus far, the next three criteria must also be met (for at least three consecutive time steps or 12 hours).
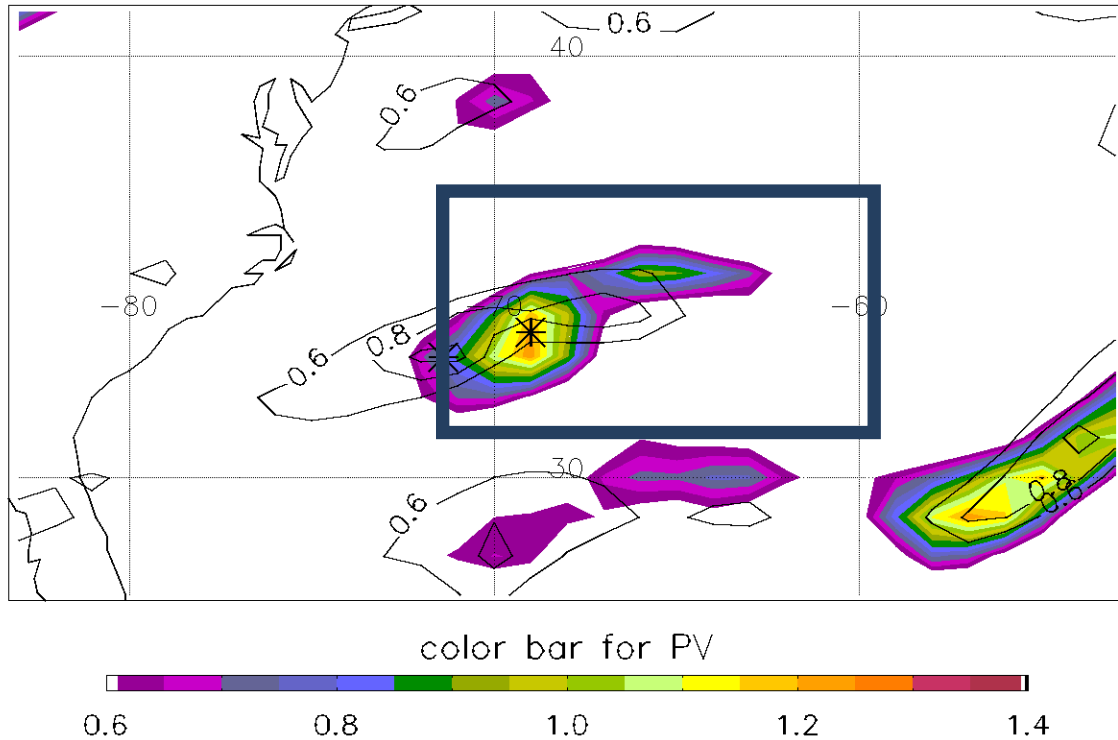
Figure 32. 850 hPa PV maximum (0.2 PVU interval) at 00 UTC 19 December 2005 (black lines) and 06 UTC 19 December 2005 (shading), superposed by the DRV locations, left asterisk marking 00 UTC 19 December 2005, and right asterisk marking 06 UTC 19 December 2005, as determined by BW12 algorithm. Note that within the blue box (which extends 12° eastward, 2° southward, and 4° northward from DRV position at 00 UTC 19 December 2005), the stronger PV maximum (the one on the left) was used to mark the future location of the DRV at 06 UTC 19 December 2005 (coinciding with right asterisk).

2.   Intense Low-Level Baroclinicity

The third criterion stipulates that the potential temperature (TH) difference at 950 hPa in a region downstream (reference green box in Figure 33) of the cyclone center must exceed 5K. Figure 33 displays the TH (shading; K) from 12 UTC 19 December 2005, as well as the 850 hPa PV outline from former position at 06 UTC 19 December 2005 (white contour) and current position at 12 UTC 19 December 2005 (black contour), and the green box down range which moves with the cyclone (position of green box

44

determined empirically). The TH difference that must meet the 5 K criteria is defined as the difference of the 10th and the 90th percentile of the TH values found within the green box.

color bar for TH
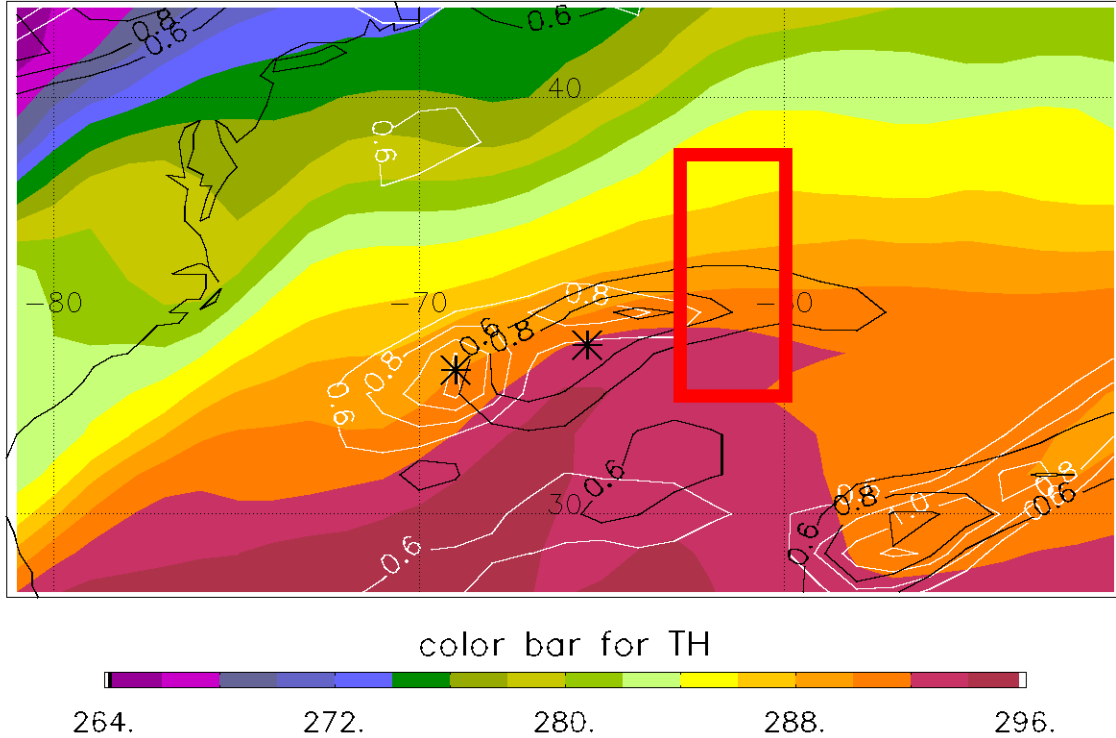
Figure 33. 950 hPa TH (potential temperature; 2K shading interval) at 12 UTC 19 December 2005, superposed by 850 hPa PV maximum (0.2 PVU interval) from former DRV position (left asterisk) at 06 UTC 19 December 2005 (white lines) and current DRV position (right asterisk) at 12 UTC 19 December 2005 (black lines). Note that within the red box (determined empirically; moving with the cyclone), the baroclinicity is determined by the difference of the 10th and the 90th percentile of the 950 hPa TH, and the baroclinicity must meet or exceed the 5K threshold.

3. Fast Propagation

To exclude TCs that often times stagnate, the BW12 algorithm imposes the fourth criterion of fast propagation to eliminate cyclones which have moved less than 1° (zonal direction) in six hours. Note that the zonal distance between the two asterisks (about 3°) in Figure 33 (as the DRV moved from 06 to 12 UTC of 19 December 2005) is indeed larger than 1°.

45

4. Very Weak Upper-Level Forcing

The averaged upper tropospheric induced (650–100 hPa) QG ascent measured at 700 hPa in the green box (reference Figure 34) encompassing the cyclone must be smaller than 0.5 cm/s, and the averaged PV at 250 hPa in that same green box must be less than 1 PVU. The goal here is to exclude ECs induced by significant UT, synoptic scale lifting (the "type B" cyclones according to PS71). The verification of upper tropospheric QG ascent being under threshold is deferred to the BW12 algorithm, but the averaged 250 hPa PV for the example at hand can be visually determined to be less than 1 PVU, as shown in Figure 34.
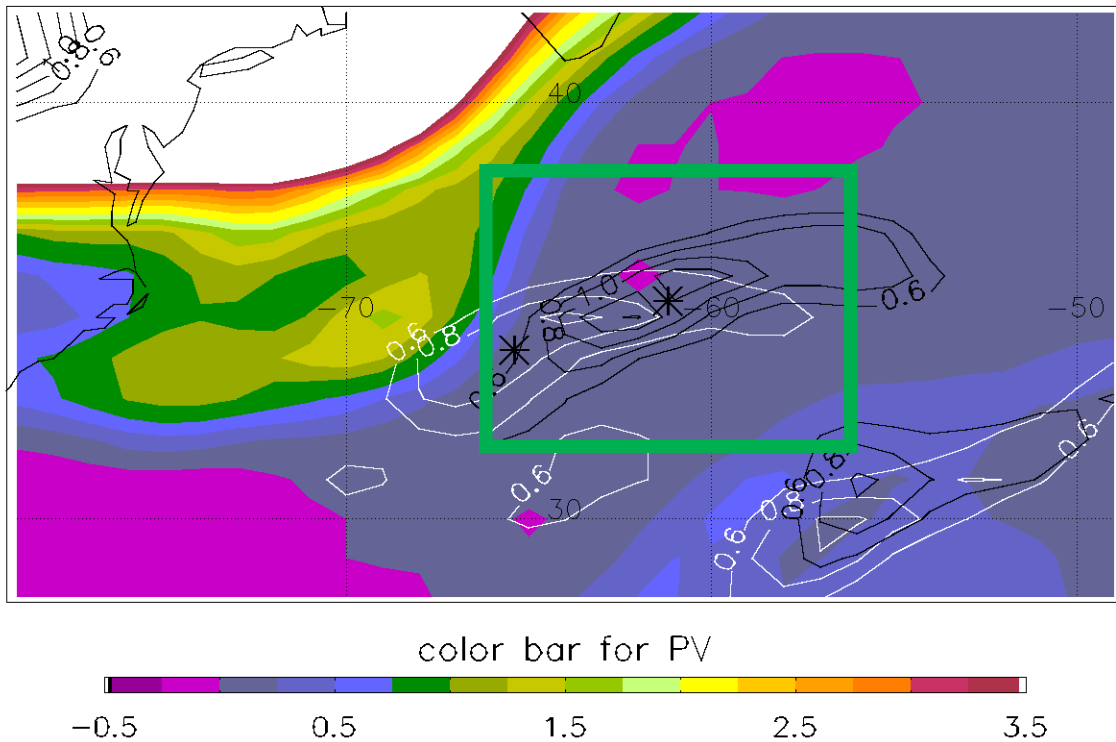
Figure 34.   250 hPa PV (shading in 0.25 PVU interval) at 18 UTC 19 December 2005, superposed by 850 hPa PV maximum (0.2 PVU interval) at former DRV position (left asterisk) at 12 UTC 19 December (white contours), and at current DRV position (right asterisk) at 18 UTC 19 December (black contours). Note that within the green box (determined empirically), the average 250 hPa PV is less than 1 PVU, which satisfies the fifth criterion.

5. Summary of DRV Identification Method

Using the algorithm outlined above, BW12 generated a list of DRVs (314) for the years 2001–2010 and shared with us for DRV research. All DRVs met the initial double criteria of MSLP minimum and lower tropospheric PV maximum for at least 24 hours. In addition they also met the last three criteria (high 950 hPa baroclinicity, fast propagation, and very weak upper tropospheric forcing) for at least three consecutive time periods (12 hours).

C. COMPOSITE METHODOLOGY

To avoid mixing temperature and moisture profiles between DRVs originated on land-locked lakes vs. ocean, a subset of the 314 DRVs was selected for composite analyses. If a DRV originated over land-locked water (such as the Great Lakes) instead of ocean, it was rejected. In addition, if a DRV formed over the Gulf of Mexico and then crossed Florida to enter the Atlantic Ocean, it was also rejected due to the prolonged air mass characteristic modification over land. Thus out of the 91 DRVs identified in the Atlantic basin, 22 were rejected. Similarly, 24 of the 223 DRVs in the Pacific basin were also rejected. Of the original 314 DRVs, 268 were included in this study: 69 from the Atlantic basin, and 199 from the Pacific basin.

1. Compositing Technique

This thesis chose the following parameters for composite analysis: Q, V, OMEGA, SLP, CH, W, PV, PVR and TH (reference Table 1 and Table 2 for definition of these terms). The DRVs are grouped and composited by basins (ATL vs. PAC), as well by seasons (cold vs. warm). In addition to the regular composites (of individual or multiple parameters), the composites of anomalies were obtained by subtracting the corresponding monthly average data from the storm in question, repeat for each storm, then average.

The primary types of composites are in the horizontal and vertical directions, as illustrated below.

a. *Horizontal Composite*

In order to make a horizontal composite of some parameter (say PV at 850 hPa) at the time of DRV formation, for all 69 DRVs in the ATL basin, begin by defining a horizontal rectangular slab, say 61° X 31°. The center of the rectangle has coordinates (0,0), while the four vertices (going clockwise from bottom left) have coordinates (-30,-15), (-30,+15), (+30,+15), and (+30,-15), as shown in Figure 35.
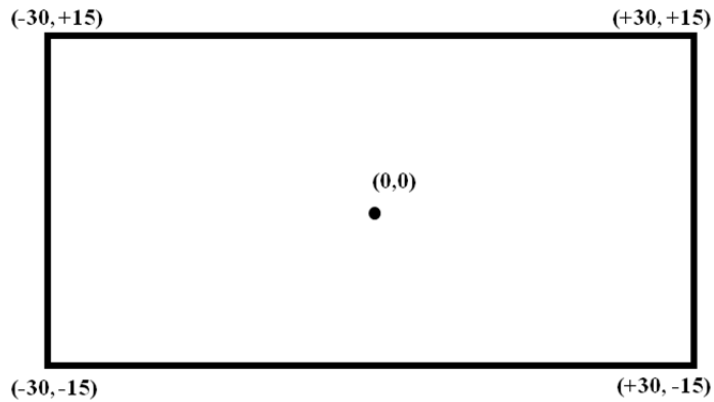
Figure 35.   A rectangular box drawn for illustration of horizontal composite.

Starting with the first DRV in the Atlantic, using the ERA-interim data for the time of the first DRV formation, capture a rectangular slab (61° X 31°) of PV values from 850 hPa, centering the data on the longitude and latitude (LAT/LON) of the DRV center. Then, regrid the center of the slab to the coordinates (0,0). Next, capture a second slab of 850 hPa PV values, re-grid the data and add the data to that of the first case. Repeat for the remaining 67 DRV cases. The final step to create the 850 hPa PV composite is to divide by the total number of storms (69). The result is shown in Figure 36.

By analogy, horizontal composite plots of 850 hPa PV could be constructed six hours prior to DRV formation, or six hours after DRV formation, or any other time relative to the DRV formation.

48
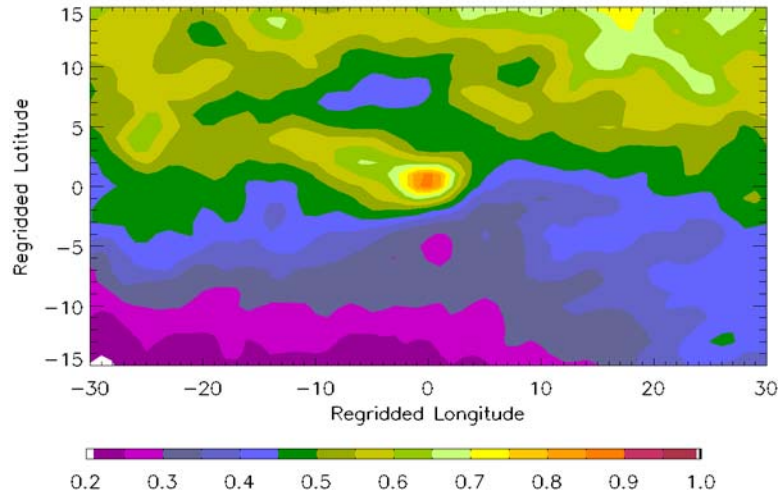
Figure 36.   850 hPa PV composite from all (69) ATL DRVs at the time of formation.

b.   *Vertical Composite*

Vertical composites are also made by extracting rectangular slabs and averaging them. The abscissa could be the longitude, latitude, or somewhere in between. The ordinate is now defined as the number of pre-defined pressure levels (60 levels altogether, for example level 12 is 850 hPa). Given that the DRV is a lower tropospheric disturbance located at some LAT/LON, the vertical slices taken for each DRV would go through its LAT/LON. The longitude-pressure PV composite of all ATL DRVs at time of formation is shown for illustration in Figure 37.
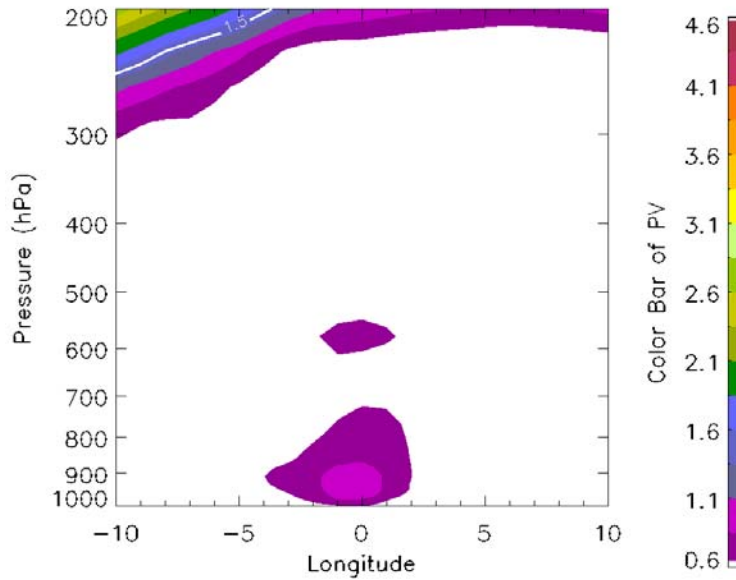
Figure 37.   Vertical composite of PV (shading; PVU) from all ATL DRVs at the time of formation.

D.   STATISTICAL SIGNIFICANCE

The Monte Carlo approach was used to determine the statistical significance of anomaly plots.   This approach relies on repeated random sampling to simulate the physical system.   For this thesis, 100 randomly-generated composites were constructed for each anomaly composite in question.   The randomly selected instantaneous ERA-interim analyses were constrained to occur: i) within plus or minus 10 calendar days of an actual event, and ii) in a different year than the observed event (so as not to include the event itself).   Next, rank the result from the actual event, against the 100 randomly sampled events, grid point by grid point, for each desired parameter.   For each grid point, if the true parameter ranked higher than 97.5% or lower than 2.5%, then the parameter was kept for that grid point.   If however, the true parameter fell within 2.5 to 97.5 % of the 100 randomly generated parameters, the parameter was set to zero for that grid point (for plotting purposes).   By the method described above, robust and statistically significant anomaly plots were generated, at or above the 95 percent confidence level.

E.   BOMB IDENTIFICATION

For each of the 314 DRVs identified by the BW12 algorithm, the complete lifecycle (six hourly history) of each storm was accessible, from the time of formation until the time the DRV was disqualified by the algorithm. A sample sub-section of such data is shown for ATL DRV#56 in Table 3.

Hours	Date/Time	Longitude	Latitude	MSLP (hPa)
0	20051218_12	-76.8	32.4	1017.23
6	20051218_18	-73.8	32.4	1016.61
12	20051219_00	-71.4	33.0	1016.58
18	20051219_06	-69.0	33.6	1013.79
24	20051219_12	-65.4	34.2	1012.75
30	20051219_18	-61.2	35.4	1009.16
36	20051220_00	-54.6	37.8	1004.79
42	20051220_06	-51.6	39.6	995.44

Table 3.   Sample data from the lifecycle of ATL DRV#56

Column one is the hours after DRV formation, and the other columns are self-explanatory. Through automated IDL (interactive data language) scripts, it was determined that DRV#56 explosively deepened from hour 18 to hour 42 (it dropped 18.35 hPa over a 24 hour period, which is equivalent to 1.1 Bergeron.   Note that the definition of a Bergeron varies with the latitude of the storm (see Equation 5 from Chapter I), and in this case it equals 16.33 hPa, using the average latitude of DRV#56 from hour 18 to hour 42 for the sake of this calculation.

THIS PAGE INTENTIONALLY LEFT BLANK

III. DRV CLIMATOLOGY

A. TEMPORAL ANALYSIS

The goal of this section is to examine the climatological characteristics of the DRVs contained in the BW12 climatology. The BW12 algorithm identified and tracked 314 DRV cases: 91 in the Atlantic (ATL) basin and 223 in the Pacific (PAC) basin. Based on the one Bergeron threshold for their deepening rate, approximately 12% of the total number were observed to deepen explosively (11 out of 91 in ATL, 22 out of 223 in PAC).

We strongly believe the stringent criteria outlined in BW12 (reference Chapter II) exclude a large number of "real" DRVs. In an attempt to keep out non-DRVs (such as ECs or TCs) from entering the climatology pool, the algorithm was so rigorous that it actually eliminated legitimate DRVs from making the final list. A prime example of such misses is the DRV that was the precursor to the East Coast Snow Storm (MMD08). With that said, we do believe the criteria did a good job of including only DRVs. With these caveats, these data were analyzed herein to shed light on DRV characteristics.

1. Annual Variability

Annual DRV count for the ATL basin from 2001 to 2010, without differentiating the bombs from non-bombs, was shown in Figure 38. The years 2001, 2002 and 2009 ranked top three in DRV production, averaging 11.3 DRVs per year. The years 2007, 2008 and 2010 were the least in terms of DRV formation, averaging 3.3 DRVs per year. In summary, from 2001 to 2010, there were 69 ocean-born DRVs (a subset of the original 91 DRVs as explained in Chapter II), so the annual average is 6.9 DRVs per year in the ATL basin, with a standard deviation of 3.4 DRVs.
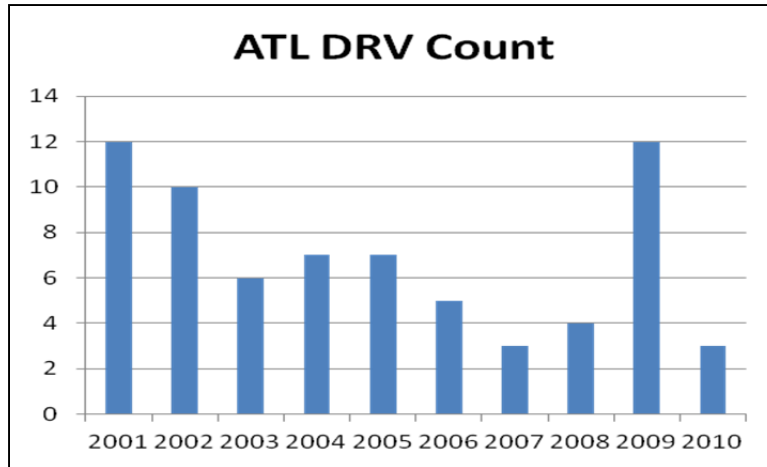
Figure 38.   Annual DRV histogram for the ATL basin from 2001 to 2010.

The annual DRV count for the PAC basin from 2001 to 2010 was summarized in Figure 39. Within the PAC basin, the years 2001, 2008 and 2010 were the top three DRV producers, averaging 25.3 DRVs per year. The slowest years were 2004, 2006 and 2009, averaging 11.7 DRVs per year. In summary, from 2001 to 2010, there were 199 ocean-born DRVs (a subset of the original 223 DRVs as explained in Chapter II) in the PAC basin, so the annual average is 19.9 DRVs with a standard deviation of 6.6 DRVs.
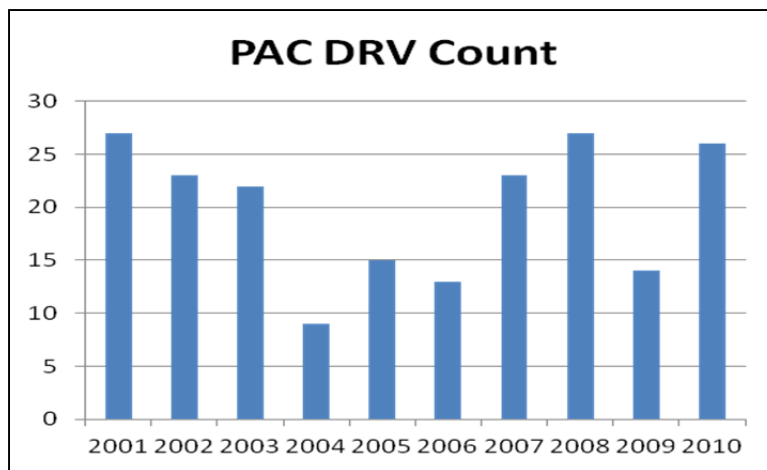
Figure 39.   Annual DRV histogram for the PAC basin from 2001 to 2010.

The DRV count for both the ATL and PAC basins from 2001 to 2010 was summarized in Figure 40. Counting both ocean basins, the years 2001, 2002 and 2008 were the top three DRV producers, averaging 34.3 DRVs per year. The slowest years

were 2004, 2005 and 2006, averaging 18.7 DRVs per year. In summary, from 2001 to 2010, there were 268 ocean-born DRVs (a subset of the original 314 DRVs as explained in Chapter II) in both the ATL and PAC basins, so the annual average is 26.8 DRVs with a standard deviation of 6.9 DRVs.
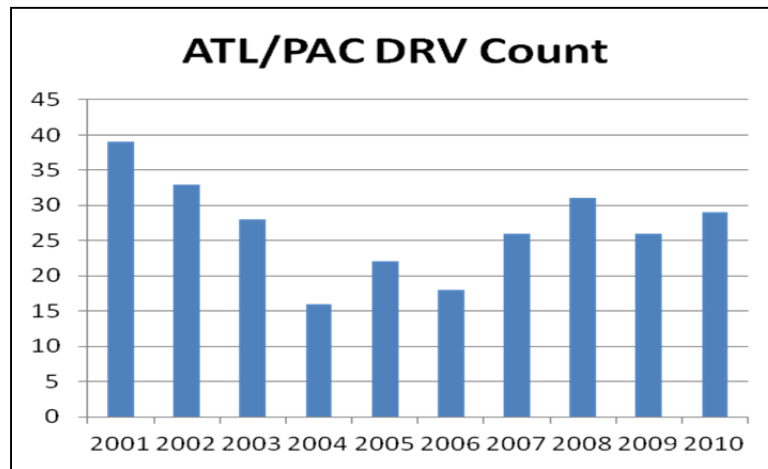
Figure 40.   Combined ATL/PAC annual DRV histogram from 2001 to 2010.

2.   Monthly Variability

The monthly DRV count for the ATL from 2001 to 2010 was shown next in Figure 41. The warm season months from May through October are the top six producers of DRVs, with August being most productive with 13 DRVs. The cold season months from November through April are the bottom six producers of DRVs, where December, January, February and April all tied at only 3 DRVs each. In summary, from 2001 to 2010, for the ATL basin, the monthly average is 5.8 DRVs, and the standard deviation is 3.0 DRVs.
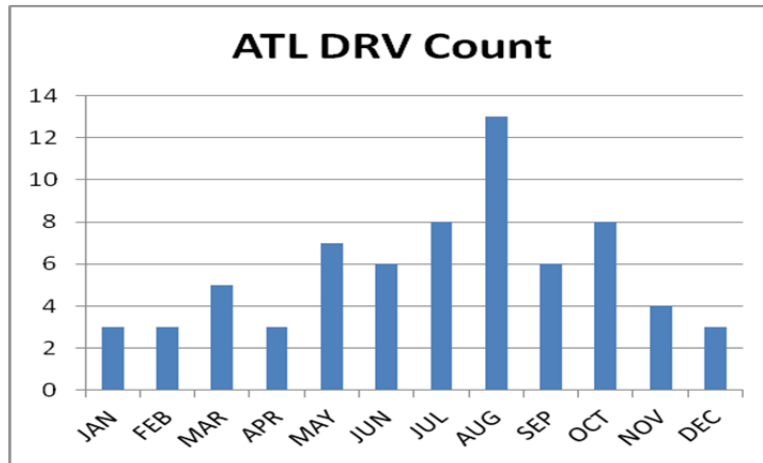
Figure 41.   Monthly DRV histogram for the ATL from 2001 to 2010.

The monthly DRV count for the PAC from 2001 to 2010 was summarized in Figure 42. The warm season months from May through October are again (same as ATL) the top six producers of DRVs, but in PAC basin September was the most productive with 37 DRVs. The cold season months from November through April are the bottom six producers of DRVs, with January totaling only 3 DRVs. In summary, from 2001 to 2010, for the PAC basin, the monthly average is 16.6 DRVs, and the standard deviation is 10.3 DRVs.
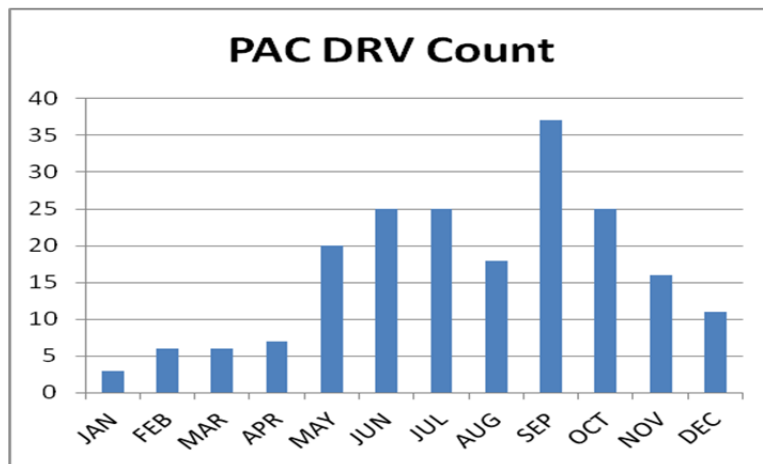
Figure 42.   Monthly DRV histogram for the PAC from 2001 to 2010.

The ATL and PAC combined monthly DRV count is shown in Figure 43. Not surprisingly, the warm season months from May through October are the top six producers of DRVs, with September the most productive, with 43 DRVs. The cold

season months from November through April are the bottom six producers of DRVs, with January totaling only 6 DRVs. In summary, from 2001 to 2010, combining the ATL and PAC basins, the monthly average is 22.3 DRVs, and the standard deviation is 12.2 DRVs
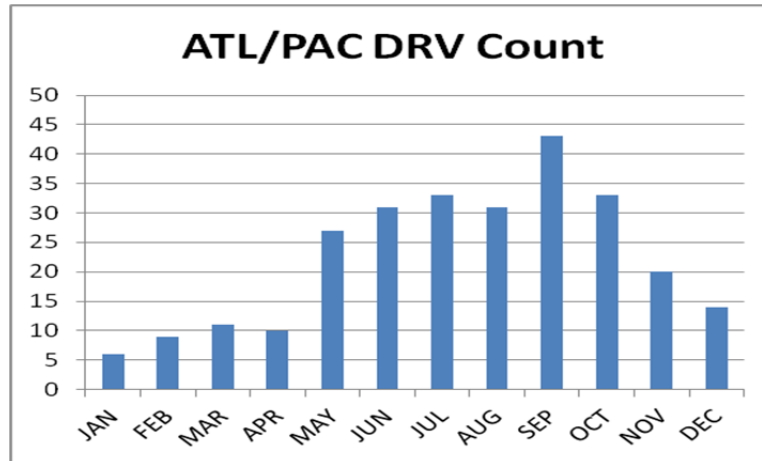
Figure 43.   Combined ATL/PAC monthly DRV histogram from 2001 to 2010.

3.   Warm vs. Cold Season Variability

More insight into the temporal variability of DRVs was revealed by consolidating the monthly data into warm (May–October) vs. cold (November–April) months, for the ATL basin from 2001 to 2010, as shown in Figure 44.
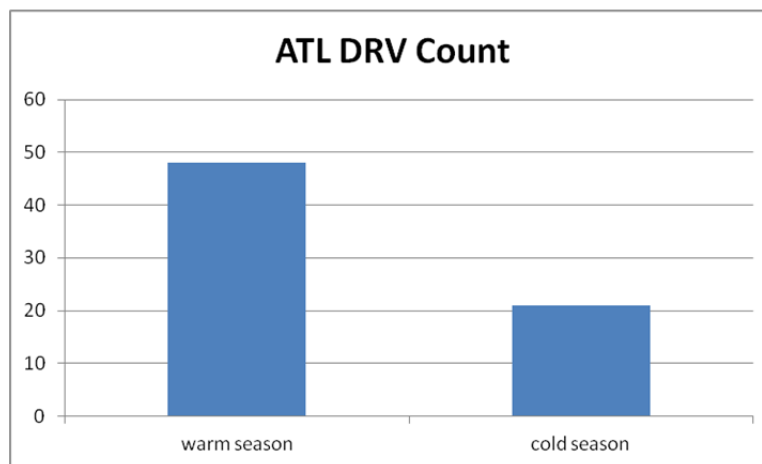
Figure 44.   Warm vs. cold season DRV histogram for ATL from 2001 to 2010.

Within the ATL basin, the warm season had about 2.3 times more DRVs than the cold season, a trend that underlines the importance of moisture to DRVs. Warm season

are associated with warmer sea surface temperature (SST), which provides more water vapor as fuel for DRV development and propagation, as outlined by PT95 (reference Figure 9 in Chapter I). A similar trend is observed in the PAC basin with 3.1 times more DRVs in warm season than cold season, as shown in Figure 45. The combined ATL/PAC warm vs. cold season DRV histogram is shown in Figure 46. For the northern hemispheric oceans, the warm season has 2.8 times more DRVs than the cold season.
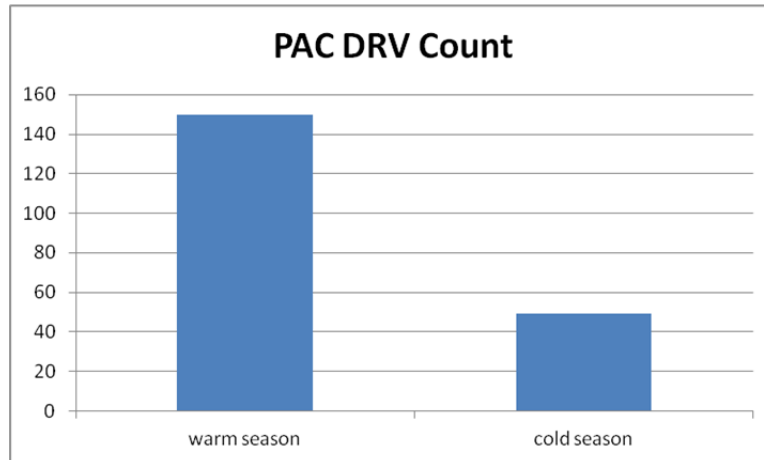
Figure 45.   Warm vs. cold season DRV histogram for PAC from 2001 to 2010.
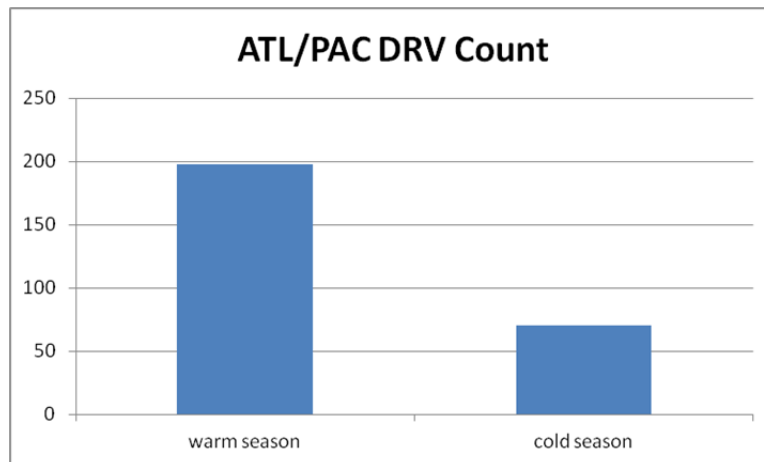
Figure 46.   Combined ATL/PAC warm vs. cold season DRV histogram from 2001 to 2010.

B. SPATIAL ANALYSIS

The spatial locations of DRV genesis were plotted to investigate any pattern, for both the ordinary non-bomb DRVs and the DRV bombs that explosively deepened. Such a climatology reveals the preferred geographical regions of DRV genesis, as well as the likely mechanisms for their generation.

1. Atlantic Basin Analysis from 2001 to 2010

The origins of DRVs formed over the ATL basin, during the warm and cold season from 2001 through 2010, were plotted in Figure 47 and Figure 48, respectively. The magenta asterisks mark the origins of DRVs that evolved into bombs, and the black triangles mark the origins of ordinary non-bomb DRVs. At first glance, the genesis location of all DRVs (both bombs and non-bombs) coincide with the general position of the Gulf Stream (see Figure 49), which is a climatologically preferred region for cyclogenesis (Zishka and Smith 1980; Sanders and Gyakum 1980; Jacobs et al. 2005).
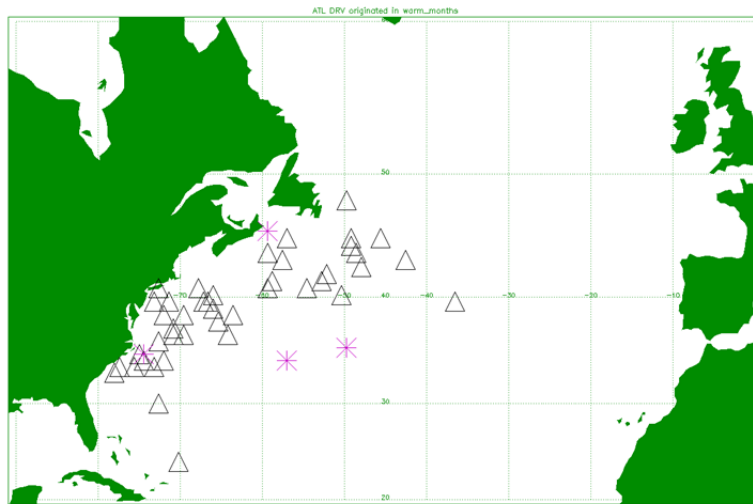
Figure 47. Location of DRV genesis in ATL basin during warm season from 2001 to 2010. The black triangles mark the origin of non-bomb DRVs, whereas the magenta asterisks mark the origin of DRV bombs.
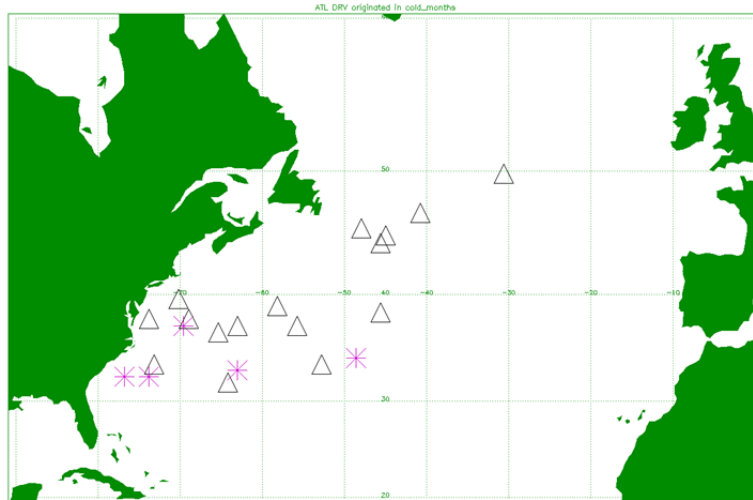
Figure 48. Location of DRV genesis in ATL basin during cold season from 2001 to 2010. The black triangles mark the origin of non-bomb DRVs, whereas the magenta asterisks mark the origin of DRV bombs.
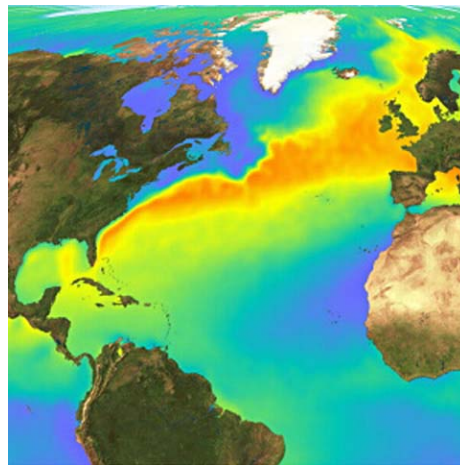
Figure 49. Position of Gulf Stream in the North Atlantic, highlighted by region of steepest sea surface temperature gradient (Laura Knight-Jadczyk, cited 2007: Fire and Ice—the Day after Tomorrow [Available online at http://www.sott.net/image/image/tmp/1168547904.692692.7800/le-gulf-stream.jpg]).

Looking very crudely at the location of DRV bombs (magenta asterisks), note that three out of four bombs during the warm season (see Figure 47), as well as four out of five bombs during the cold season (see Figure 48), preferentially originated near the southern boundary of the genesis distribution. This suggests that the DRVs originating at lower latitudes have a better chance of deepening explosively. It is possible that the

60

lower latitude regions are associated with warmer SST, which equates to an abundant source of moisture and latent heat conversion of the DRVs. Or perhaps disturbances in lower latitude regions have a longer DRV-phase growth time period before interacting with the DT. At this time, there are simply not enough cases to say anything with much conviction.

The frequency contours of DRV genesis (without differentiating bombs and non-bombs) in ATL basin during warm season from 2001 to 2010 were plotted in Figure 50. Raw non-zero frequencies appear in each 5° X 5° quadrilateral of latitude and longitude. Isopleths represent smoothed frequencies, obtained as one eighth of the sum of six times the raw central frequency plus the sum of the surrounding raw frequencies (formula after Figure 3 caption from SG80).

In agreement with former assessment, the favored region of DRV formation coincides well with the generic location of the Gulf Stream.
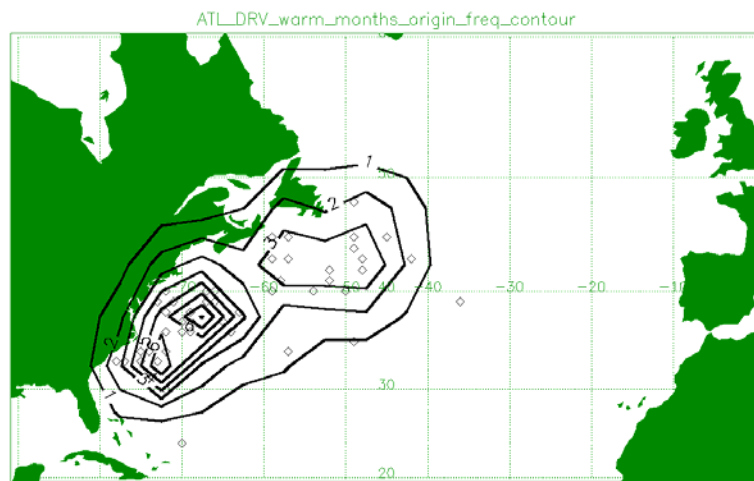
Figure 50.   Frequency contour of DRV genesis in ATL basin during warm season from 2001 to 2010.

The frequency contours of DRV genesis (without differentiating bombs and non-bombs) in ATL basin during cold season from 2001 to 2010 were plotted in Figure 51. Even with only 21 DRVs during the cold season (versus 48 DRVs in the warm season), the smoothed frequency contour bears the same pattern as the warm season.
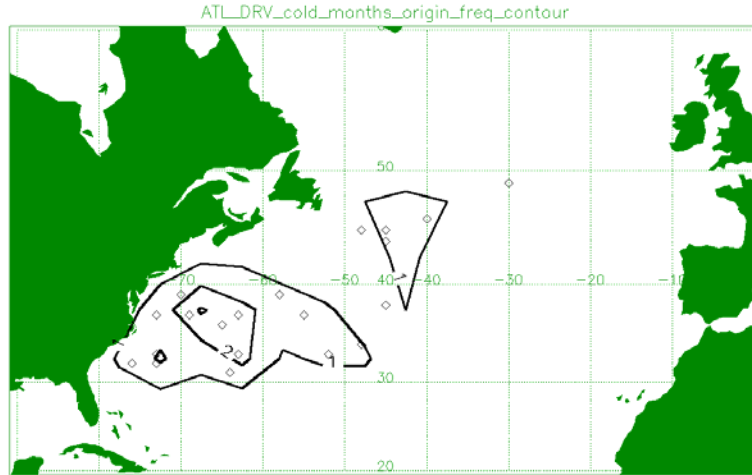
Figure 51.   Frequency contour of DRV genesis in ATL basin during cold season from 2001 to 2010.

The trajectories of ATL DRVs during the warm season of 2001–2010 are plotted in Figure 52. The tracks of non-bomb DRVs are marked in black, whereas the tracks of DRV bombs are in magenta. In general, a typical DRV tracked from west to east, with a bent toward the north over its lifecycle.
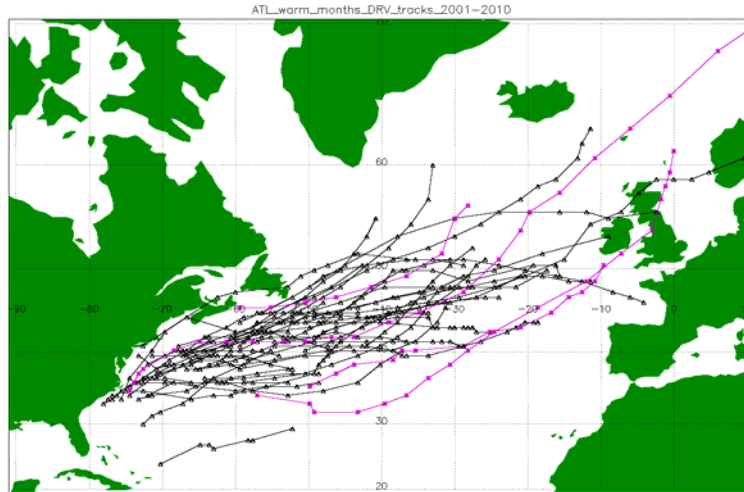
Figure 52.   Trajectories of ATL DRVs during warm season from 2001 to 2010. The black lines mark the tracks of non-bomb DRVs, whereas the magenta lines mark the DRV bombs.

The trajectories of DRVs during the cold season of 2001–2010 are plotted in Figure 53. As in the warm season, the tracks of non-bomb DRVs are marked in black,

whereas the tracks of DRV bombs are marked in magenta. On average the DRVs tracked from west to east, with a slight northward movement over its lifecycle.
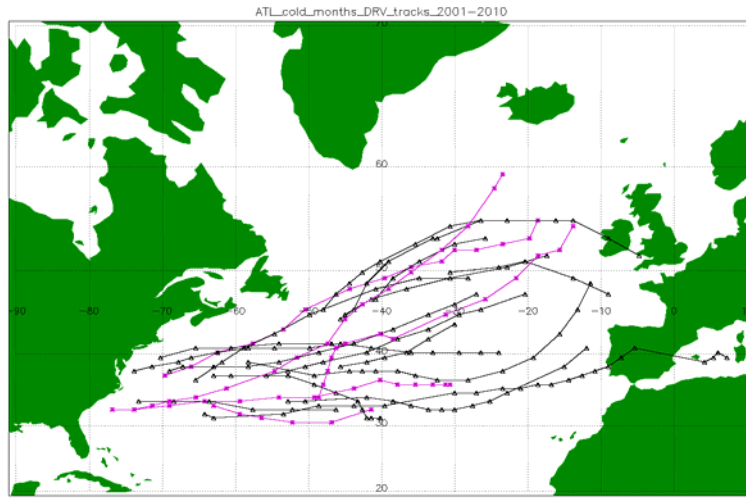
Figure 53.   Trajectories of ATL DRVs during cold season from 2001 to 2010. The black lines mark the tracks of non-bomb DRVs, whereas the magenta lines mark the DRV bombs.

2.   Pacific Basin Analysis from 2001 to 2010

The origins of DRVs formed over PAC during the warm and cold season from 2001 through 2010, were plotted in Figure 54 and Figure 55, respectively.
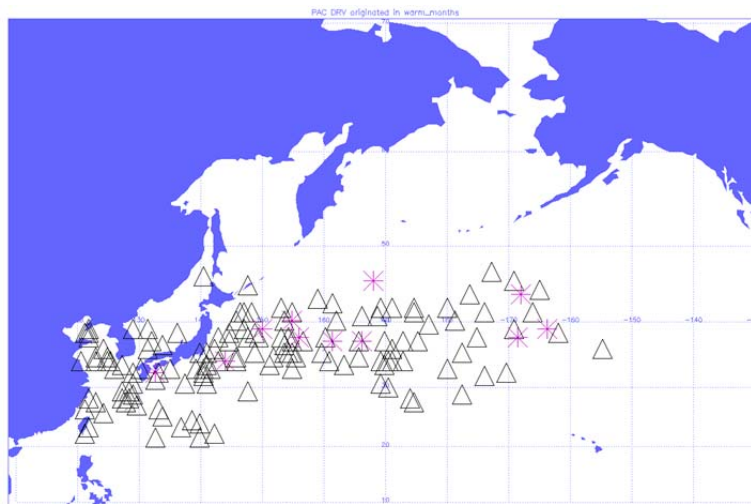
Figure 54.   Location of DRV genesis in PAC during warm season from 2001 to 2010. The black triangles mark the origin of non-bomb DRVs, whereas the magenta asterisks mark the origin of DRV bombs.
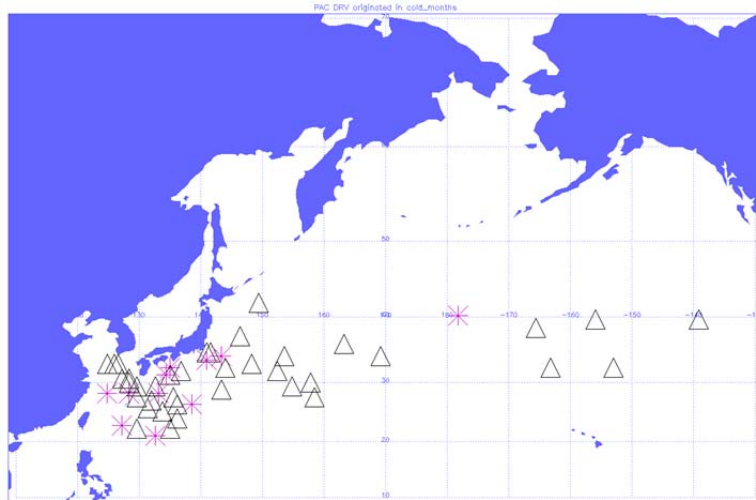
Figure 55. Location of DRV genesis in PAC during cold season from 2001 to 2010. The black triangles mark the origin of non-bomb DRVs, whereas the magenta asterisks mark the origin of DRV bombs.

Using the same convention as ATL, the magenta asterisks mark the origins of DRV bombs, and the black triangles mark the origins of non-bomb DRVs. At first look, the DRVs (in particular the bombs during the cold season) tend to form near the general position of the Kuroshio Current (see Figure 56), which is an area of elevated moisture and baroclinicity, favorable for cyclogenesis.
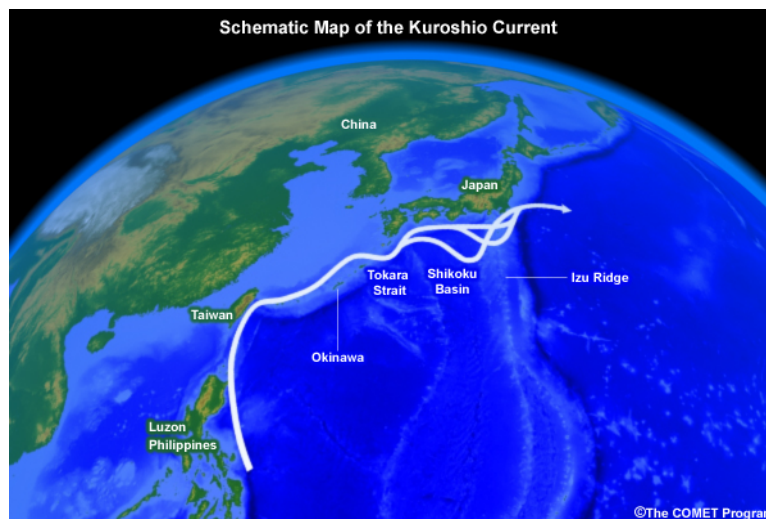
Figure 56. General position of the Kuroshio Current (The COMET Program, cited 2010: A Forecaster's Overview of the Northwest Pacific. [Available online at https://www.meted.ucar.edu/search/details.php?id=18785]).

The frequency contours of DRV genesis, without differentiating bombs and non-bombs, in PAC basin during the warm season from 2001 to 2010 were plotted in Figure 57. Contour value maximums are located south of the Korean Peninsula, southeast of the Kanto Plain, and east of Honshu Island, Japan.
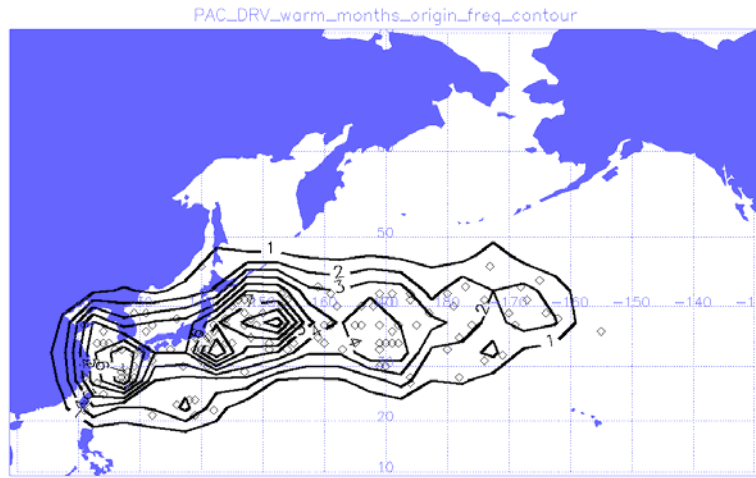
Figure 57.   Frequency contour of DRV genesis in PAC during warm season from 2001 to 2010.

The frequency contours of DRV genesis in PAC basin during the cold season from 2001 to 2010 are plotted in Figure 58. Note that even with less DRVs (49) in the cold season (versus 150 in the warm season), the contour value maxima are located in the same general region as the warm season, but more localized over the W PAC.
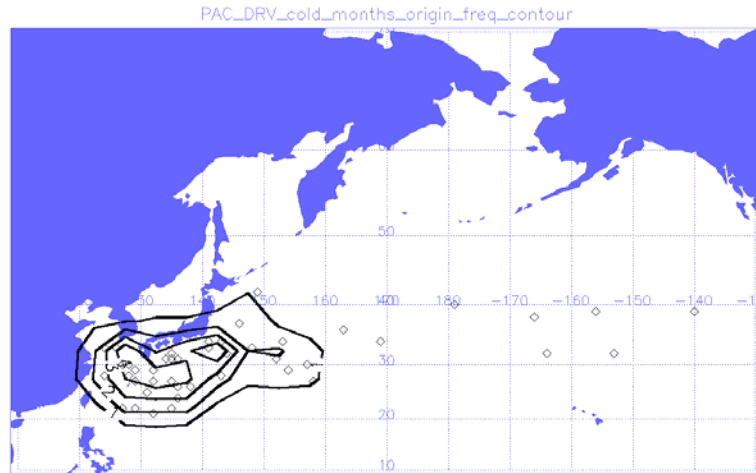
Figure 58.   Frequency contour of DRV genesis in PAC basin during cold season from 2001 to 2010.

The tracks of PAC DRVs during the warm and cold season of 2001-2010, are plotted in Figure 59 and Figure 60, respectively. As in the survey of ATL cases, the tracks of non-bomb DRVs are marked in black, whereas the tracks of bombs are marked in magenta. In general, the typical PAC DRV also tracked from west to east, with at times forceful northward movement over its lifecycle. Upon closer look, the majority of DRV bombs (magenta tracks) during both warm and cold season tend to finish their lifecycle by curving northward. Horizontal and vertical cross sections of explosively deepening DRVs (reference Chapter V) have shown that, both type A and type C DRVs inevitably interact with DTs just before reaching 1 Bergeron pressure drop. Since DTs are lower and more attainable to the north, it makes sense that the DRV bombs tend to curve northward and deepen explosively.
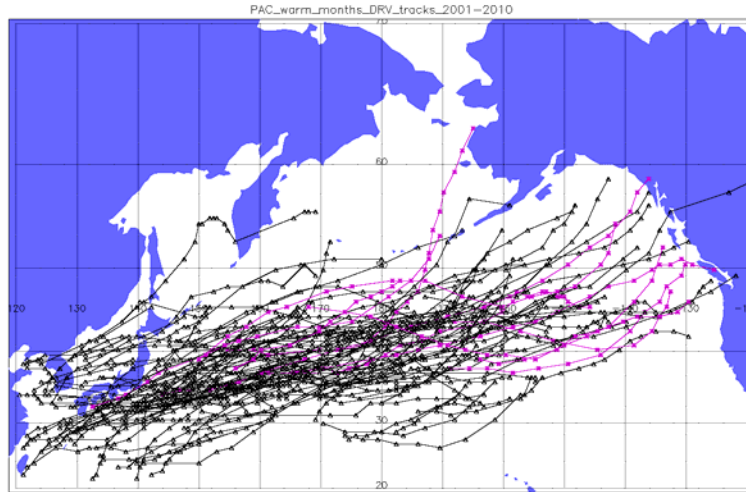
Figure 59.   Trajectories of PAC DRVs during warm season from 2001 to 2010. The black lines mark the tracks of non-bomb DRVs, whereas the magenta lines mark the DRV bombs.
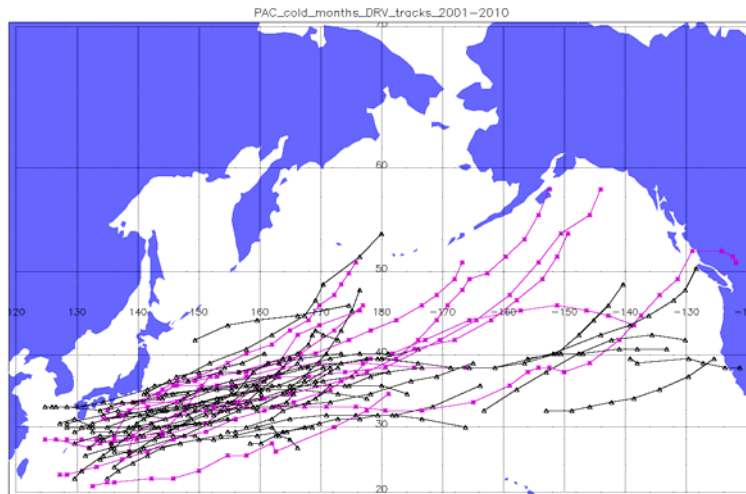
Figure 60.   Trajectories of PAC DRVs during cold season from 2001 to 2010. The black lines mark the tracks of non-bomb DRVs, whereas the magenta lines mark the DRV bombs.

C. BASIC PARAMETERS ANALYSIS

The DRVs were sorted (by basin, season, and bomb status) into eight groups as shown in Table 4.

1. ATL Warm Non-Bomb	5. ATL Warm Bomb
2. ATL Cold Non-Bomb	6. ATL Cold Bomb
3. PAC Warm Non-Bomb	7. PAC Warm Bomb
4. PAC Cold Non-Bomb	8. PAC Cold Bomb

Table 4.   DRVs sorted by basin, season and bomb status (eight groups).

Five basic parameters were computed/averaged/plotted for each group of DRVs (as sorted above) for a cursory survey of how they differ in Table 5. For clarity, the first four groups (non-bombs) are shown in the left-panel (in blue), and the last four groups (bombs) are shown in the right-panel (in red).

1. Total DRV Count
2. Duration of DRVs
3. Initial Pressure at Time of DRV Formation
4. Lowest Pressure Attained during Life of DRV
5. Largest Pressure Drop during Life of DRV (item #3 minus item #4)

Table 5.   List of basic parameters.

1.   Total DRV Count

The DRV counts in each group are plotted as shown in Figure 61. As noted before, there are more non-bomb DRVs during the warm season, in comparison to the cold season (Figure 61 left-panel). However, there were roughly equal number of DRV bombs during both warm and cold season (Figure 61 right-panel), which meant the DRVs are more likely to bomb during the cold season.
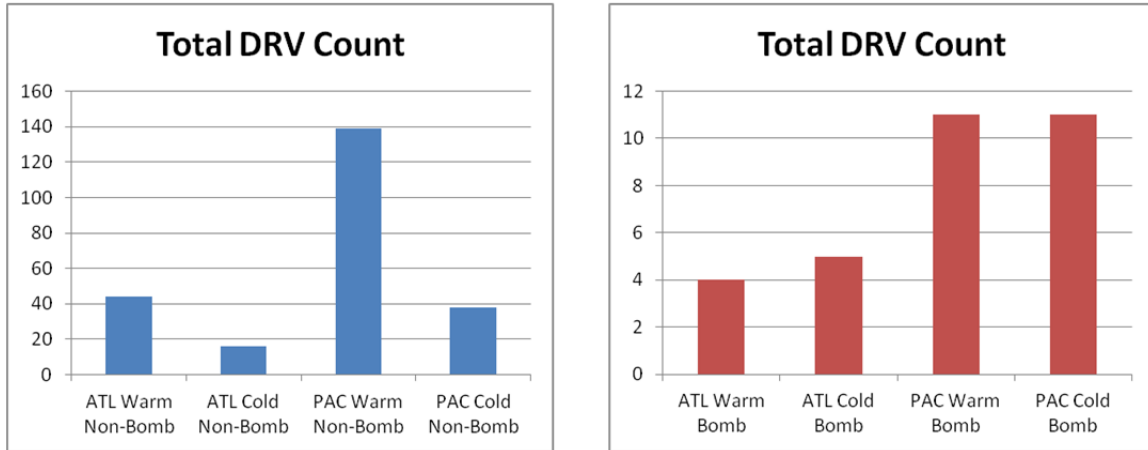
Figure 61.   Left panel contains total non-bomb DRV count in groups separated by basin and season. Right panel is set up in the same manner, showing the data for DRV bombs.

2.   Duration of DRVs

The average duration of DRVs in each group are plotted as shown in Figure 62. Note that the average life of non-bomb DRVs in the warm season are slightly longer than that in the cold season (Figure 62 left-panel), and the same goes for the DRV bombs (Figure 62 right-panel). Note also that the average life of DRV bombs are approximately 36 hours longer than the non-bomb DRVs (comparing right-panel to left-panel).
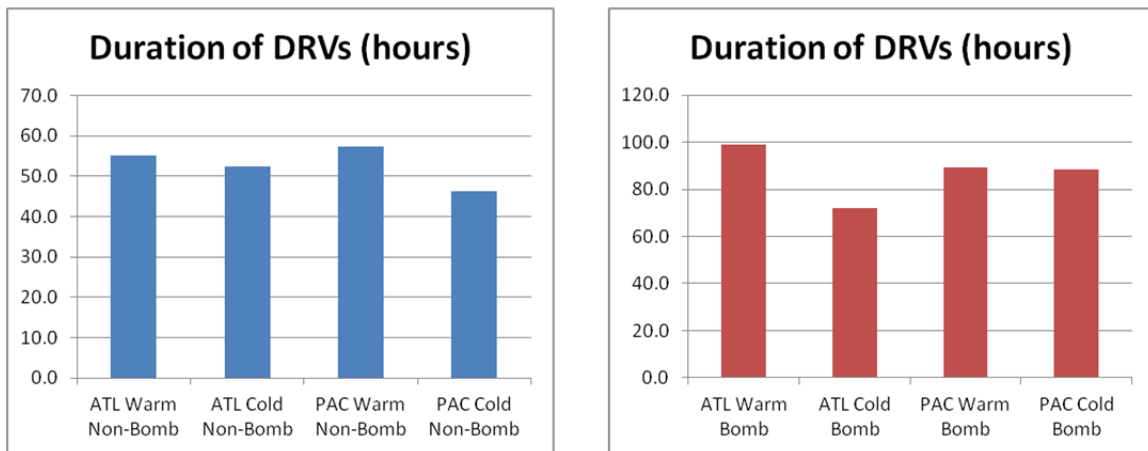
Figure 62.   Left panel contains duration of non-bomb DRVs in groups separated by basin and season. Right panel is set up the same, containing the data for DRV bombs.

3. Initial Pressure at Time of DRV Formation

The average pressure at initial time of DRV formation in each group are plotted as shown in Figure 63. Note that the eight groups average to 1008 hPa for their initial pressure (considering both left and right-panels in Figure 63).
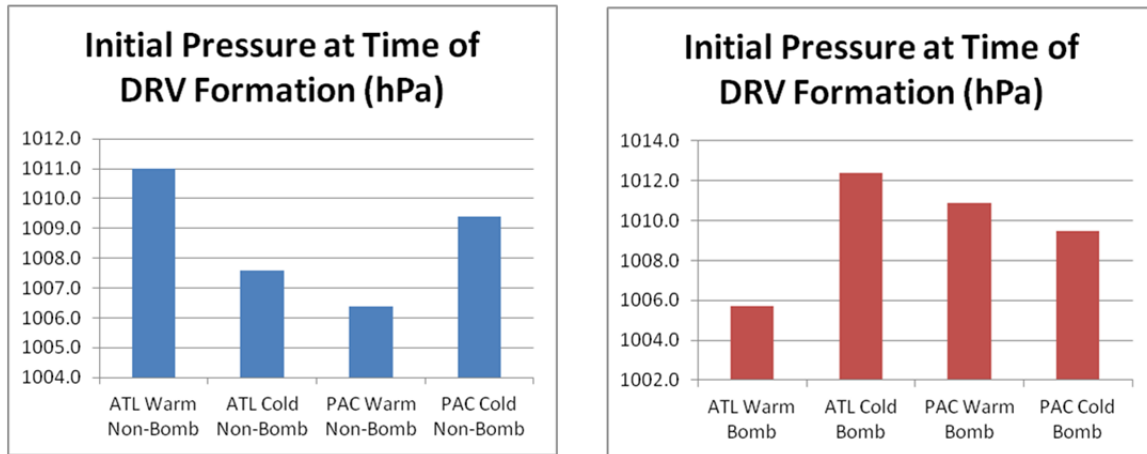
Figure 63. Left panel contains average initial pressure at time of non-bomb DRV formation in groups separated by basin and season. Right panel is set up the same, containing the data for DRV bombs.

4. Lowest Pressure Attained during Life of DRV

The lowest pressure attained during the life of DRV in each group are averaged and plotted as shown in Figure 64. The non-bomb DRVs groups average about 1001 hPa for lowest pressure (Figure 64 left-panel), but the DRV bombs groups average around 965 hPa (Figure 64 right-panel).
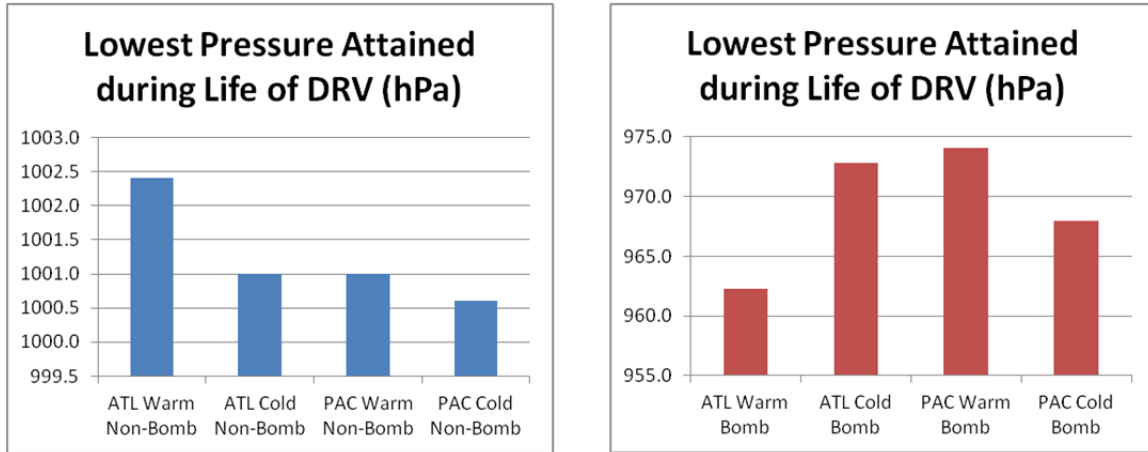
Figure 64.   Left panel contains average lowest pressure attained during the life of non-bomb DRV in groups separated by basin and season. Right panel contains the average lowest pressure attained during the life of DRV bombs, also in groups separated by basin and season.

5.   Largest Pressure Drop during Life of DRV

Finally the largest pressure drop during life of DRV are averaged and plotted as shown in Figure 65. Note that the bomb groups average about 40 hPa pressure drop (Figure 65 right-panel), whereas the non-bomb groups average only about 7 hPa pressure drop (Figure 65 left-panel).
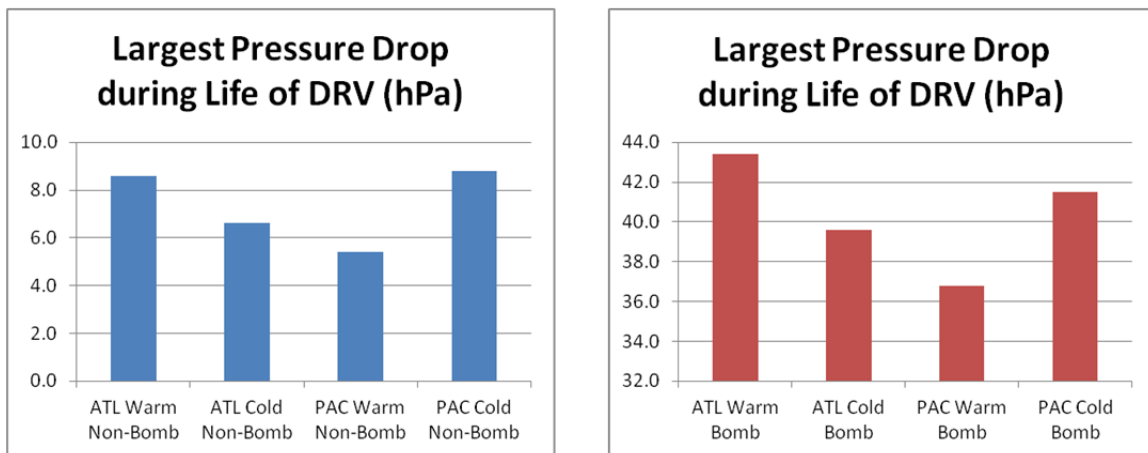
Figure 65.   Left panel contains average maximum pressure drop during the life of non-bomb DRV in groups separated by basin and season. Right panel is set up the same, containing the data for DRV bombs.

71

D. HIGH IMPACT WEATHER ANALYSIS

As mentioned earlier in Chapter I, Sanders and Gyakum (1980) defined a "bomb" as an extratropical cyclone (EC) that deepened by at least one Bergeron in 24 hours. The term "bomb" was used here to describe a DRV that underwent explosive cyclogenesis, and the term "non-bomb" was used to describe a DRV that did not undergo explosive cyclogenesis, an ordinary DRV so to speak.

1. Annual Variability

It is insightful to take another look at the annual DRV count for the ATL basin from 2001 to 2010, this time with the bombs and non-bombs colored in red and blue respectively, as shown in Figure 66.
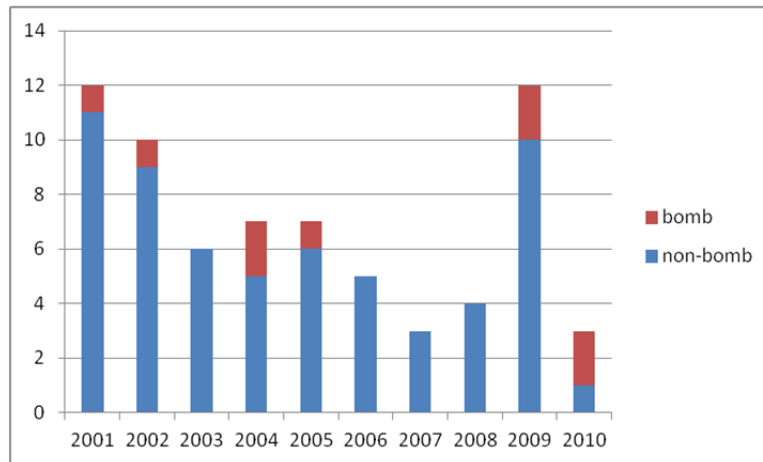
Figure 66.   Annual DRV histogram for the ATL basin from 2001 to 2010.

Note that for the ATL basin, no bombs were reported in 2003, 2006, 2007 and 2008. To be sure, there existed explosively deepened ECs in the ATL during these years, but either none of them were of DRV origin, or those of DRV origin were excluded by the BW12 algorithm. The years 2004, 2009 and 2010 each had two DRVs that underwent explosive cyclogenesis, while the years 2001, 2002 and 2005 each had one DRV that bombed. A total of 9 DRVs bombed among 69 DRVs (13%) within the ATL basin.

The annual DRV count for the PAC basin from 2001 to 2010 is summarized in Figure 67.
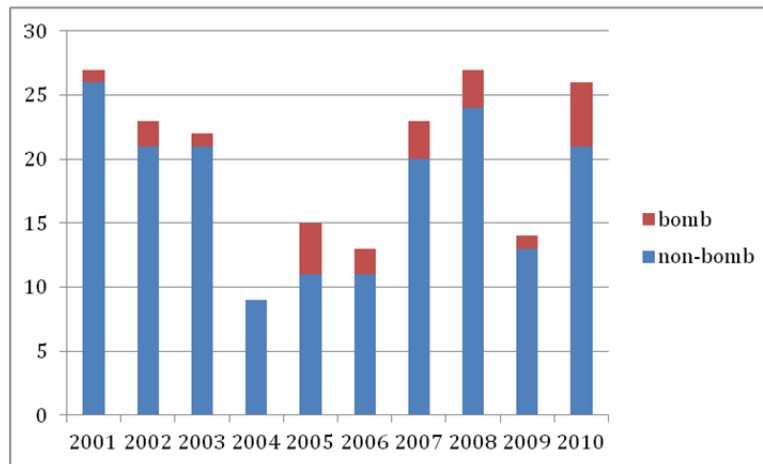
Figure 67.   Annual DRV histogram for the PAC basin from 2001 to 2010.

As in the ATL, the non-bomb (regular) DRVs were depicted by the blue bars, and the explosively deepened DRVs (bombs) were depicted by the red bars. The year 2010 ranked first for bomb formation, 5 of its 26 DRVs deepened explosively. The year 2005 ranked second, 4 of its 15 DRVs bombed. The year 2004 reported no bombs, which meant while there were ECs that explosively deepened in 2004, none of them were of DRV origins. Note that a total of 22 DRVs bombed among 199 DRVs (11%) within the PAC. Combining the statistics from both ATL and PAC basins, 31 out of 268 DRVs bombed, which equated to approximately 12%, as shown in Figure 68.
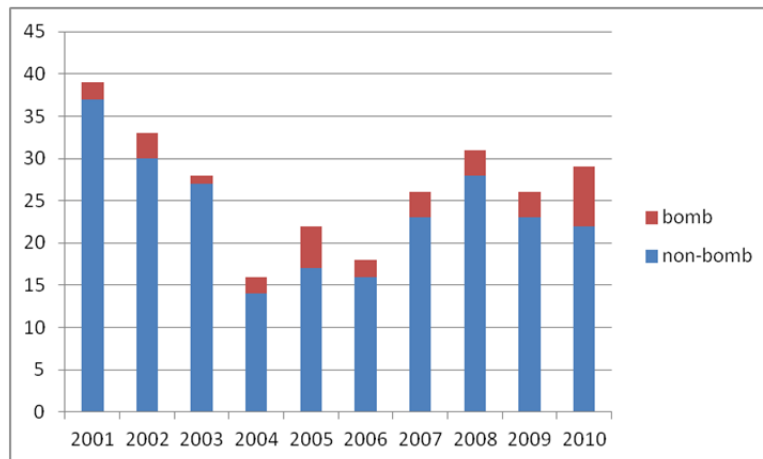
Figure 68.   Combined ATL/PAC annual DRV histogram from 2001 to 2010.

2. Monthly Variability

The monthly DRV count for the ATL from 2001 to 2010 was summarized next in Figure 69. Note that zero DRV deepened explosively from April through August, which included most of spring and all of summer. The scarcity of bomb could be attributed to DT meandering further north from spring to summer. Since DT is the surrogate of upper tropospheric (UT) support to DRVs, the increased distance between DT and DRVs (recall DRVs preferentially originate over the lower latitudes) meant less DRVs are able to obtain upper tropospheric support. This condition reversed in September through March as the DT worked its way back toward the equator, resulting in at least one bomb each month.
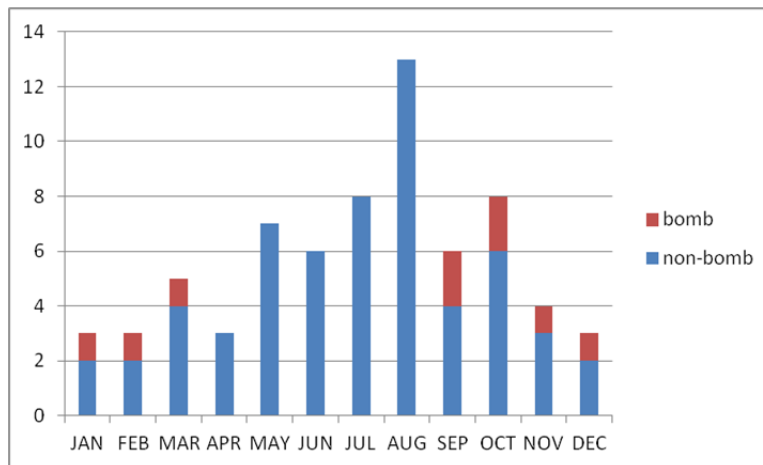
Figure 69.   Monthly DRV histogram for the ATL from 2001 to 2010.

The monthly DRV count for the PAC from 2001 to 2010 was summarized in Figure 70. Similar to the ATL, spring and summer were quieter months for bombs in the PAC. While the months March, June and August had zero bombs, the months of April, May and July had only one or two bombs. Similar to the ATL, October was the most productive month with 6 out of its 25 DRVs bombing. The next highest bomb producer was February, with 4 out of its 6 DRVs bombing, and the third place going to September with 3 bombs out of its 37 DRVs. The ATL/PAC combined monthly DRV count is shown in Figure 71.
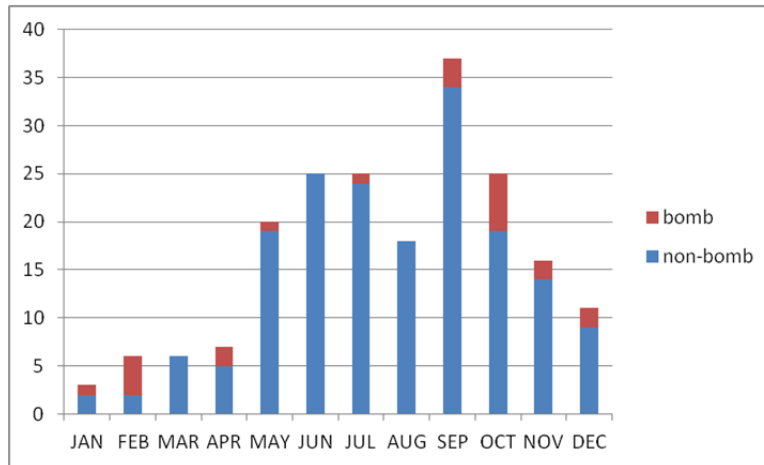
Figure 70.   Monthly DRV histogram for the PAC from 2001 to 2010.
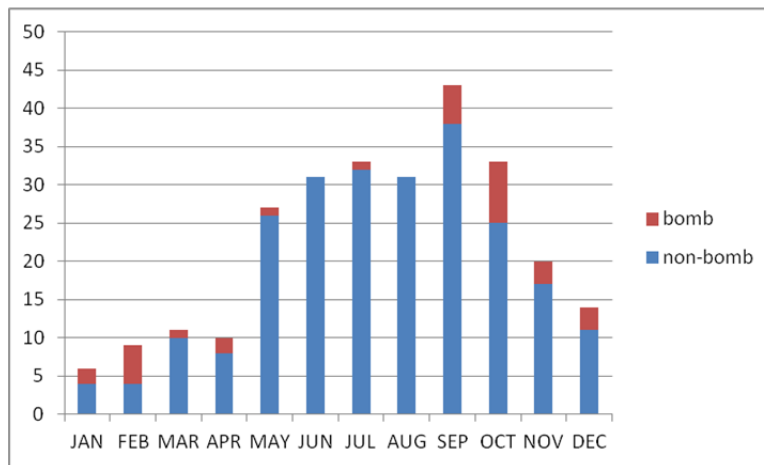
Figure 71.   Combined ATL/PAC monthly DRV histogram from 2001 to 2010.

3.   Warm vs. Cold Season Variability

More insight into the temporal variability of DRVs was revealed by consolidating the monthly data into warm (May–October) vs. cold (November–April) months for the ATL, PAC and both basins combined from 2001 to 2010, as shown in Figure 72, Figure 73 and Figure 74.
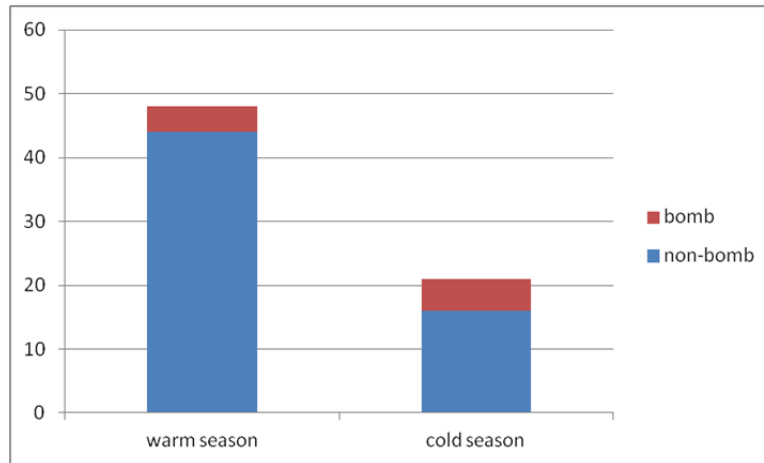
Figure 72.   Warm vs. cold season DRV histogram for ATL from 2001 to 2010.
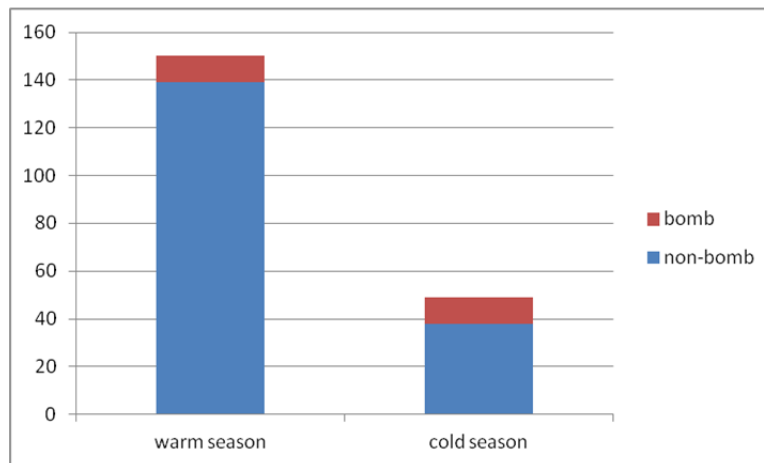
Figure 73.   Warm vs. cold season DRV histogram for PAC from 2001 to 2010.

Note that, although the cold season had one-third as many DRVs as the warm season, the number of bombs (red bars) equal or exceed (as is the case in ATL) the number of bombs during the warm season. This means that the DRVs in the cold season have a higher relative frequency of becoming bombs, than the DRVs in the warm season. This could be attributed to the fact that colder season has stronger temperature gradients, which implies stronger jets and stronger tropopause-level waveguides. More robust waveguides would allow for a larger number of robust DT anomalies, which are more conducive to interact with DRVs and bomb.
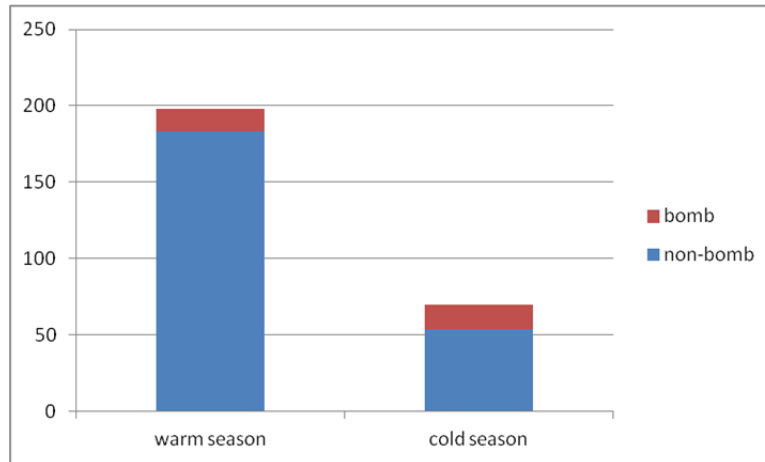
Figure 74.   Combined ATL/PAC warm vs. cold season DRV histogram from 2001 to 2010.

THIS PAGE INTENTIONALLY LEFT BLANK

IV.   SUMMARY OF COMPOSITE STUDIES

The composite structures of the DRVs from 2001–2010 identified by BW12 are examined here. These results can be directly compared to that of previous work examining idealized and observed DRVs. The goal herein was to determine if the limited number of DRV studies in the prior literature are indeed representative of a large number of "real world" DRVs, which have been identified using an objective technique.

A.   COMPOSITES AT TIME OF DRV FORMATION

In making composite plots at the time of DRV formation, the 268 DRVs were sorted into four groups separated by seasons and basins (without differentiating the bombs from the non-bombs) as shown in Table 5.

Groups	# of DRVs
ATL COLD	21
ATL WARM	48
PAC COLD	49
PAC WARM	150

Table 6.   Four groups defined for composite studies.

As described in Chapter III, the composites were constructed by averaging horizontal slices through the center of DRVs. The ATL COLD group is of particular interest since three out of four case studies mentioned in Chapter I happened in ATL during the cold season.

1.   Necessary Ingredients

a.   *Moisture*

Moisture is integral for DRV growth. This can be seen in the horizontal composites of Q (specific humidity; g H_2O/kg air) at 884 hPa (pressure level chosen for the robust signals), which contain strong signals of the moisture parameter, as shown in

Figure 75. Both ATL WARM and PAC WARM DRV groups showed a local maximum (greater than 11.5 g H_2O/kg air) of moisture right over the center of the DRVs (regridded to 0,0). The data for ATL COLD and PAC COLD identify moist tongues (Q greater than 8.5 g H_2O/kg air) oriented SW to NE, extending through the center of the DRVs. Also note the steep meridional moisture gradients displayed in all four groups, positioned between (0,0) and 5° north of the DRV center. As seen in the next subsection, this is due to the large meridional temperature gradient.
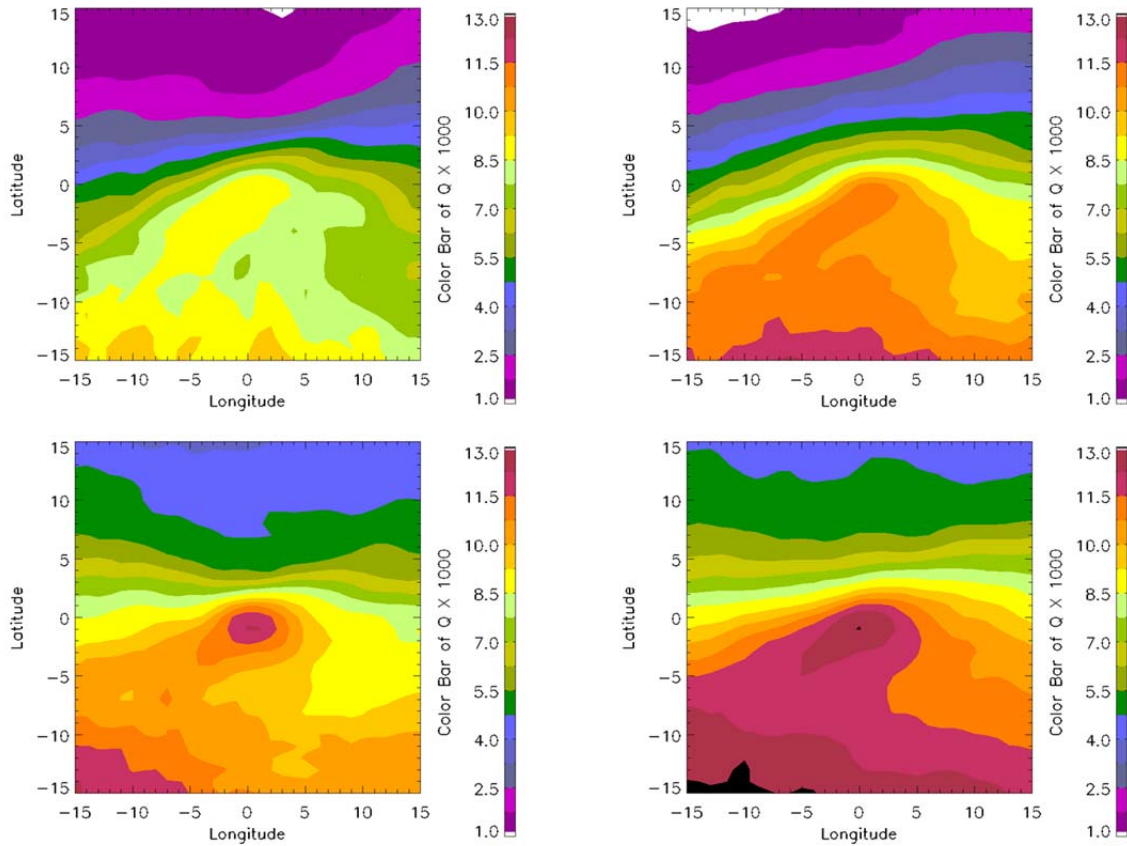
Figure 75. Horizontal composite of Q (specific humidity; g H_2O/kg Air) @884 hPa of ATL COLD, PAC COLD, ATL WARM and PAC WARM DRVs, during the years 2001–2010, are shown in top-left, top-right, bottom-left and bottom-right-panels, respectively.

b.   *Baroclinicity*

Baroclinicity is also ubiquitous with DRV formation. In the horizontal composites of TH (potential temperature; K) at 884 hPa (pressure level chosen for the robust signals), the data revealed large meridional temperature gradients, pointing from north to south, as shown in Figure 76 (ATL COLD, PAC COLD, ATL WARM and PAC WARM DRVs, during the years 2001–2010, are shown in top-left, top-right, bottom-left and bottom-right-panels, respectively). As is to be expected, the TH composites during the cold season (ATL COLD and PAC COLD groups) exhibited stronger temperature gradients than the warm season composites (ATL WARM and PAC WARM groups). The ATL COLD group averaged 10K change over 5°, and the sharpest temperature gradient occurred between (0,0) and 5° north of the DRV center. This is consistent with previous research that has observed DRV genesis to occur primarily on the south side of the baroclinic zone (W02, MM05, MMD08, BW11). The PAC COLD group averaged 6K change over 5°, but the sharpest temperature gradient occurred between (0,0) and 5° south of the DRV center. ATL WARM and PAC WARM groups have warmer temperature overall, but the temperature changes average to 5K over 5°. There is a definite change in the orientation of the baroclinic zone from SW to NE in the Cold season, to more zonal in the Warm seasons. This might be climatological because the DRVs preferentially form over the warm currents (Gulf Stream in ATL and Kuroshio Current in PAC), which are oriented SW to NE.
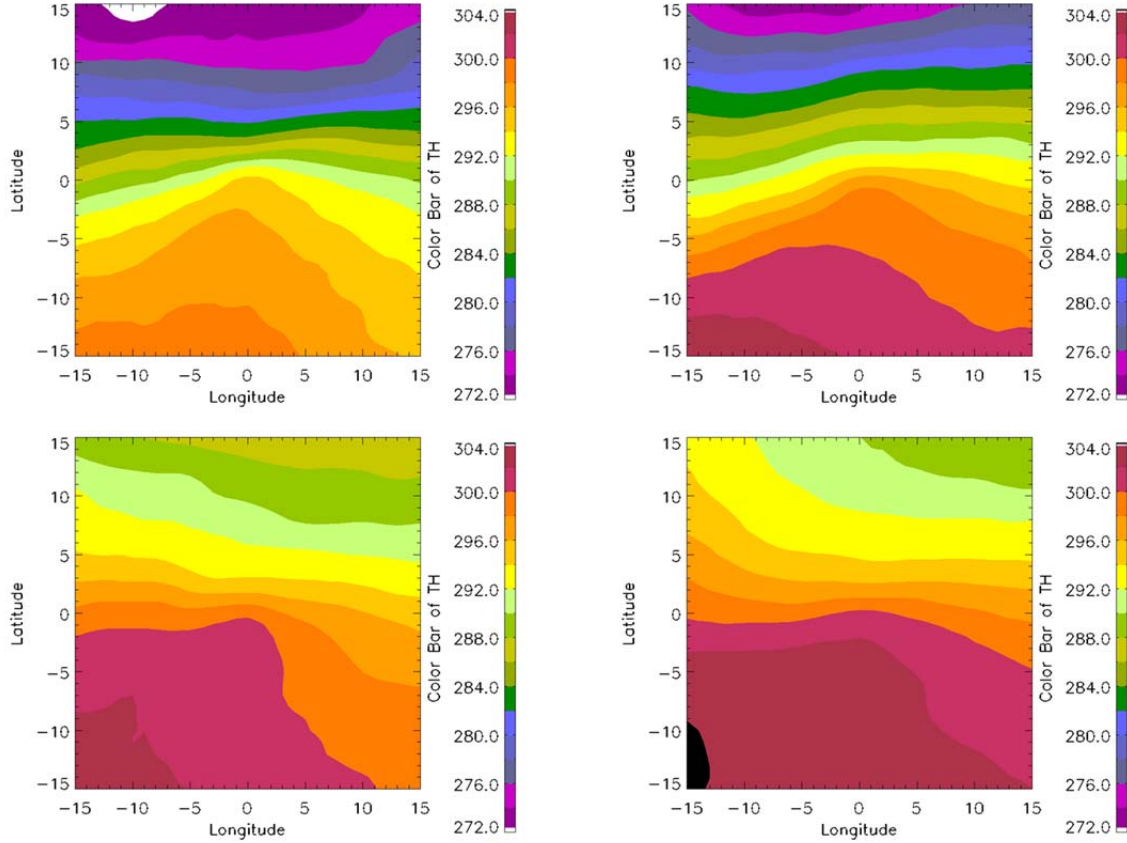
Figure 76.   Horizontal composite of TH (potential temperature; K) @884 hPa of ATL COLD, PAC COLD, ATL WARM and PAC WARM DRVs, during the years 2001–2010, are shown in top-left, top-right, bottom-left and bottom-right-panels, respectively.

2.   Disturbance Structure

In comparison to a typical EC (extratropical cyclone), a DRV is significantly shorter in both its horizontal and vertical extent.   The horizontal PV composites at 930 hPa (pressure level chosen for the robust signals) of DRVs for all four groups (ATL COLD, ATL WARM, PAC COLD and PAC WARM), are shown in top-left, top-right, bottom-left, and bottom-right-panels of Figure 77, respectively. By using 0.6 PVU as the color-shading cutoff, note that the 930 hPa PV composites (which embodies DRVs) assume elliptical shapes, where the transverse to conjugate diameter is about 700 to 350 km (these distances are consistent with idealized and observed DRVs as short scale disturbances). The elliptical shape also makes sense, since the previous PV anomaly is to

the west of the newly-generated PV anomaly, which in general move ENE, hence the elliptical shape oriented along the baroclinic zone.
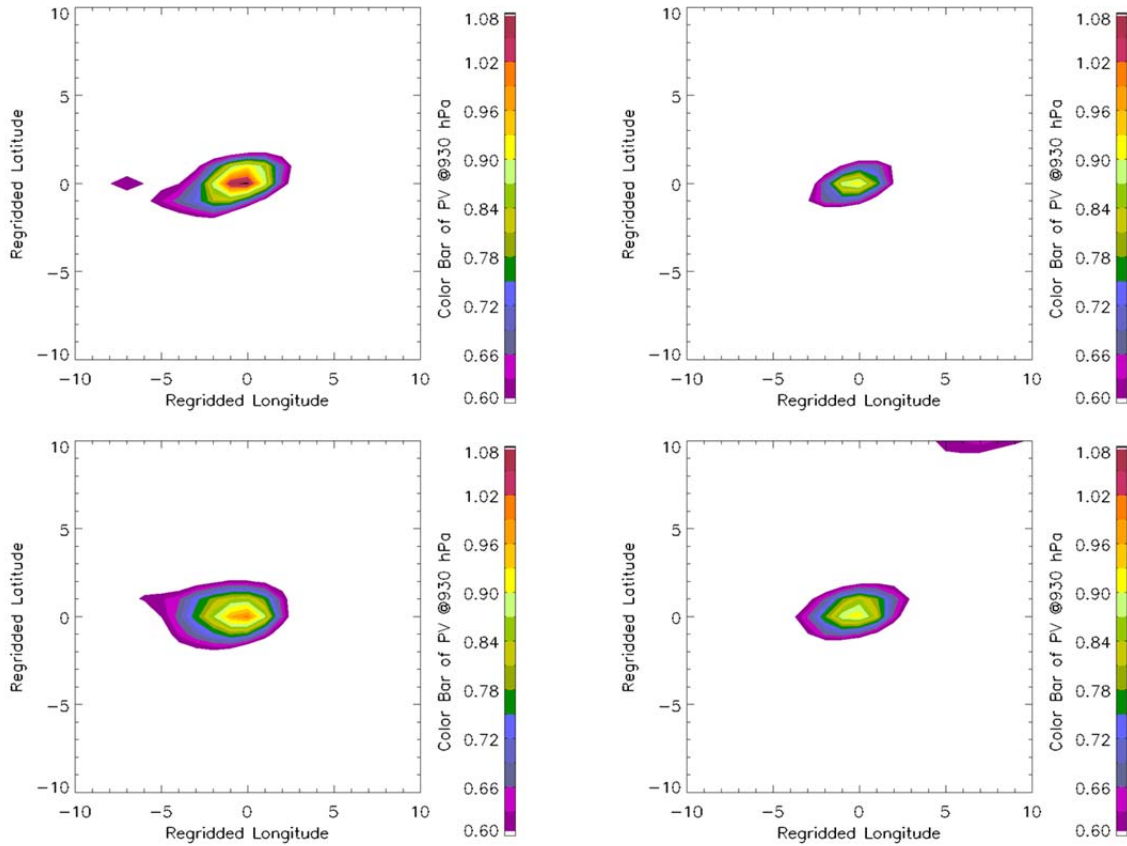
Figure 77.   Horizontal composite of PV (potential vorticity; PVU) @930 hPa of ATL COLD, PAC COLD, ATL WARM and PAC WARM DRVs, during the years 2001–2010, are shown in top-left, top-right, bottom-left and bottom-right-panels, respectively.

The vertical PV composites, sliced at 30° angle through the DRVs (from the NW to SE), for all four groups (ATL COLD, ATL WARM, PAC COLD and PAC WARM), are shown in top-left, top-right, bottom-left, and bottom-right-panels of Figure 78, respectively. Again by using 0.6 PVU as the color-shading cutoff, the enhanced lower tropospheric PV (which embody DRVs) are consistent with the idealized and observed DRVs as being short scale disturbances. Also note that because slices were made at 30° angle through the DRVs, the composites were able to capture the lowering of the DT (dynamic tropopause) further toward the northwest, as indicated by the sloping 1.5 PVU

white lines. This again is an indication that the DRV genesis is occurring to the south of the main axis of the baroclinic zone. The horizontal scale exhibited in the composites range between 3° to 6°, which equates to between 300 to 600 km (distance estimated based on average DRV latitude of 37°).
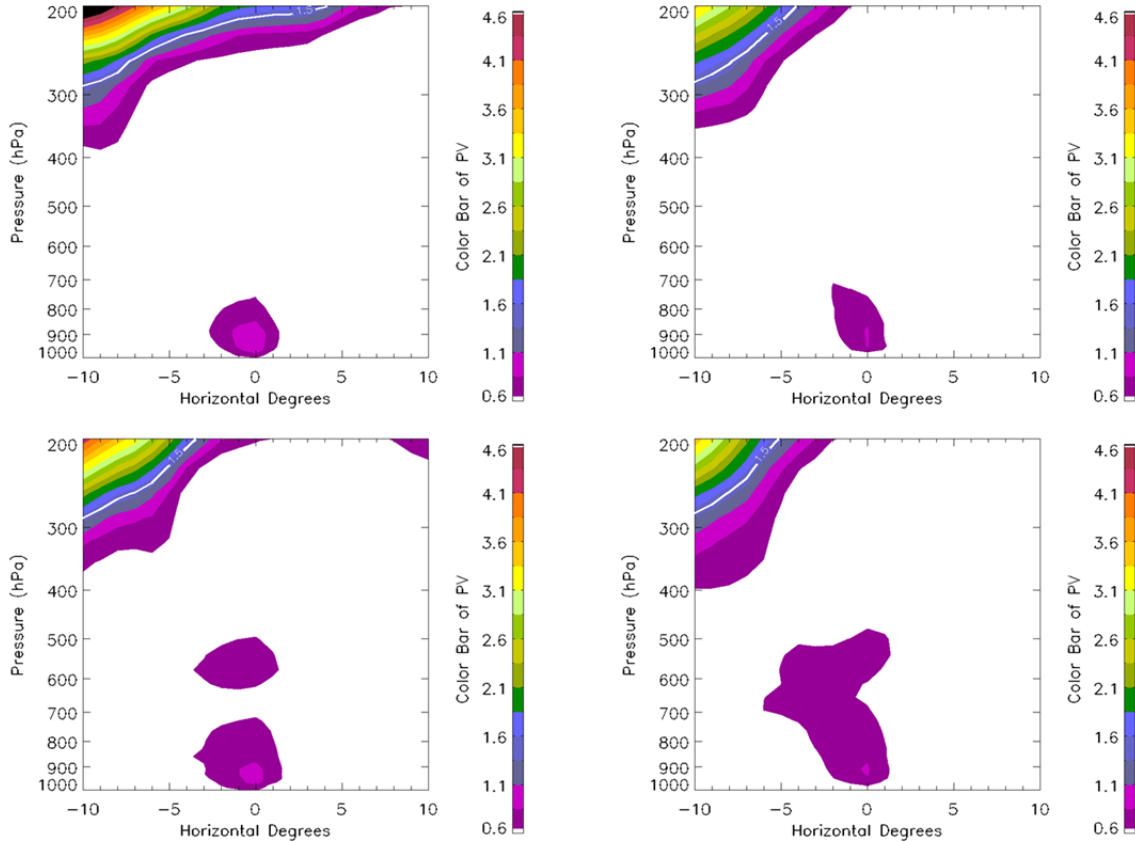
Figure 78.   Vertical (WNW to ESE slice at 30°) composite of PV (potential vorticity; PVU) centered over DRVs of ATL COLD, PAC COLD, ATL WARM and PAC WARM, during the years 2001–2010, are shown in top-left, top-right, bottom-left and bottom-right-panels, respectively.   The horizontal scale equates to approximately 1000 km for every 10 degrees (for average DRV latitude of 37°).   The DT (dynamic tropopause) is approximated by the 1.5 PVU white line.

A DRV does not require upper tropospheric forcing, because it is a self-sustaining entity that thrives on the diabatic production of positive lower tropospheric PV. The horizontal composites of 930 hPa PV (shading; PVU), MSLP (black contours; every 2 hPa) and the dynamic tropopause or DT (orange contour; 2 PVU isoline @ 250 hPa -

proxy to upper tropospheric support) of all four groups of DRVs, from 2001 to 2010, are shown in Figure 79 (ATL COLD, PAC COLD, ATL WARM and PAC WARM DRVs, are shown in top-left, top-right, bottom-left and bottom-right-panels, respectively). It appears that the DRVs, for all four groups, tend to form about 6° south of the DT, between shallow upper tropospheric trough and ridge couplets. Even though there appears to be some interaction between the DRVs and the DT from these composites, this thesis defers to the BW12 algorithm for assurance that the ascent attributed to upper tropospheric forcing (650 to 100 hPa) is less than 0.5 cm/sec (not discernible).
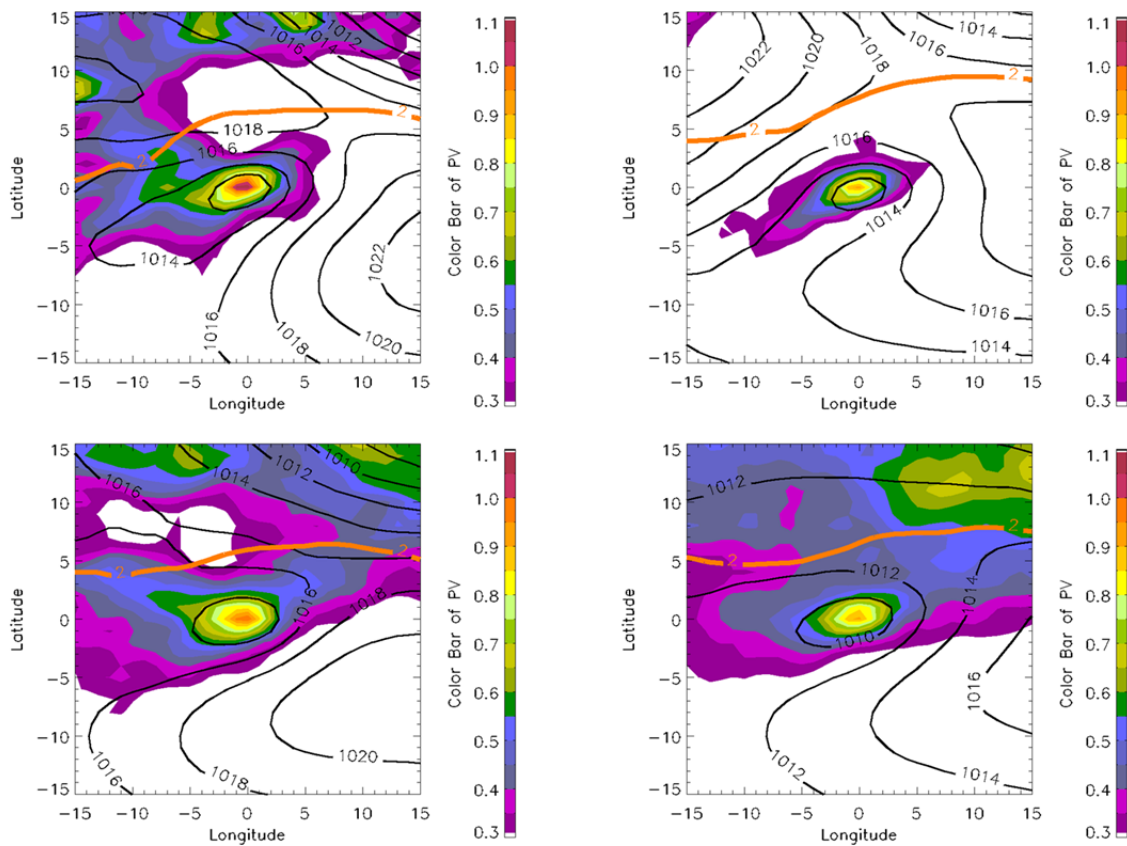
Figure 79.   Horizontal composite of 930 hPa PV (shading; PVU), MSLP (black contours; every 2 hPa), and DT (orange contour; 2 PVU isoline @250 hPa) for ATL COLD, PAC COLD, ATL WARM and PAC WARM DRVs, during the years 2001–2010, are shown in top-left, top-right, bottom-left and bottom-right-panels, respectively.

3. Diabatic Dominance

Vertical composites of diabatic heating (black contour; K/day) and temperature anomaly (shading; K) for ATL COLD, PAC COLD, ATL WARM and PAC WARM DRVs, during the years 2001–2010, are shown in top-left, top-right, bottom-left and bottom-right-panels of Figure 80, respectively. Recall from Chapter I, the collocation of positive diabatic heating and positive temeprature anomaly directly equates to the diatbatic production of eddy APE. Since the temperature anomaly scale is the same for all four groups, it is apparent that the diabatic conversion of APE is much more prominent during the cold season (ATL COLD and PAC COLD groups) in comparison to the warm season (ATL WARM and PAC WARM groups).
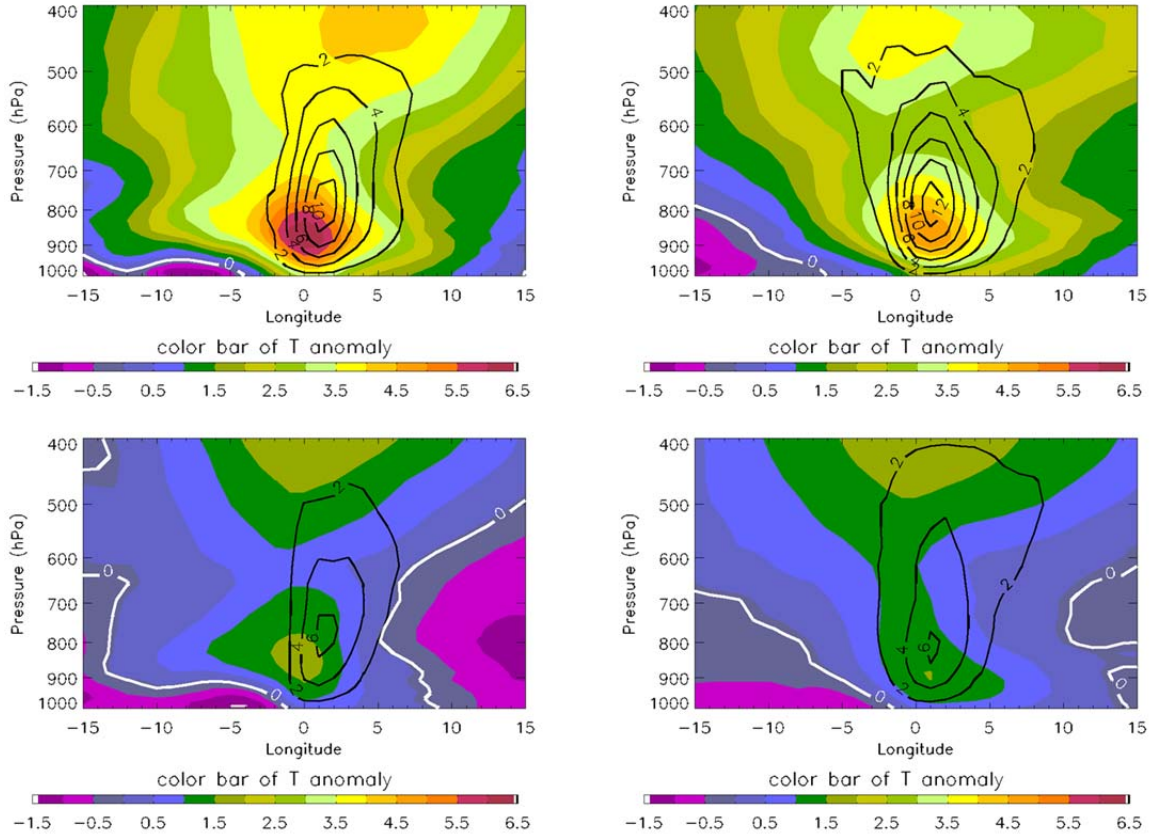
Figure 80. Vertical composites of diabatic heating (black contour; K/day, interval of 2) and temperature anomaly (shading; K) for ATL COLD, PAC COLD, ATL WARM and PAC WARM DRVs, during the years 2001–2010, are shown in top-left, top-right, bottom-left and bottom-right-panels of Figure 81, respectively.

The above composite structure bears a strong resemblance to that seen in extreme winter storm Lothar (W02), the East Coast Snowstorm (MMD08), the N ATL Cyclone (BW11), as well as the MM5 simulation (Moore, Montgomery and Davies 2012 [submitted]), in top-left, top-right, bottom-left and bottom-right-panels of Figure 81, respectively.
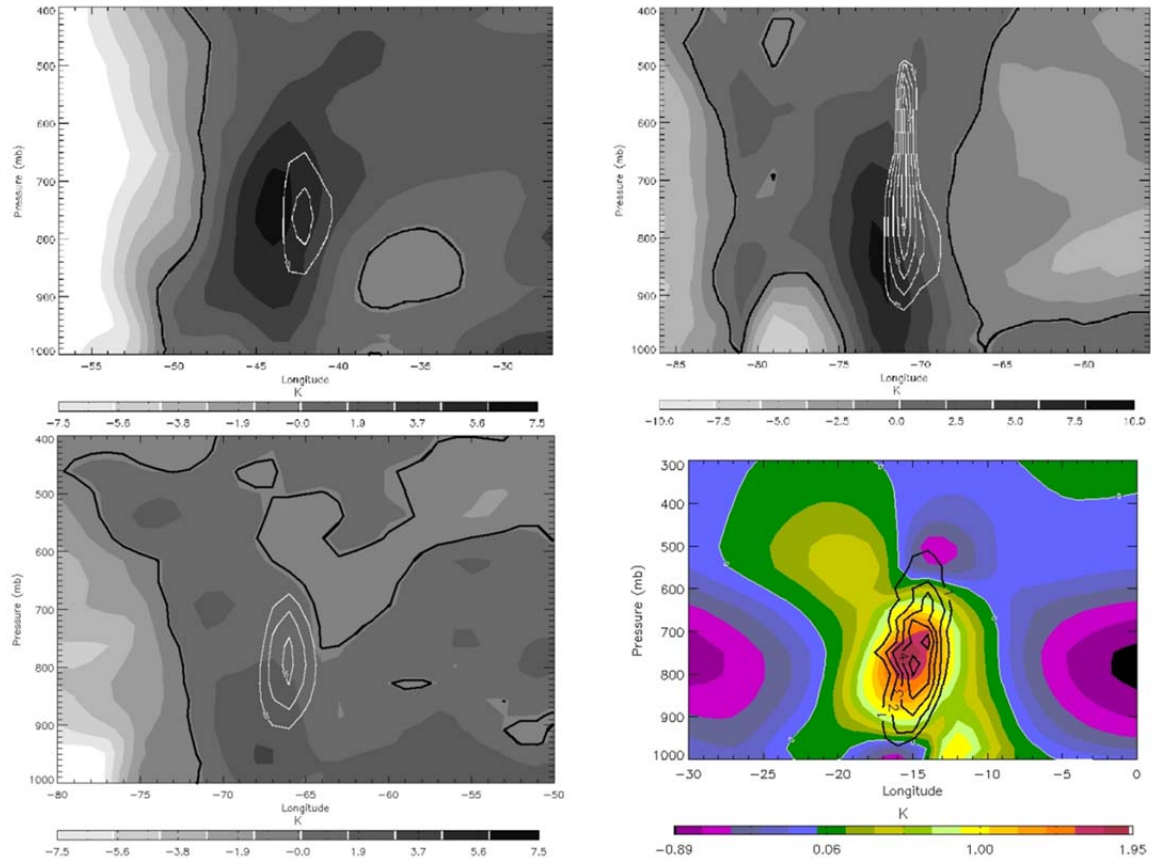
Figure 81.   Longitude pressure cross section for extreme winter storm Lothar on 00 UTC 25 December 1999 at 43N (W02; top-left), the East Coast snowstorm on 00 UTC 25 February 2005 at 37N (MMD08; top-right), and the North Atlantic cyclone on 00 UTC 19 December 2005 at 34N (BW11; bottom-left), showing temperature anomaly (shading, K) and diabatic heating (white contour; K/6 hr, contour starts at 20 in intervals of 5). Longitude pressure cross section of temperature anomaly (shading; K) and diabatic heating (black contour; K/day) for 2D SG model simulation of DRV growth at day 4.5, 40N (MM04; bottom-right).

Even though diabatic effects can attribute for up to 60% of storm intensity for some ECs, a typical EC is dominated by baroclinic process, whereas a DRV is dominated

by the diabatic process, as shown back in Figure 13. As mentioned in Chapter I, Mak (1994) stated that perturbation PV would increase where latent heating increases with height, and decrease where latent heating decreases with height. In other words, diabatic heating would give rise to significant local positive or negative PV generation where there is a sharp vertical gradient in the heating rate (while there is zero net PV change within the convective column). The vertical composites of PV generation rate or PVR (color shade; PVU/hr), superposed by diabatic heating or CH (black contours, positive values only; K/day, contour interval of 1.5), for all four DRV groups, are shown in Figure 82.
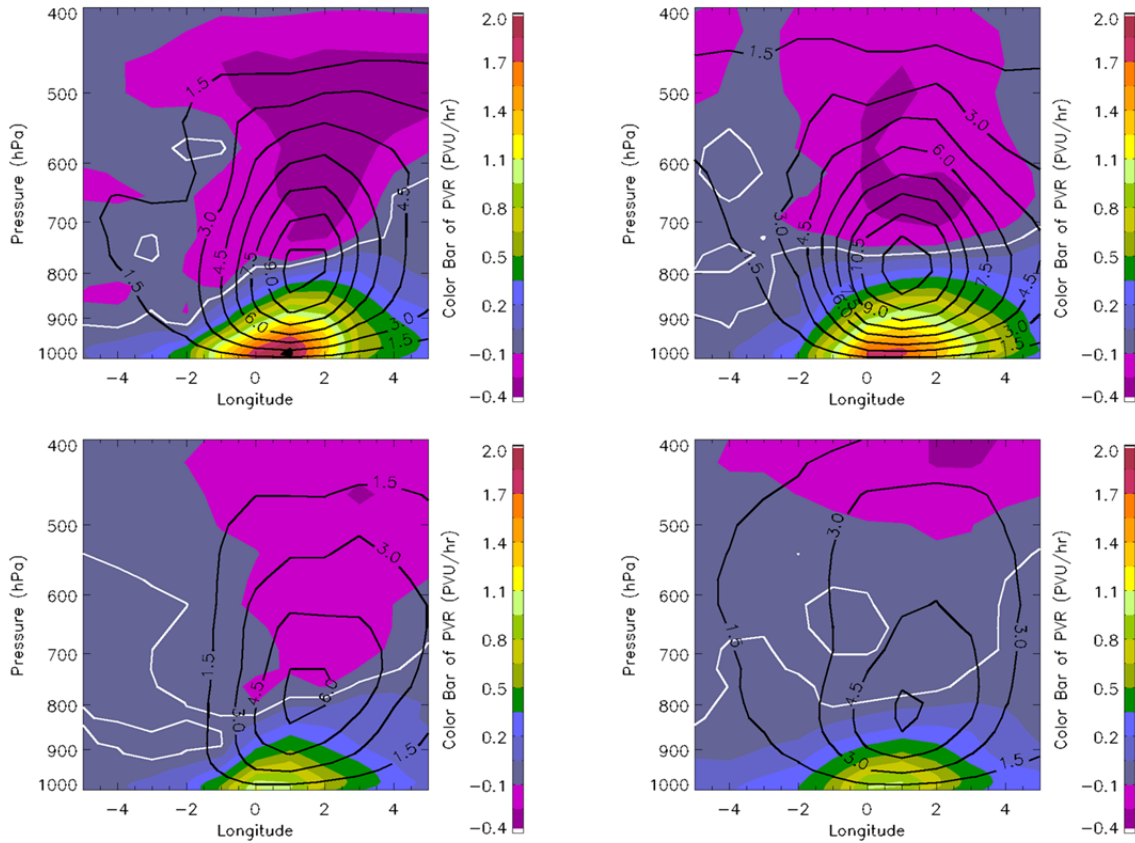
Figure 82. Vertical composites of PV generation rate or PVR (shading; PVU/hr), superposed by diabatic heating or CH (black contours, positive values only; K/day), for ATL COLD, PAC COLD, ATL WARM and PAC WARM DRV groups from 2001 to 2010, in top-left, top-right, bottom-left and bottom-right-panels, respectively. The white line represents PVR value of 0, delineating the negative PVR above from the positive PVR below.

4. Consistency with Literature

For intellectual curiosity, the composite results were compared to that of previous work examining idealized and observed DRVs. This comparison revealed that the limited number of DRV studies in the peer-reviewed literature *are* representative of the larger number of "real world" DRVs, as identified by BW12 algorithm during the years 2001–2010.

Vertical composite of PV, TH and V (as shown in Figure 83) were constructed at the time of DRV formation, for all four groups (as outlined in the beginning of this chapter). Note that all four panels of Figure 83 are qualitatively similar to left-panel of Figure 17 (Lothar), as well as left-panel of Figure 22 (East Coast Snowstorm), with a distinct positive PV anomaly associated with the DRV. To the east of this anomaly, there is strong flow from the south to the north. In addition, there is a clear warm core structure evident in the TH field.
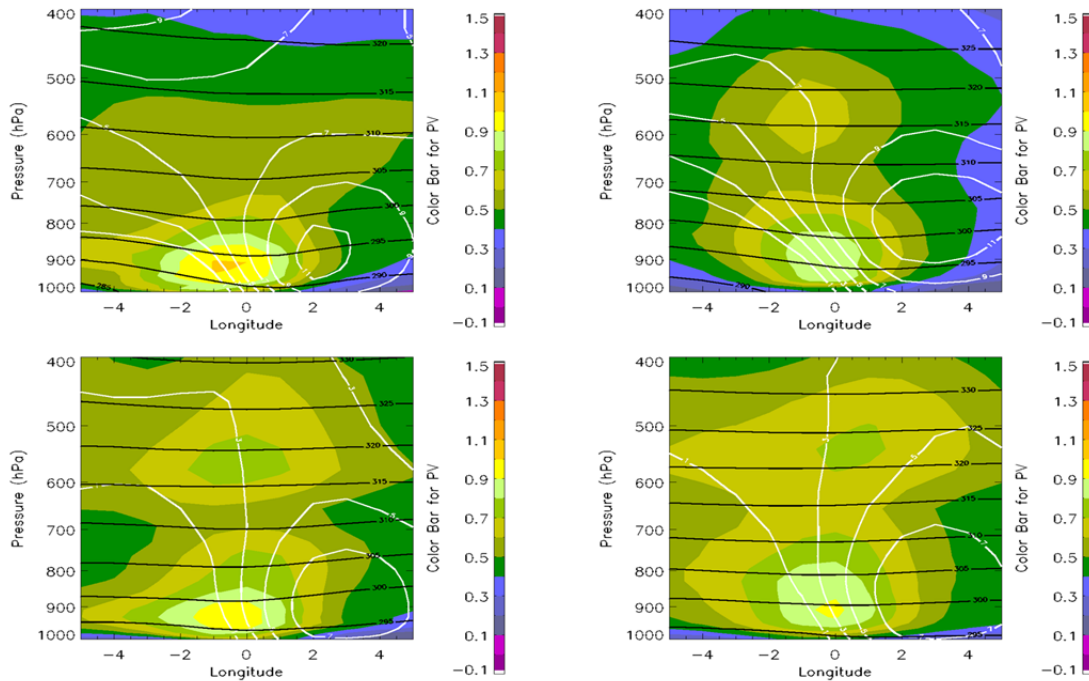
Figure 83. Vertical composites of PV (shading; PVU), TH (K) and V (white contours; positive values only in 2 m/s interval) for ATL COLD, PAC COLD, ATL WARM and PAC WARM DRV groups during the years 2001–2010, in top-left, top-right, bottom-left and bottom-right-panels, respectively. Note their structural similarity to the vertical composites of PV, TH and V from Lothar (Figure 17 left-panel) and East Coast Snowstorm (Figure 22 left-panel).

In the same vein, vertical composites of PV generation rate or PVR (shading; PVU/hr) and vertical velocity or W (black contours; positive values only in 1.5 m/s interval) were constructed as shown in Figure 84. Note their structural similarity to the right-panels of Figure 17 and Figure 22, with rising motion (which implies latent heat release) depicted by positive values of W. Positive PV production is evident at the lower levels, with PV depletion at higher levels.
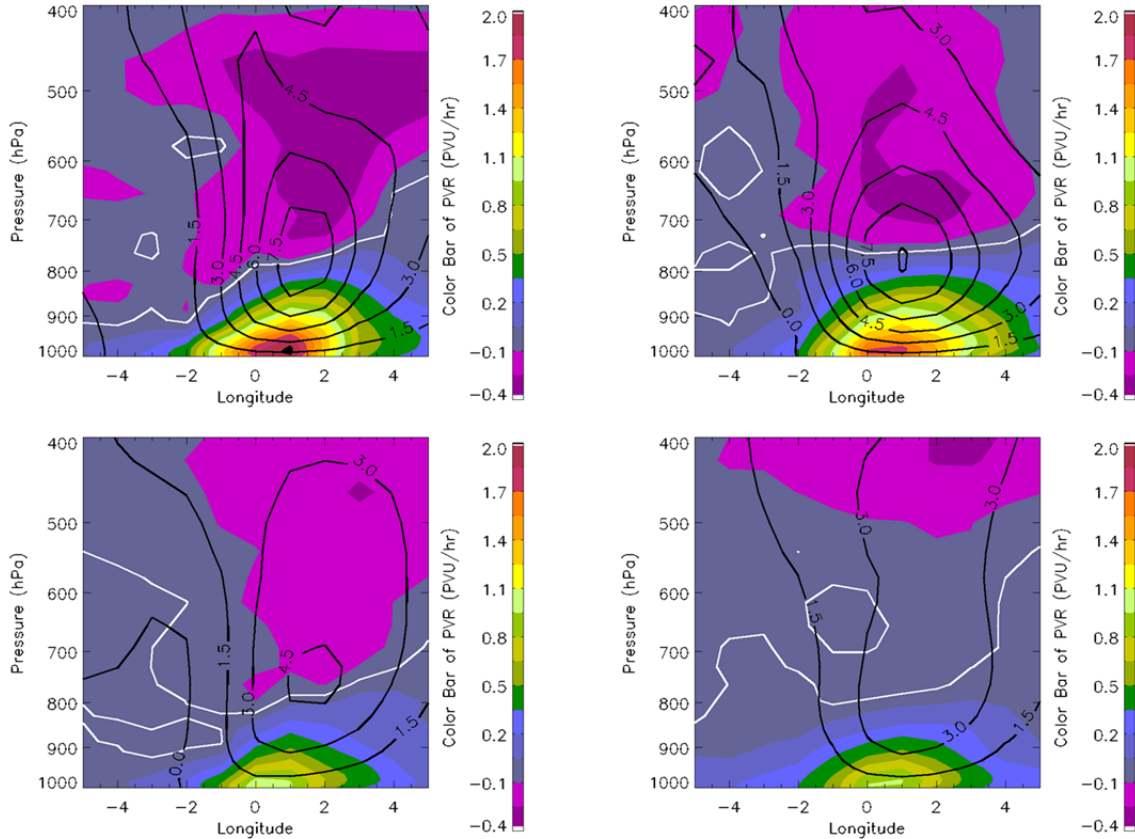
Figure 84.   Vertical composite of PV generation rate or PVR (shading; PVU/hr) and vertical velocity or W (black contours; positive values only in 1.5 m/s interval) for ATL COLD, PAC COLD, ATL WARM and PAC WARM DRV groups during the years 2001–2010, in top-left, top-right, bottom-left and bottom-right-panels, respectively. Note their structural similarity to the vertical composites of PVR and W from Lothar (right-panel of Figure 17) and East Coast Snow Storm (right-panel of Figure 22).

B. STATISTICALLY SIGNIFICANT ANOMALY PLOTS 6 TO 24 HOURS PRIOR TO DRV FORMATION

In the light of the 12% DRVs which functioned as precursors and/or pathways to explosive cyclogenesis, improvement in DRV predictability is highly desirable. Statistically significant anomalous signals before DRV genesis could be leveraged as possible DRV predictors (pending further research).

1. ATL COLD

Spatially centered on the LAT/LON of DRVs (at time of formation), a series of statistically significant anomaly plots of Q were made, for ATL COLD group from 2001 to 2010, stepping back 6, 12, 18 and 24 hours prior to time of DRV formation, as shown in top-left, top-right, bottom-left and bottom-right-panels of Figure 85. Note that as time moves further back, the location of Q anomlay maximum also shifted gradually to WSW, depicting the average track of DRVs to be from WSW to ENE. Even though the intensity of Q anomaly maximum successively diminishes with each backward time step, the signal is coherent and of possible use for further research in DRV predictability.

Figure 85.　Series of statistically significant horizontal anomaly plots of Q for ATL COLD DRVs from 2001 to 2010. Top-left is 6 hours prior to DRV time of formation. Top-right is 12 hours prior to DRV time of formation. Bottom-left is 18 hours prior to DRV time of formation. Bottom-right is 24 hours prior to DRV time of formation.

Similar conclusion can be drawn by making a series of statistically significant anomaly plots of TH, also spatially centered on the LAT/LON of DRVs (at time of formation), for ATL COLD group from 2001 to 2010, stepping back 6, 12, 18 and 24 hours prior to time of DRV formation, as shown in top-left, top-right, bottom-left and bottom-right-panels of Figure 86. In addition to the anomalous baroclinicity, these plots also point out the warm core within the DRVs.

Figure 86.   Series of statistically significant horizontal anomaly plots of TH for ATL COLD DRVs group from 2001 to 2010. Top-left is 6 hours prior to DRV time of formation. Top-right is 12 hours prior to DRV time of formation. Bottom-left is 18 hours prior to DRV time of formation. Bottom-right is 24 hours prior to DRV time of formation.

2.   PAC COLD

As done previously for the ATL COLD DRV group, a series of statistically significant anomaly plots of Q were made, centering on LAT/LON of DRV at time of formation, for the PAC COLD group from 2001 to 2010, stepping back 6, 12, 18 and 24 hours prior to time of DRV formation, as shown in top-left, top-right, bottom-left and bottom-right-panels of Figure 87. In comparison to ATL COLD group, the PAC COLD group has more robust anomalous Q signals depicting the possible locations of DRVs prior to formation.

93

Figure 87.   Series of statistically significant horizontal anomaly plots of Q for PAC COLD DRVs from 2001 to 2010. Top-left is 6 hours prior to DRV time of formation. Top-right is 12 hours prior to DRV time of formation. Bottom-left is 18 hours prior to DRV time of formation. Bottom-right is 24 hours prior to DRV time of formation.

A series of statistically significant anomaly plots of TH were constructed, centering on LAT/LON of DRV at time of formation, for the PAC COLD group from 2001 to 2010, stepping back 6, 12, 18 and 24 hours prior to time of DRV formation, as shown in top-left, top-right, bottom-left and bottom-right-panels of Figure 88. This time, the ATL COLD group has more robust anomalous TH signals depicting the possible locations of DRVs prior to formation, in comparison to the PAC COLD group.

Figure 88.   Series of statistically significant horizontal anomaly plots of TH for PAC COLD DRVs group from 2001 to 2010. Top-left is 6 hours prior to DRV time of formation. Top-right is 12 hours prior to DRV time of formation. Bottom-left is 18 hours prior to DRV time of formation. Bottom-right is 24 hours prior to DRV time of formation.

3.   ATL WARM

As done previously for the COLD groups, a series of statistically significant anomaly plots of Q were made for the ATL WARM group. The anomaly plots were also centered on LAT/LON of DRV at time of formation, from 2001 to 2010. The anomaly plots were obtained by stepping back 6, 12, 18 and 24 hours prior to time of DRV formation, as shown in top-left, top-right, bottom-left and bottom-right-panels of Figure 89. In comparison to ATL COLD group, even though the SSTs are warmer during the warm season, the ATL WARM group has slightly less intense anomalous Q signals.
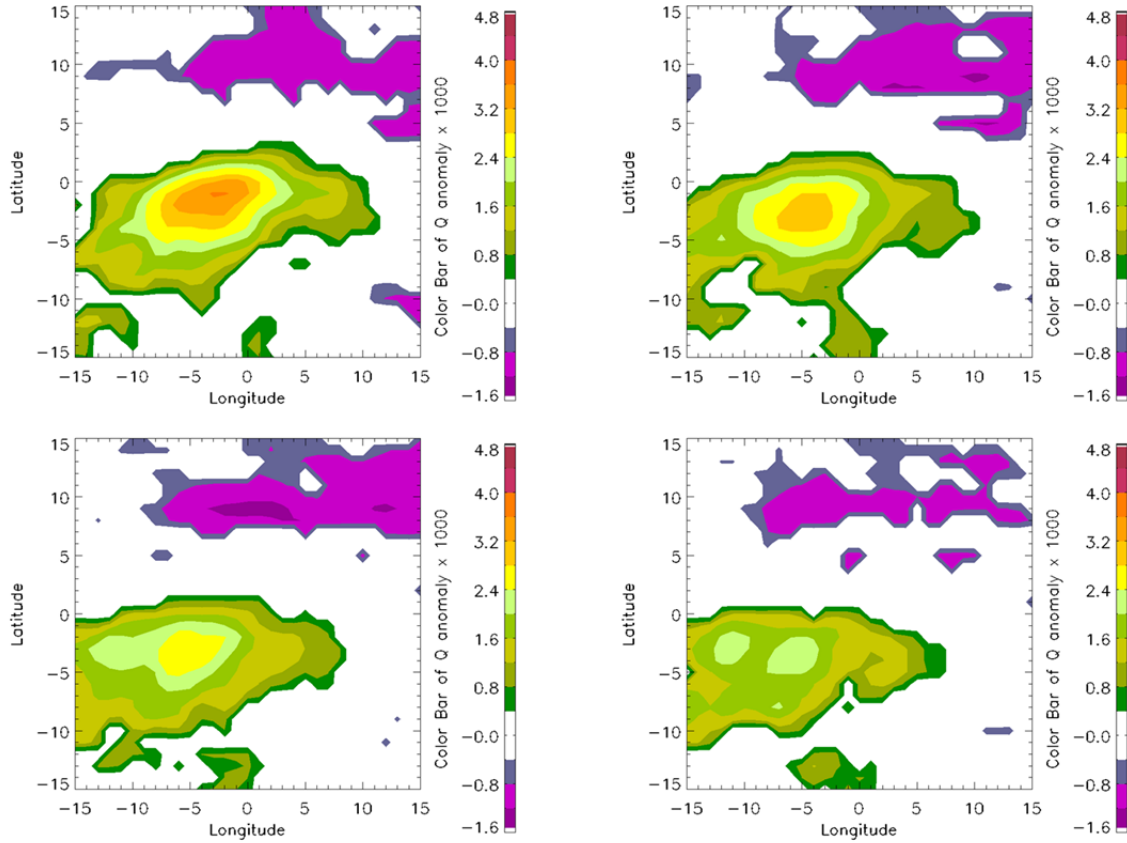
Figure 89.   Series of statistically significant horizontal anomaly plots of Q for ATL
              WARM DRVs from 2001 to 2010. Top-left is 6 hours prior to DRV time of
              formation. Top-right is 12 hours prior to DRV time of formation. Bottom-left
              is 18 hours prior to DRV time of formation. Bottom-right is 24 hours prior to
              DRV time of formation.

A similar series of statistically significant anomaly plots of TH for ATL WARM
group are shown in Figure 90. The plots were obtained by centering on LAT/LON of
DRV at time of formation, during the warm seasons of 2001 through 2010, but stepping
back 6, 12, 18 and 24 hours prior to time of DRV formation. In comparison to the ATL
COLD group, even though the temperatures are warmer during the warm season, the
ATL WARM group had much weaker anomalous TH signals, which may not be useful
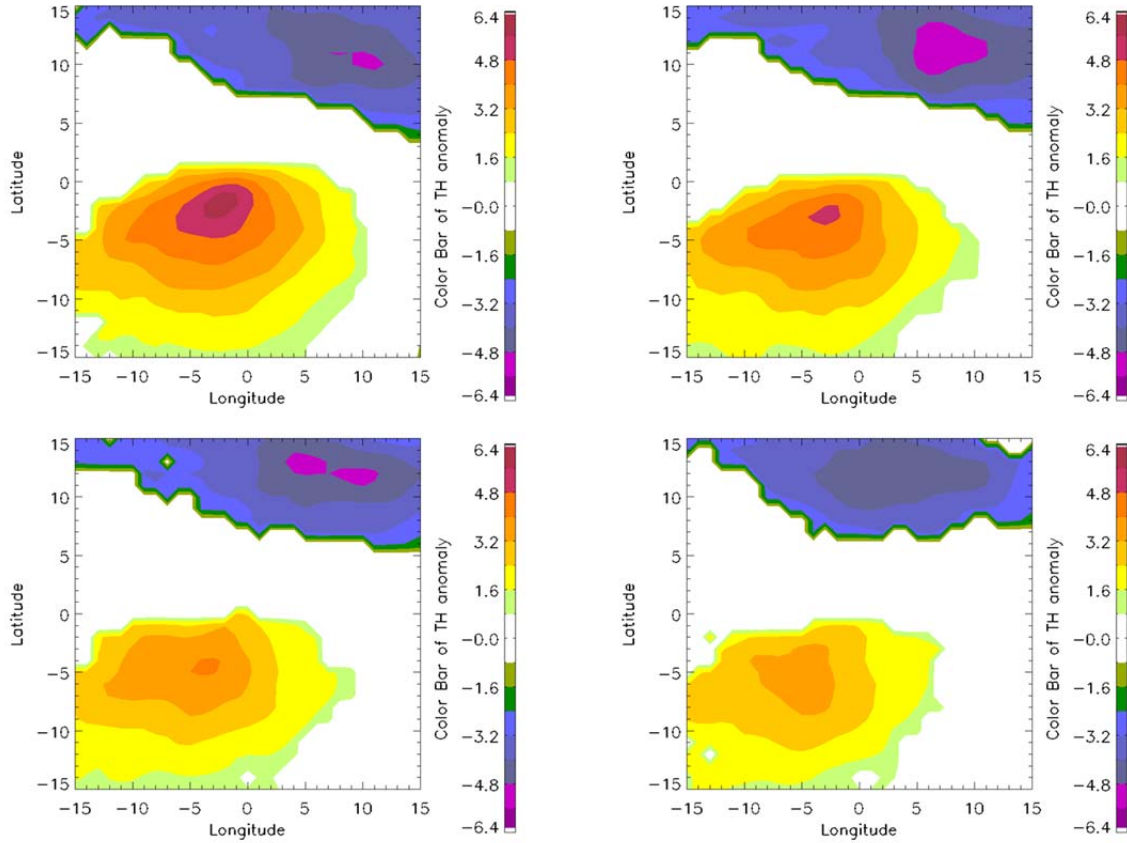for DRV predictability.

Figure 90.   Series of statistically significant horizontal anomaly plots of TH for ATL
WARM DRVs group from 2001 to 2010. Top-left is 6 hours prior to DRV
time of formation. Top-right is 12 hours prior to DRV time of formation.
Bottom-left is 18 hours prior to DRV time of formation. Bottom-right is
24 hours prior to DRV time of formation.

4.   PAC WARM

As done previously for the other three groups, a series of statistically significant
anomaly plots of Q were made for the PAC WARM group from 2001 to 2010, centering
on LAT/LON of DRV at time of formation. The plots were obtained by stepping back
6, 12, 18 and 24 hours prior to time of DRV formation, as shown in top-left, top-right,
bottom-left and bottom-right-panels of Figure 91. In comparison to PAC COLD group,
even though the SSTs are warmer during the warm season (therefore more moisture is
available), the PAC WARM group has slightly less robust anomalous Q signals,
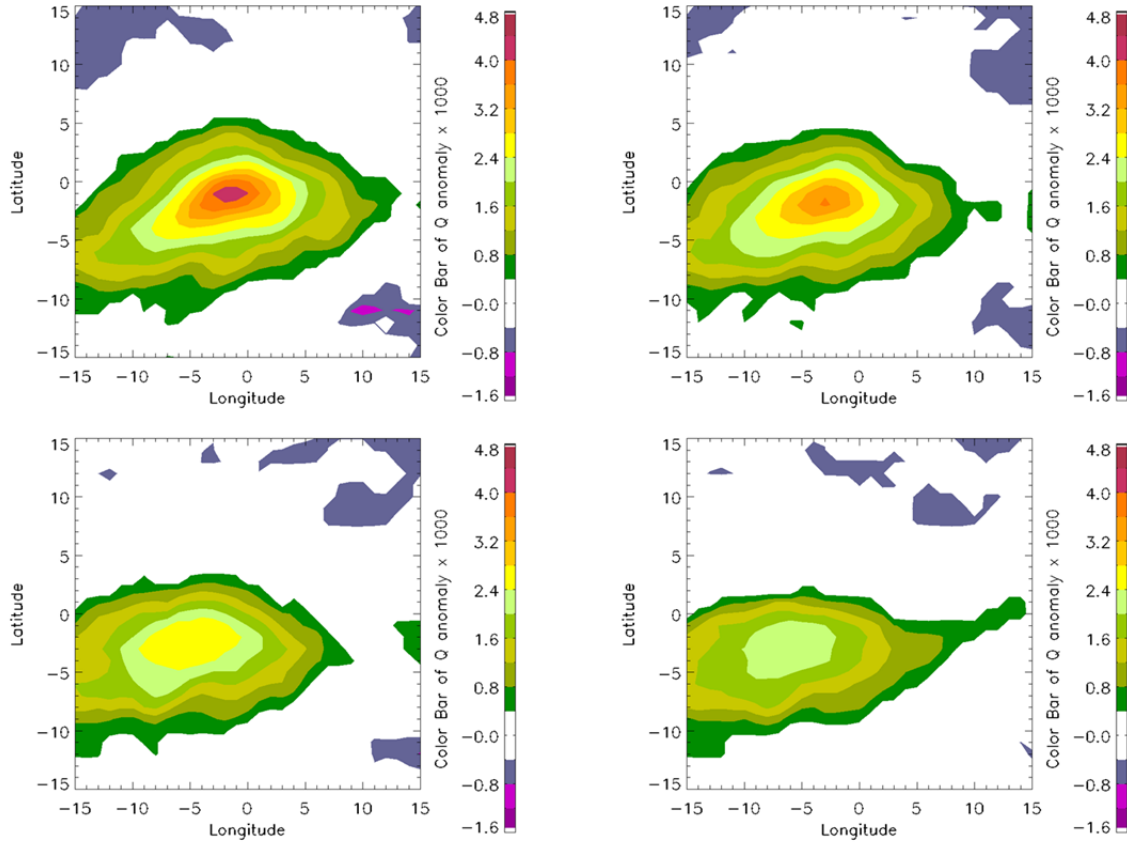depicting the possible locations of DRVs prior to formation.

97
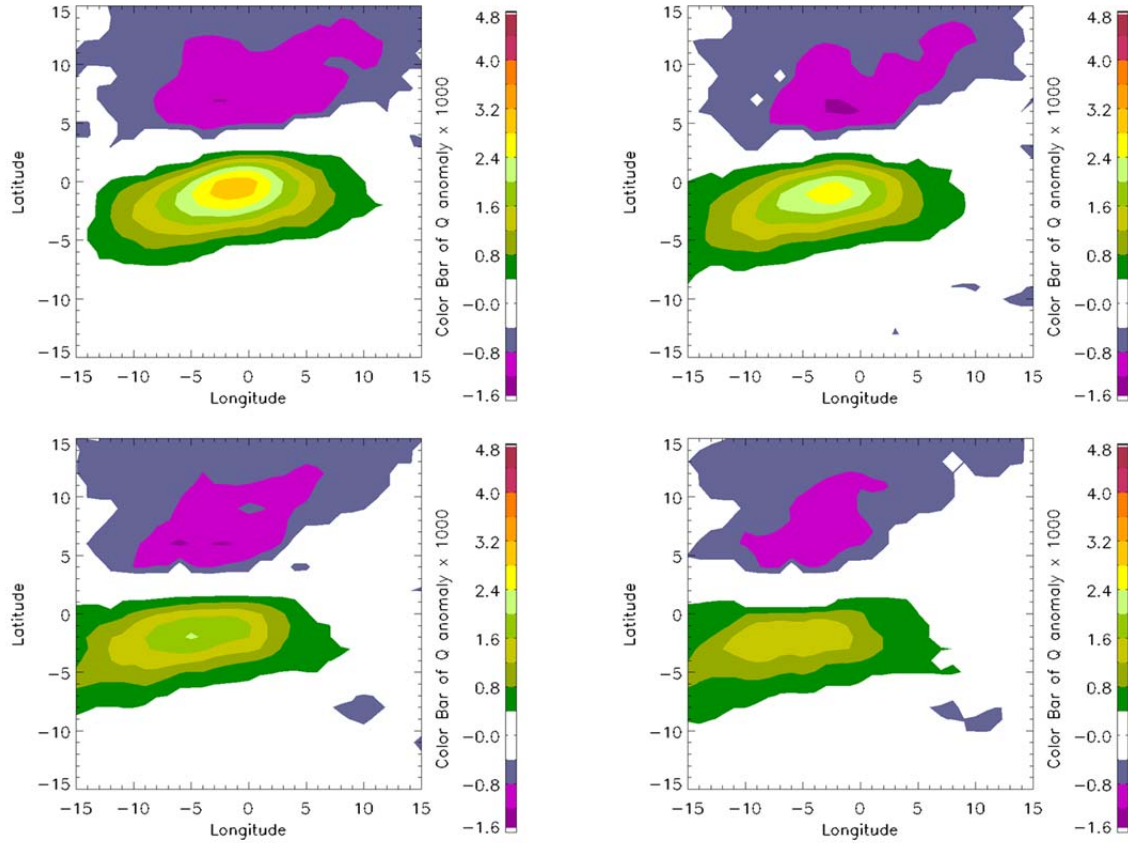
Figure 91.   Series of statistically significant horizontal anomaly plots of Q for PAC
WARM DRVs from 2001 to 2010. Top-left is 6 hours prior to DRV time of
formation. Top-right is 12 hours prior to DRV time of formation. Bottom-left
is 18 hours prior to DRV time of formation. Bottom-right is 24 hours prior to
DRV time of formation.

Same series of statistically significant anomaly plots of TH, centering on
LAT/LON of DRV at time of formation, for the PAC WARM group from 2001 to 2010,
stepping back 6, 12, 18 and 24 hours prior to time of DRV formation, are shown in top-
left, top-right, bottom-left and bottom-right-panels of Figure 92. Similar to what was
seen in the ATL basin, when compared to the PAC COLD group, even though the
temperatures are warmer during the warm season, the PAC WARM group had much
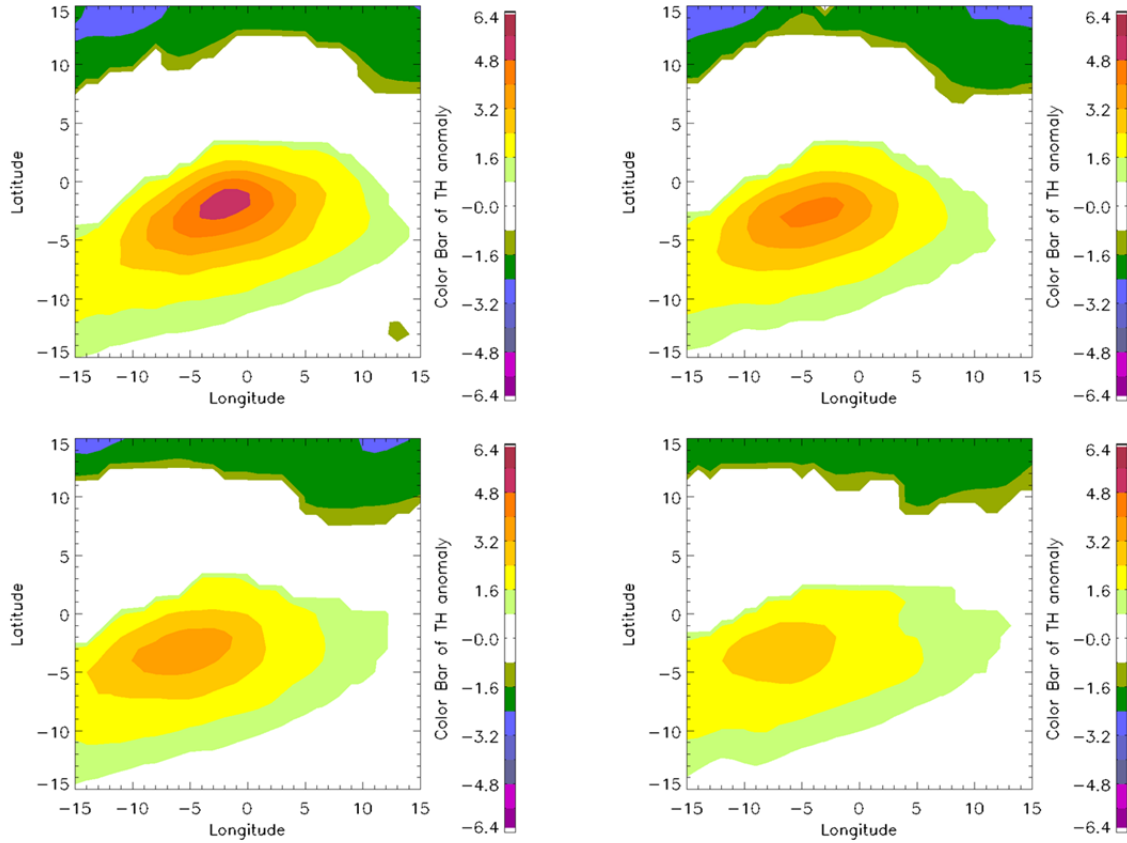weaker anomalous TH signals, for DRV predictability utilization.
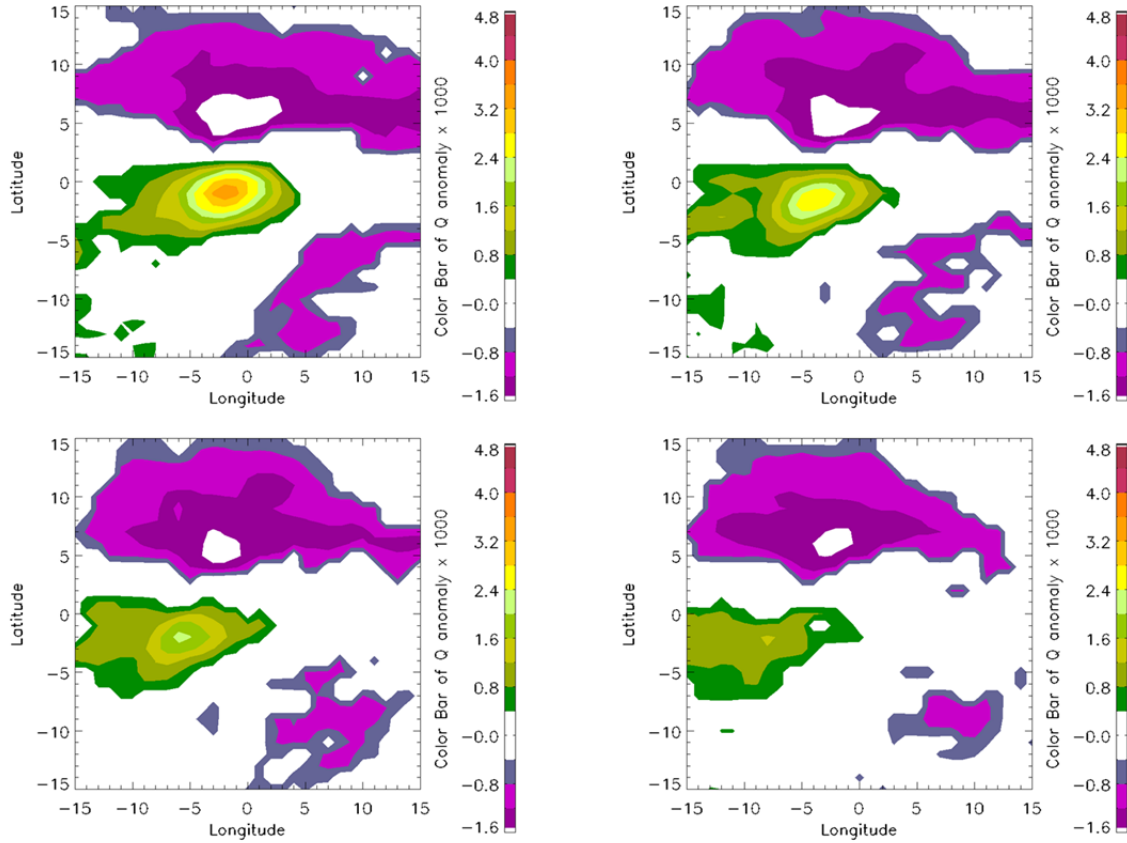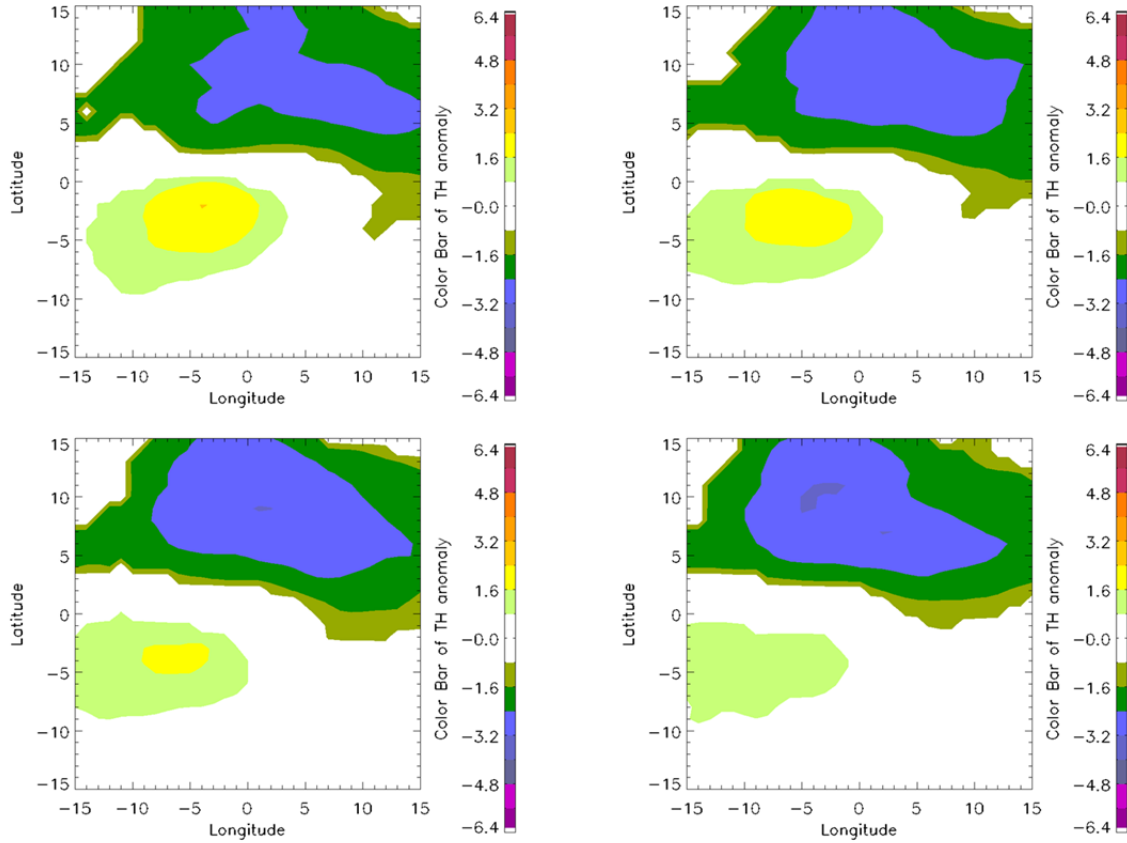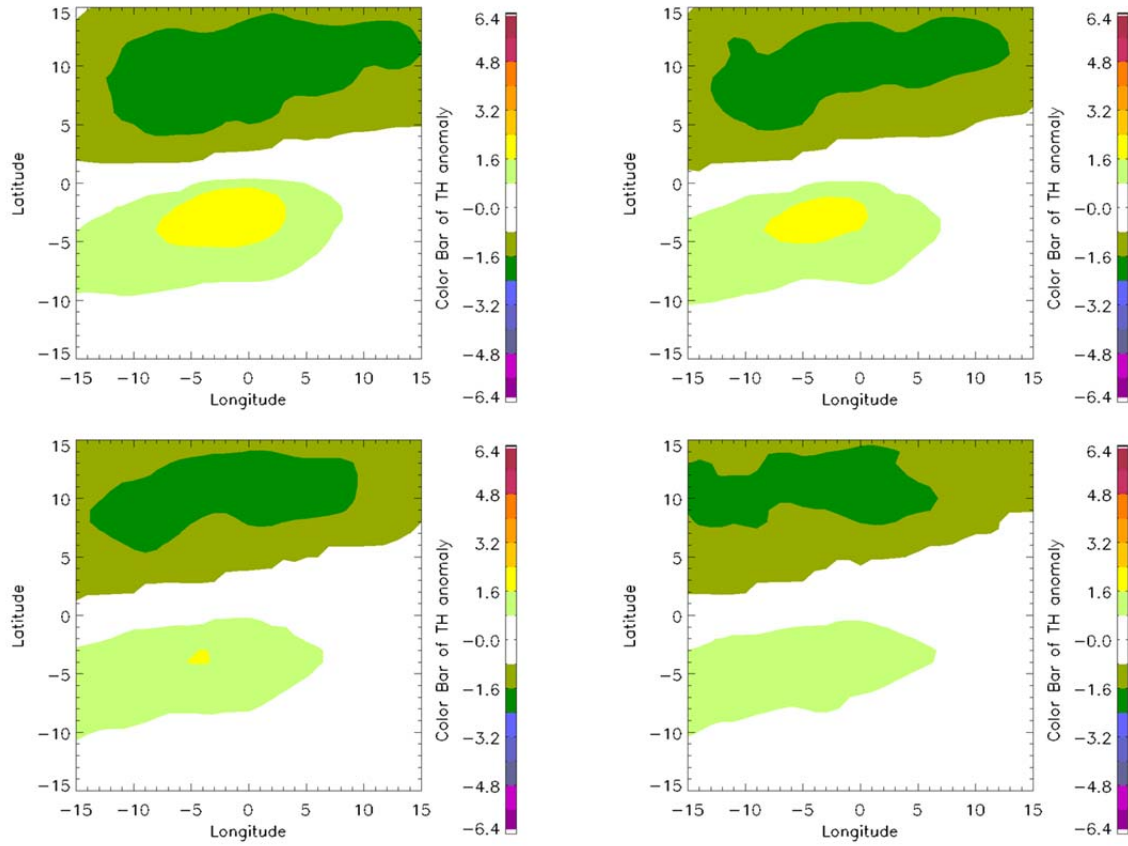
Figure 92.   Series of statistically significant horizontal anomaly plots of TH for PAC WARM DRVs group from 2001 to 2010. Top-left is 6 hours prior to DRV time of formation. Top-right is 12 hours prior to DRV time of formation. Bottom-left is 18 hours prior to DRV time of formation. Bottom-right is 24 hours prior to DRV time of formation.

THIS PAGE INTENTIONALLY LEFT BLANK

V.   HIGH IMPACT WEATHER

A.   TYPE A VS. TYPE C EXPLOSIVE CYCLOGENESIS WITH DRV ORIGINS

1.   Determination of Explosive Cyclogenesis Types (A or C)

As previously discussed in Chapter I, type A cyclogenesis starts with a pre-existing surface cyclone without upper tropospheric support, but eventually affects an upper cold trough as the surface low intensifies. On the other hand, type C cyclogenesis starts with pre-existing upper *and* lower tropospheric disturbances, while the upper tropospheric levels play a greater role. Of the 31 cases where the DRVs explosively deepened, nine (30%) of them were type A, and 22 (70%) were type C. The type of cyclogenesis was *subjectively* determined, by inspecting the interaction between the DRV and the associated upstream DT (dynamic tropopause). The bomb was designated as type A if, during the 24 hours when the disturbance underwent explosive deepening, the DT was ridging (or flat) and/or relatively distant from the DRV. On the other hand, the bomb is of type C mechanism if, during the 24 hours of explosive deepening, the DT had a pre-existing upstream trough that approached and phase-locked with the DRV. Illustrations follow.

2.   Example of Type A Explosive Cyclogenesis

a.   *Horizontal Slice with DT, MSLP and 930 hPa PV*

With fixed background map, horizontal slices of 930 hPa PV (shading; PVU), dynamic tropopause or DT (orange contour; 2 PVU isoline @ 250 hPa), and MSLP (black contours; in 2 hPa interval) of PAC DRV#2 were captured in six-hour time steps, from 06 UTC 13 February to 12 UTC 14 February, 2001, as shown in Figure 93. Note that between 06 UTC 13 February and 18 UTC 13 February (top-two and middle-left-panels), the DT grew flatter and stayed distant from the DRV (black asterisk). Then over the next six hours, the DRV affected a "kink" in the DT, and *pulled* the tropopause fold toward itself (middle-right-panel). Then by 06 UTC 14 February the DRV phase-locked with DT and reached 1 Bergeron pressure drop by 12 UTC 14 February.
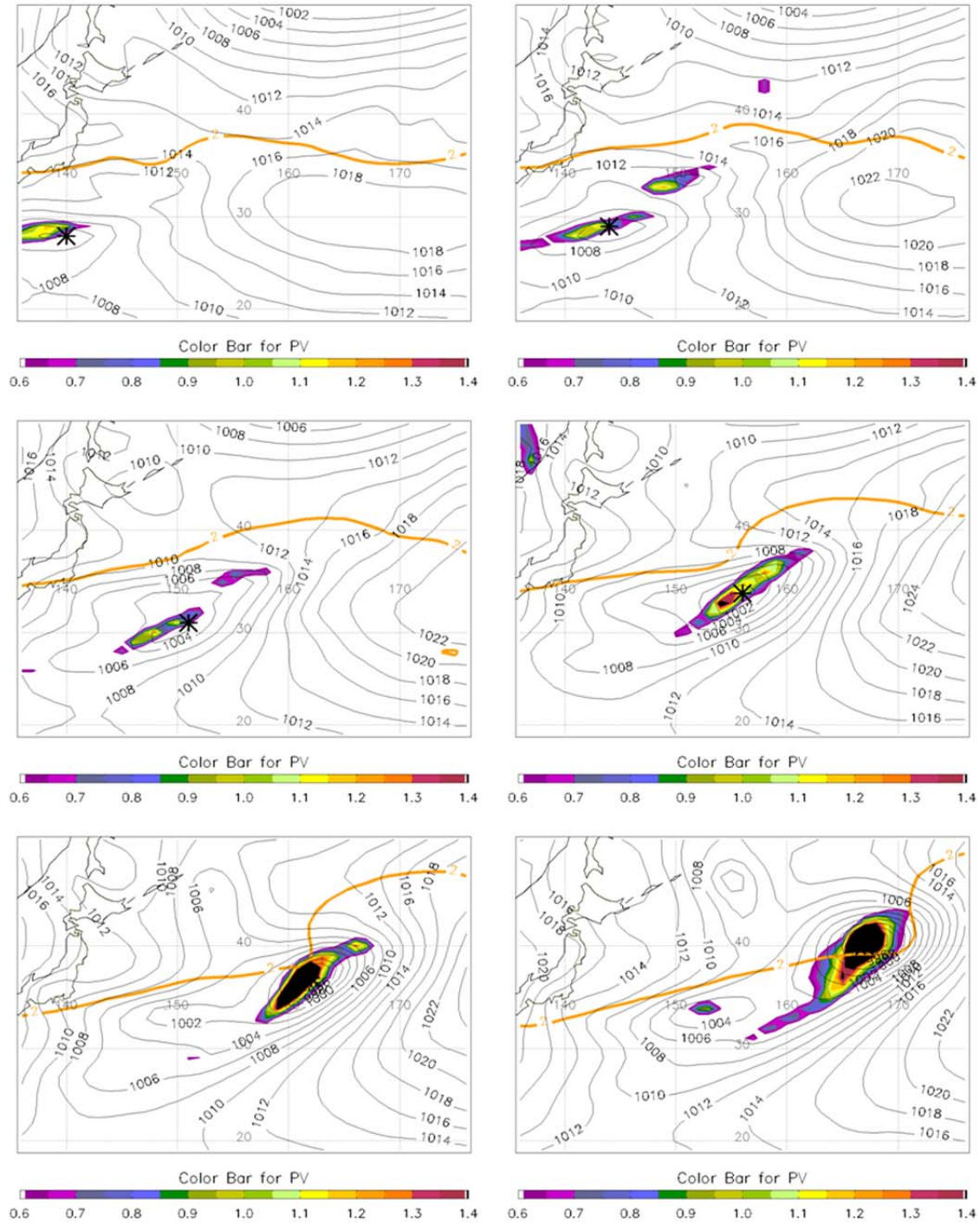
Figure 93. Horizontal slices of 930 hPa PV (shading; PVU), dynamic tropopause or DT (orange contour; 2 PVU isoline @250 hPa), and MSLP (black contours; in 2 hPa interval) of PAC DRV#2 (bomb), in six-hour time steps, from 06 UTC 13 February to 12 UTC 14 February 2001.

b. Vertical PV Slice

Moving with the LAT/LON of the DRV, vertical slices (northwest to southeast at 30°) of PV (shading; PVU) of PAC DRV#2 were captured, in six-hour time steps, from 06 UTC 13 February to 12 UTC 14 February, 2001, as shown in Figure 94. Note that from 06 UTC to 18 UTC of 13 February 2001 (top-two and middle-left-panels), the DRV was self-sustaining as the DT drifted slightly closer. Then, over the next six hours, the DRV affected a sizable change in the DT and started to pull the tropopause downward (middle-right-panel). By 06 UTC 14 February 2001, the DRV phase-locked with DT, forming a continuous PV tower, and reached 1 Bergeron pressure drop by 12 UTC 14 February 2001.

Figure 94.   Vertical slices of PV (shading; PVU), with 1.5 PVU white contour as tropopause, of PAC DRV#2 (bomb), in six-hour time steps, from 06 UTC 13 February to 12 UTC 14 February, 2001.

3.   **Example of Type C Explosive Cyclogenesis**

a.   *Horizontal Slice with DT, MSLP and 930 hPa PV*

Again with fixed background map, horizontal slices of 930 hPa PV (shading; PVU), dynamic tropopause or DT (orange contour; 2 PVU isoline @ 250 hPa), and MSLP (black contours; in 2 hPa interval) of ATL DRV#56 (N ATL cyclone in BW11) were captured, in six-hour time steps, from 00 UTC 19 December to 06 UTC 20 December, 2005, as shown in Figure 95. Note that between 00 to 06 UTC of 19 December 2005 (top-two panels), the DT was flat and distant from the DRV (black asterisk). Then over the next six hours, a distinct trough appeared in the DT upstream of the DRV (middle-left-panel). Over the next 18 hours, this DT trough continued to propagate eastward until it phase-locked with the DRV and reached 1 Bergeron pressure drop at 06 UTC 20 December 2005.
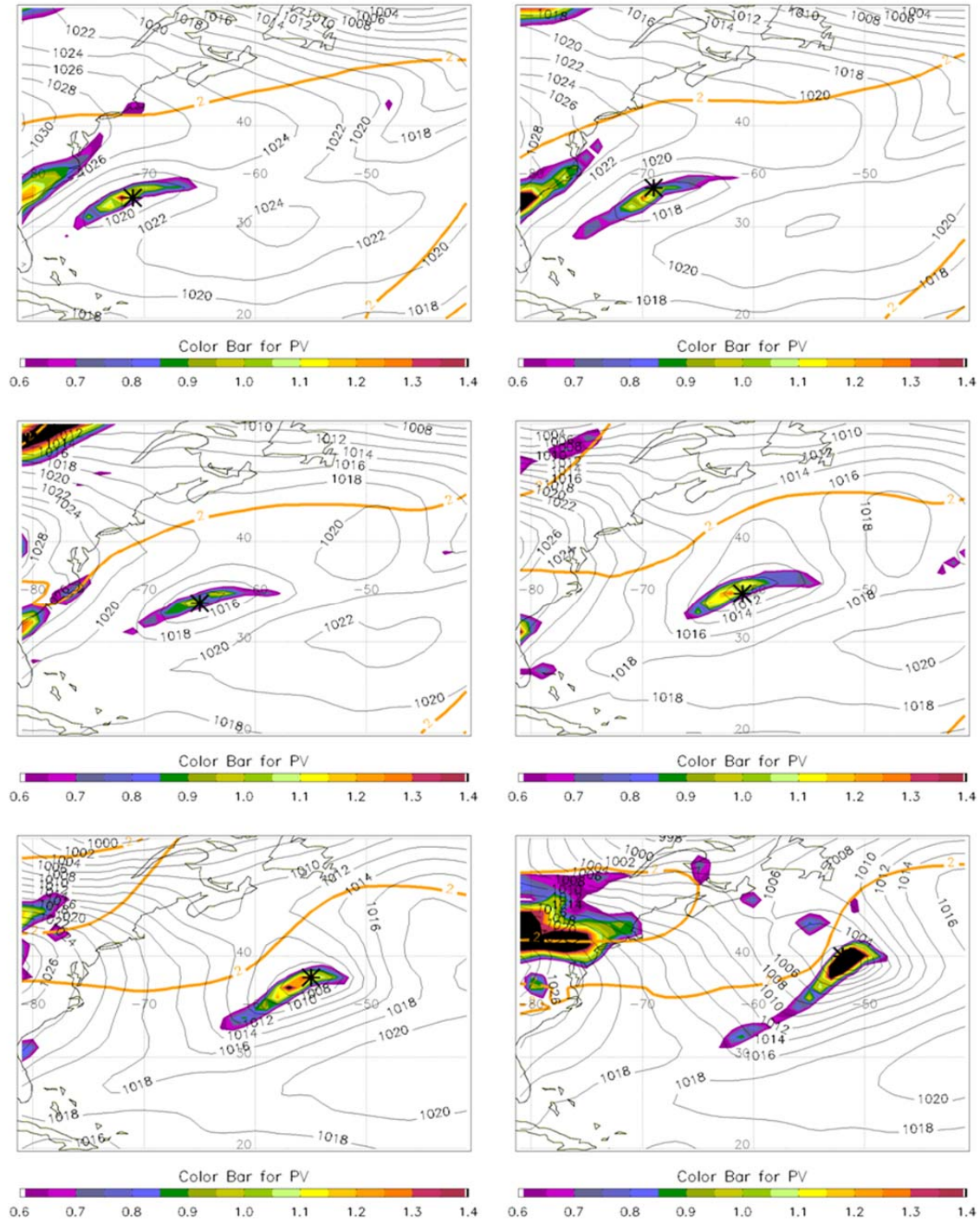
Figure 95. Same as Figure 93, except for ATL DRV#56 (N ATL cyclone from BW11). The six panels are from 00 UTC 19 December to 06 UTC 20 December 2005, in six-hour time steps.

b. Vertical PV Slice

Moving with the LAT/LON of the DRV, vertical slices (northwest to southeast at 30°) of PV (shading; PVU) of ATL DRV#56 were captured, in six-hour time steps, from 00 UTC 19 December to 06 UTC 20 December, 2005, as shown in Figure 96. Note that from 00 to 18 UTC of 19 December 2005 (top-two and middle-two panels), the DRV was self-sustaining with limited vertical growth even as the DT trough drew closer. Then over the next 12 hours, the DRV grew vertically through interaction with the lowering DT, and reached 1 Bergeron pressure drop by 06 UTC 20 December 2005.
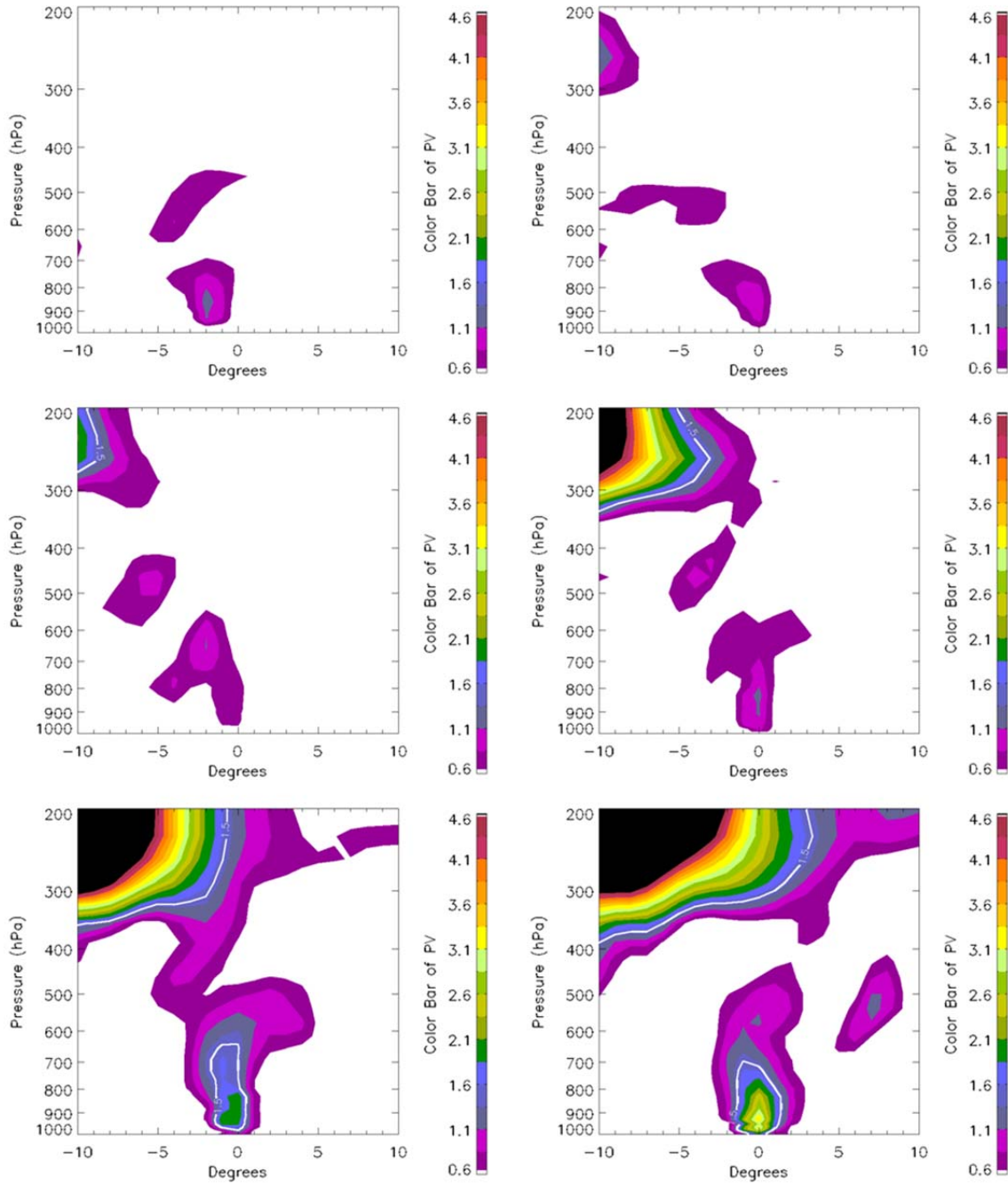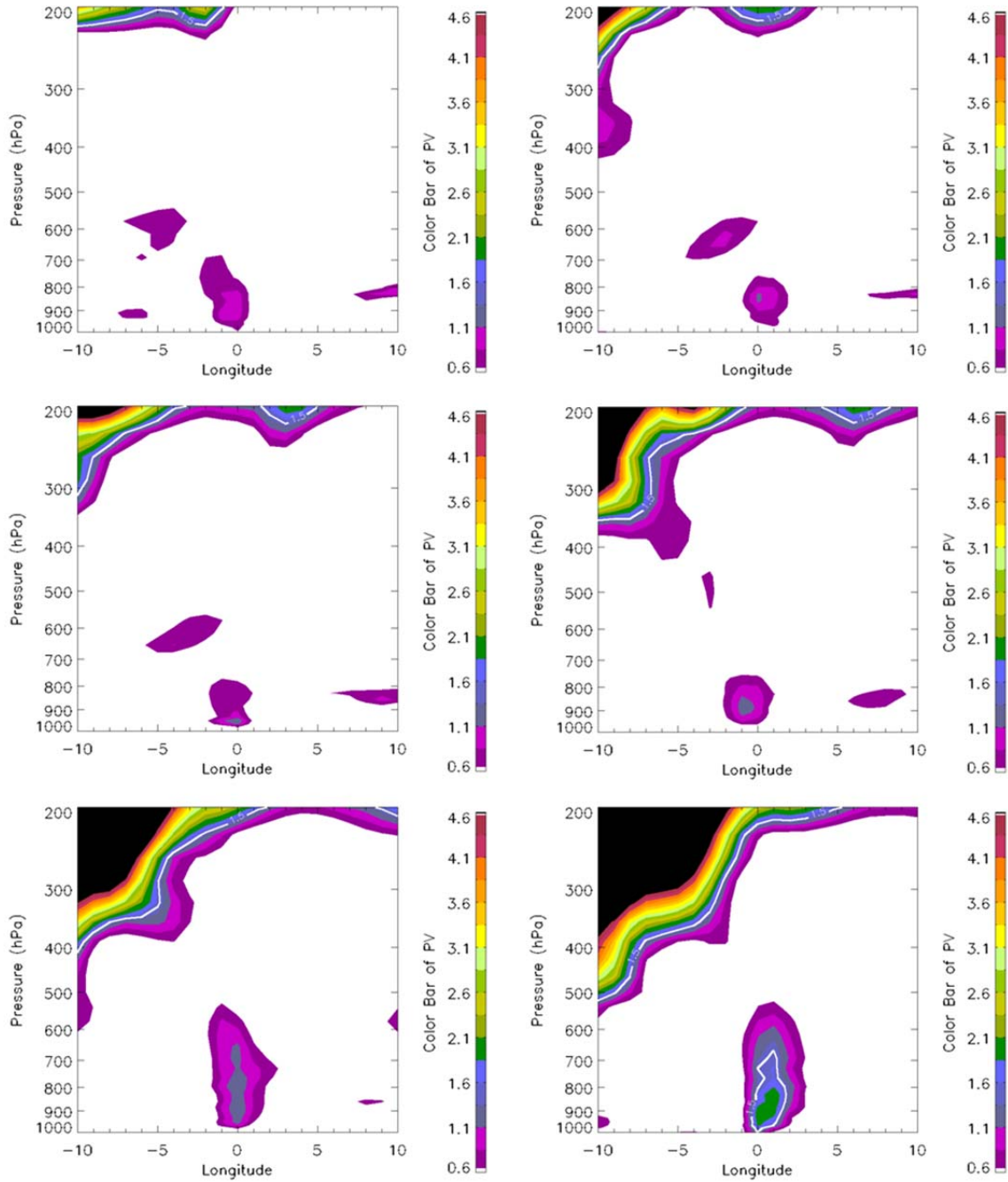
Figure 96. Vertical slices of PV (shading; PVU), with 1.5 PVU white contour as DT, of ATL DRV#56 (bomb), in six-hour time steps, from 00 UTC 19 December to 06 UTC 20 December 2005.

B.   COMPOSITES OF BOMB VS. NON-BOMB DRVS

Within each of the four default groups (ATL COLD, ATL WARM, PAC COLD and PAC WARM), DRVs that bombed were separated from the ones that did not bomb, resulting in four additional types of horizontal composites (using the 4 panel template), at the time of DRV formation: top-left-panel shows composites of Q within DRV bombs, bottom-left-panel shows composites of Q within non-bomb DRVs, top-right-panel shows composites of TH within DRV bombs, and the bottom-right-panel shows composites of TH within non-bomb DRVs.

1.   ATL COLD

In terms of moisture, the bomb group (top-left-panel) had higher values of Q maximum near the LAT/LON of DRV formation (regridded to 0,0), compared to that of the non-bomb group (bottom-left-panel). In terms of baroclinicity, the bomb group (top-right-panel) exhibited a larger meridional temperature gradient than that of the non-bomb group (bottom-right-panel). As show in MM05, both larger baroclinicity and moisture content lead to a faster growing disturbance. It seems reasonable to hypothesize that a faster growing DRV is more conducive to subsequent explosive deepening.
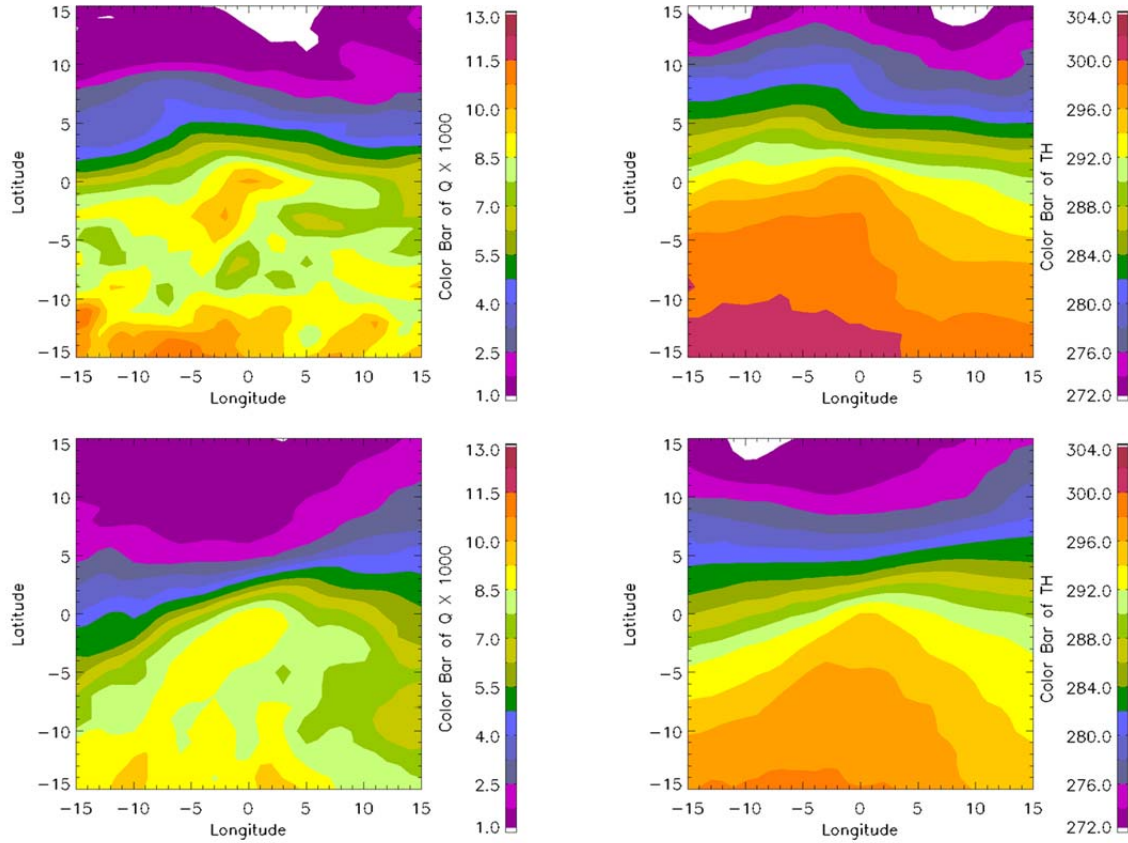
Figure 97.   Within the ATL COLD DRVs, the top-left-panel shows composites of Q (shading; g H$_2$O/kg air) within DRVs that bombed, and the bottom-left-panel shows composites of Q (shading; g H$_2$O/kg air) within DRVs that did not bomb. The top-right-panel shows composites of TH (shading; K) within DRV that bombed, and the bottom-right-panel shows composites of TH (shading; K) within DRVs that did not bomb. All composites made at time of DRV formation.

2.   ATL WARM

The same conclusion can be drawn here as for the ATL COLD group: the DRVs that bombed were in a more favorable environment (in terms of moisture content and baroclinicity) at time of formation, than the DRVs that did not bomb. The bomb group (top-left-panel) had higher values of Q maximum near the LAT/LON of DRV formation (regridded to 0,0), compared to that of the non-bomb group (bottom-left-panel). The bomb group (top-right-panel) also exhibited a larger meridional temperature gradient than that of the non-bomb group (bottom-right-panel).
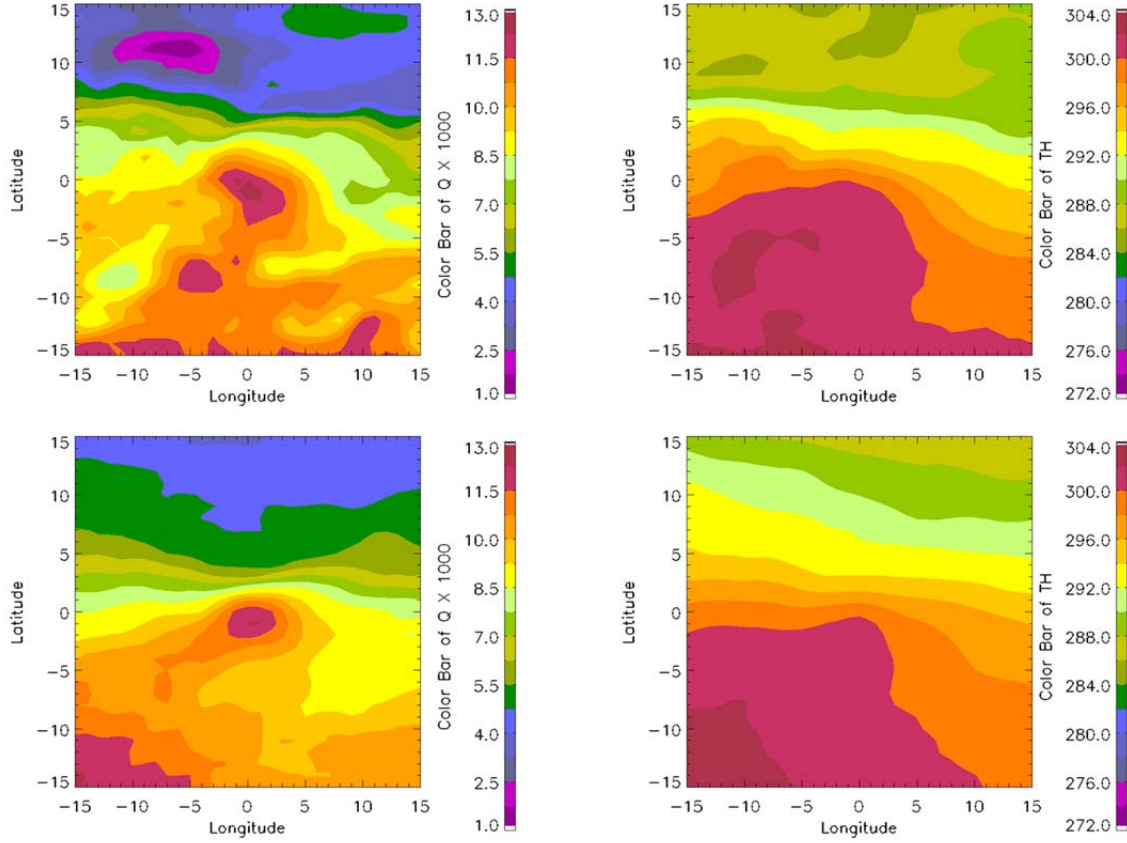
Figure 98.   Same set up as Figure 97, except for the ATL WARM DRVs.

3.   PAC COLD

The same conclusion cannot be drawn here as in the ATL basin. The difference between the bomb and non-bomb DRVs is subtle. In fact, it appears that the non-bomb group has the more favorable environment (in terms of moisture content and baroclinicity) at time of formation, than the DRVs that bombed. The bomb group (top-left-panel) had slightly lower values of Q maximum near the LAT/LON of DRV formation (regridded to 0,0), compared to that of the non-bomb group (bottom-left-panel). The bomb group (top-right-panel) also had a slightly smaller meridional temperature gradient than that of the non-bomb group (bottom-right-panel).
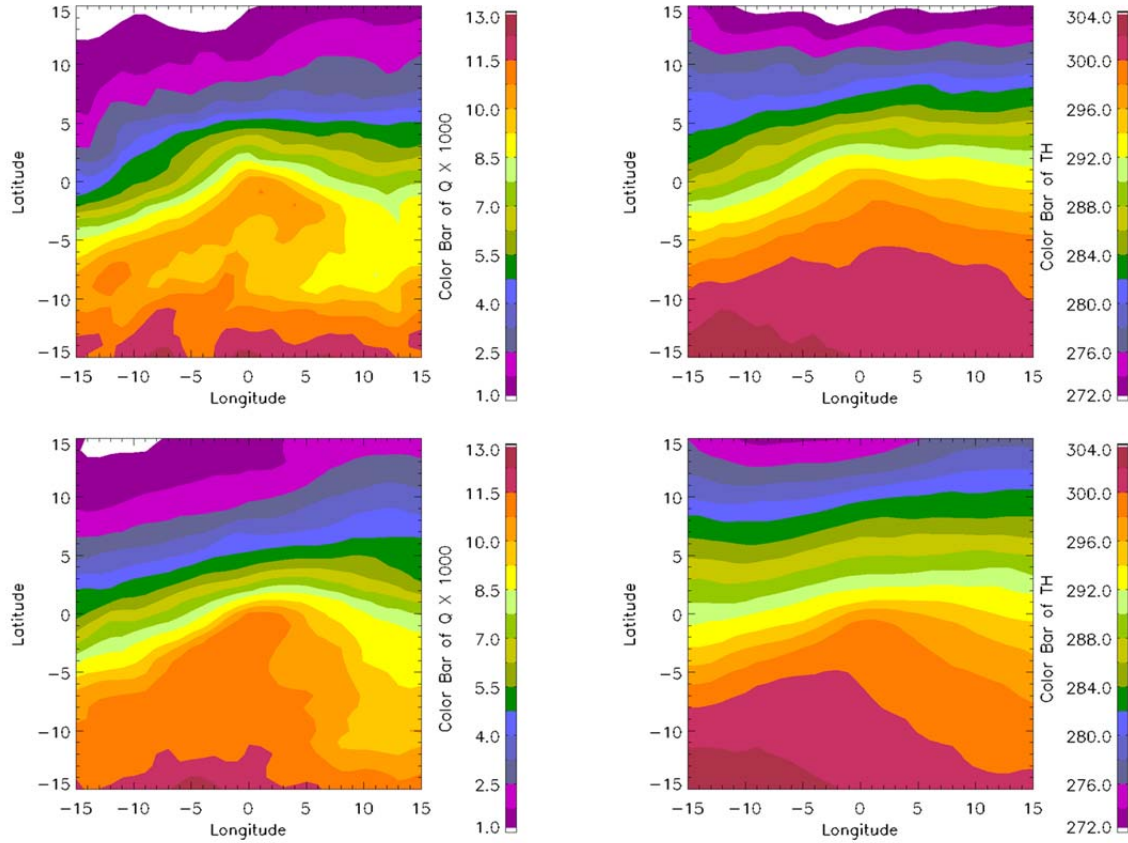
Figure 99.   Same as Figure 97, except for the PAC COLD DRVs.

4.   PAC WARM

The observations in PAC WARM group are quite interesting. The difference between the bomb and non-bomb DRVs is no longer subtle, with the non-bomb group having the higher moisture content (bottom-left-panel), and the bomb-group having the higher baroclinicity values (top-right-panel), surrounding the DRVs. This could be interpreted to mean that stronger temperature gradients, which imply a stronger jet (and a stronger upper tropospheric anomaly), are more conducive to bomb formation within the PAC WARM group.
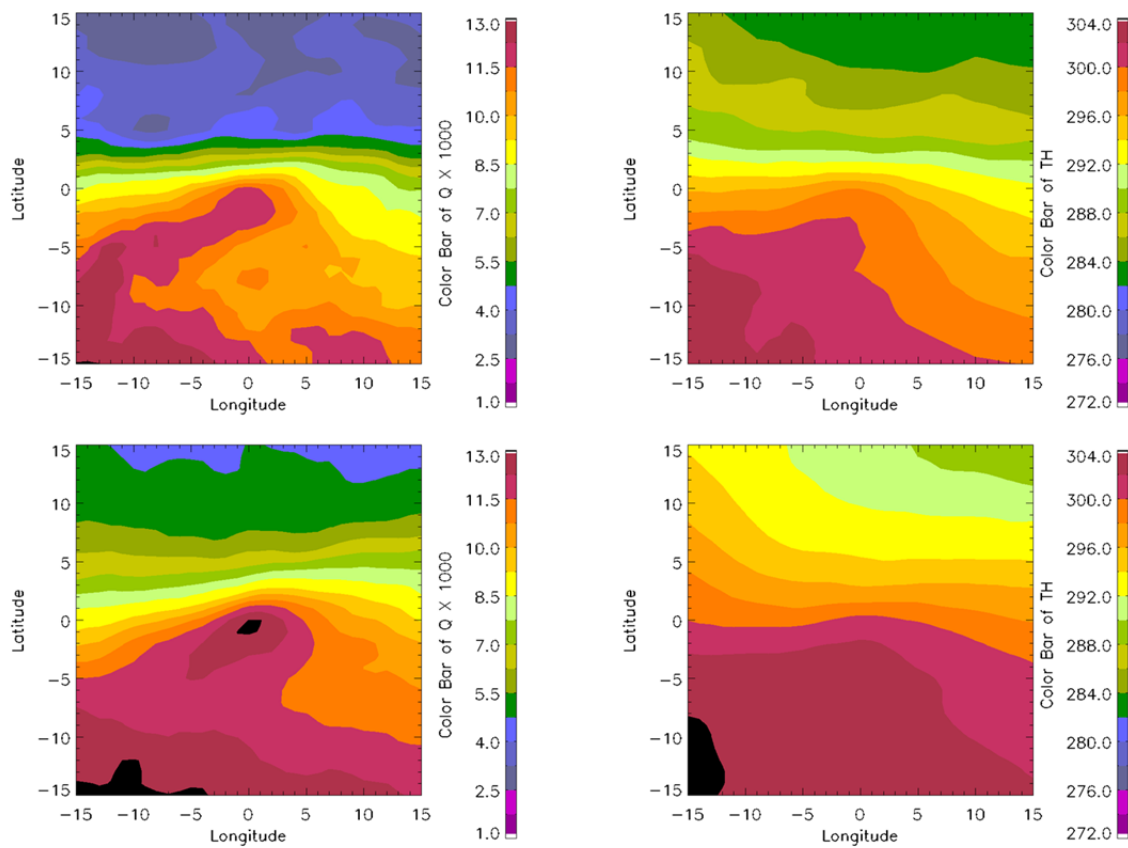
Figure 100.   Same set up as Figure 97, except for the PAC WARM DRVs.

113

THIS PAGE INTENTIONALLY LEFT BLANK

VI.   DISCUSSION AND CONCLUSION

The overarching goal of this research project was to add to the general knowledge of DRV dynamics. To date there have been a limited number of DRV studies in the literature, whether they be idealized or case study examinations. To vastly expand the scope of DRV research, this thesis utilized a 10-year, objective DRV climatology prepared by Boettcher and Wernli (2012).

Within the 268 ocean-born DRVs utilized for this study, about three times as many DRVs form during the warm season, as compared to the DRVs born during the cold season. The affinity to warmth was seen again as DRVs preferentially form in proximity of the Gulf Stream and the Kuroshio Current. A composite analysis of the identified DRVs revealed a similar disturbance structure to that previously reported. The DRVs are characterized by a low-level PV maximum in a region devoid of significant upper-level forcing. The necessary ingredients of moisture and baroclinicity are clearly identified. In agreement with the interpretation offered by Mak (1994), the composites showed that PV perturbations (production or destruction) occur where diabatic heating (CH) changes with height (increase or decrease). The process of diabatic conversion to eddy APE can be visualized by vertical composites, showing the covariance of positive diabatic heating and a positive temperature perturbation.

Statistically significant anomalous signals in the lower tropospheric specific humidity and potential temperature fields *before* the time of DRV genesis were identified. The structure and time of these signals proved to be coherent. A future avenue of DRV research would be to investigate the usefulness of these signals in a predictive sense.

The composite analyses were separated into four groups (sorted by basins and seasons). The cold season is defined as November through April, whereas the warm season is from May through October. Note that three out of four published DRV case studies fell into the ATL COLD group, which makes up only 8% of the 2001–2010 DRV climatology (16% of the bombs). Even the "Perfect Storms" occurred near the end of

115

October, which is bordering the beginning of the cold season. There is a notable lack of research into the other three groups, but some insights were gained through analysis of the composite methodology described in Chapter IV.

It was evident that the composite plots from this thesis bear a strong resemblance to the equivalent DRV plots in published literature, which lends credence to the existing model studies, and also establishes the existing case studies as non-outliers. As mentioned above, even though ATL COLD is the smallest group with only 21 DRVs, it contained five times more "real DRVs" than the case studies combined.

When split into "bomb" versus "non-bomb" clusters, the PAC WARM group showed interesting anomalous Q and TH trends. The non-bomb cluster had higher moisture content, while the bomb-cluster had higher baroclinicity values. This could be interpreted to mean that stronger temperature gradients, which imply a stronger jet as well as stronger upper tropospheric perturbations, are more conducive to bomb formation within the PAC WARM group.

A final word on type A cyclogenesis. Some published works have cast doubt on the existence of type A cyclones as defined by Petterssen and Smebye (1971). In this work, it was determined that nine observed cases fit the characteristics of the Type A development. All of these storms explosively deepened. As such, we believe that type A cyclones are *alive* and *well* over the Northern Hemispheric ocean basins.

LIST OF REFERENCES

Boettcher, M., and Wernli H., 2011: Life cycle study of a diabatic Rossby wave as a precursor to rapid cyclogenesis in the North Atlantic–Dynamics and forecast performance. *Mon. Wea. Rev.*, **139,** 1861–1878.

_____, and _____, 2012 *(Submitted)*: A 10-year climatology of diabatic Rossby-waves in the northern hemisphere. *Mon. Wea. Rev.*

Conzemius, R. J., R. W. Moore, M. T. Montgomery and C. A. Davis, 2007: Mesoscale convective vortex formation in a weakly sheared moist neutral environment. *J. Atmos. Sci.,* **64,** 1443–1466.

Dunkerton, T. J., M. T. Montgomery, and Z. Wang, 2009: Tropical cyclogenesis in a tropical wave critical layer: easterly waves. *Atmos. Chem. Phys.,* **9,** 5587–5646.

Fantini, M., and A. Buzzi, 1993: Numerical experiments on a possible mechanism on cyclogenesis in the Antarctic region. *Tellus*, **45A,** 99–113.

Gyakum, J. R., P. J. Roebber, and T. A. Bullock, 1992: The role of antecedent surface vorticity development as a conditioning process in explosive cyclone intensification. *Mon. Wea. Rev.,* **120,** 1465–1489.

Holton, J. R., 1992: Synoptic-Scale Motions II: Baroclinic Instability. *An Introduction to Dynamic Meteorology*, R. Dmowska and J.R. Holton, Eds., Academic Press, 228–264.

Jiang, H. and D. J. Raymond, 1995: Simulation of a mature mesoscale convective system using a nonlinear balance model. *J. Atmos. Sci.,* **52,** 161–174.

Jones, S. C., P. A. Harr, J. Abraham, L. F. Bosart, P. J. Bowyer, J. L. Evans, D. E. Hanley, B. N. Hanstrum, R. E. Hart, F. Lalaurette, M. R. Sinclair, R. K. Smith and C. Thorncroft, 2003: The extratropical transition of tropical cyclones: forecast challenges, current understanding, and future directions. *Wea. Forecasting,* **18,** 1052–1092.

Lorenz, E. N., 1955: Available potential energy and the maintenance of the general circulation. *Tellus*, **7**, 157–167.

Mak, M., 1994: Cyclogenesis in a conditionally unstable moist baroclinic atmosphere. *Tellus,* **46A,** 14–33.

Montgomery, M. T. and B. F. Farrell, 1991: Moist surface frontogenesis associated with interior potential vorticity anomalies in a semigeostrophic model. *J. Atmos. Sci.,* **48,** 343–367.

_____, and _____, 1992: Polar low dynamics. *J. Atmos. Sci.,* **49,** 2484–2505.

Moore, R. W., and M. T. Montgomery, 2004 (MM04): Reexamining the dynamics of short-scale, diabatic Rossby waves and their role in midlatitude cyclogenesis. *J. Atmos. Sci.,* **61,** 754–768.

_____, and _____, 2005 (MM05): Analysis of an idealized, three-dimensional diabatic Rossby vortex: A coherent structure of the moist baroclinic atmosphere. *J. Atmos. Sci.,* **61,** 754–768.

_____, and _____, and H. C. Davies, 2008 (MMD08): The integral role of a diabatic Rossby vortex in a heavy snowfall event. *Mon. Wea. Rev.,* **136,** 1878–1897.

_____, and _____, and _____, 2012 (*Submitted*): Dynamical processes culminating in diabatic Rossby vortex genesis. Part I: An idealized numerical model study. *Mon. Wea. Rev.*

_____, and O. Martius, and H. C. Davies, 2008: Downstream development and Kona low genesis. *Geophys. Res. Lett.,* **35,** L20814, doi:10.1029/2008GL035502, 2008.

Norquist, D. C., E. E. Recker, and R. J. Reed, 1977: The energetics of African wave disturbances as observed during phase III of GATE. *Mon. Wea. Rev.*, **105**, 334–342.

Parker, D. J., and A. J. Thorpe, 1995 (PT95): Conditional convective heating in a baroclinic atmosphere: A model of convective frontogenesis. *J. Atmos. Sci.,* **52,** 1699–1711.

Petterssen S. and Smebye S. J., 1971 (PS71): On the development of extratropical cyclones, *Quart. J. R. Met. Soc.,* **97,** 457–482.

Raymond, D. J. and H. Jiang, 1990 (RJ90): A theory for long-lived mesoscale convective systems. *J. Atmos. Sci.,* **47,** 3067–3077.

Riviere, G., P. Arbogast, K. Maynard, and A. Joly, 2010: The essential ingredients leading to the explosive growth stage of the European wind storm Lothar of Christmas 1999. *Quart. J. Roy. Meteor. Soc.,* **136,** 638–652.

Sanders, F. and Gyakum, J. R., 1980 (SG80): Synoptic-dynamic climatology of the "Bomb." *Mon. Weather Rev.,* **108,** 1589–1606.

Wernli, H., 2002: Diabatic Rossby Waves, *EGS XXVII General Assembly,* Nice, 21–26 April 2002, abstract #3957.

_____, S. Dirren, M. A. Liniger, and M. Zillig, 2002: Dynamical aspects of the life cycle of the winter storm "Lothar" (14–26 December 1999). *Quart. J. Roy. Meteor. Soc.,* **128,** 405–427.

INITIAL DISTRIBUTION LIST

1. Defense Technical Information Center
   Ft. Belvoir, Virginia

2. Dudley Knox Library
   Naval Postgraduate School
   Monterey, California